uc3m | Universidad Carlos III de Madrid

BACHELOR'S DEGREE IN MECHANICAL ENGINEERING

Academic course 2018/2019

Bachelor thesis

"A Biomechanical Analysis of Bicycle Helmets using FEM"

David Sepúlveda López

Tutor:

Marcos Rodríguez Millán

Co-Tutor:

Jacobo Antona-Makoshi

Expected place and location of presentation:

11/07/2019 Classroom: 7.1.J05

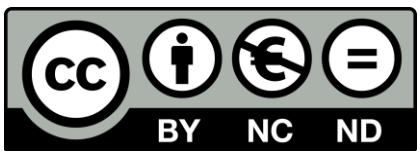

ABSTRACT

This thesis evaluates, by means of finite element methods the possible head injuries that might occur during an EN 1078 standard impact setting, as well as the energy percentage absorbed by the helmet in the same conditions.

In this thesis, the geometry of a commercially available bicycle helmet has been modelled using CATIA. The helmet model geometry has then been meshed with quadrilateral and hexahedral elements using Hypermesh software. The last step of the thesis was performing helmeted head impact simulations using LS-DYNA software.

The impacts upon which this thesis is based on are the EN 1078 flat anvil and curbstone anvil shock absorbing capacity tests, which are the EU standards for bicycle helmet safety evaluations. To validate the results, a comparison between the resultant acceleration and impact time between this study and previous studies was made. The EN 1078 flat anvil test has been validated and the set-up for the EN 1078 curbstone anvil test has been deemed correct. The acceleration results deemed the helmet safe by the EN 1078 standard.

The head injury criteria assessed for the EN 1078 flat anvil test suggest 50% probability of skull fracture and a 75% concussion probability. A HIC value of 970.2 was obtained, indicating an 88% probability of moderate injury and 49% of serious injury. It was also found that DAI injuries are in the threshold of reaching a 50% probability of occurrence.

The head injury criteria assessed for the EN 1078 curbstone anvil test indicates a 50% probability of concussion. A HIC value of 224.2 was obtained, which associates to 7% probability of moderate injury and 3% of serious injury. It was also found that DAI injuries are 11.1 kPa away from the 50% probability threshold.

Regarding the additional tests made, the following results were obtained: the PU Foam has little effect on the absorption properties of the helmet and its main use is rider comfort. The importance of the modeling the straps in the simulation is demonstrated, since they keep the head attached to the helmet at all times. Depending on impact speed the helmet can absorb up to 50% of the impact energy. It is proposed that bicycle helmets must be mandatory for all people regardless of age, since the effectiveness of the helmet has also been demonstrated at low impact speeds. An analysis made to the different densities of the EPS Foams showed that in order to achieve a more distributed impact, with a low HIC value and low maximum acceleration it is recommended to use an EPS Foam with a larger density. Curves of injury probability against impact speed were developed showing that minor injuries start to happen at 10 km/h, severe at 15 Km/h and the most extreme injuries at 20 Km/h. The critical value for untreatable damage in the impact is 29.4 Km/h. Even though the effectiveness of the helmet has been proven in this study, it has also been found that at high speeds the cyclist can suffer untreatable damage; therefore, new research on helmets and cyclist safety is required to increase the likelihood of survival.

It is proposed to lower the bicycle speed limits to 20 km/h in city shared pathways, and to limit the speed of electric bikes to reach a maximum of 20 km/h without rider input to keep extreme injury modes within reasonable values in the worst-case-scenario impact.

Keywords: **Head Injury, EPS, Impact, Safety.**

AKNOWLEDGEMENTS

This thesis is for my wonderful parents and my sister: Felix, Esther and Raquel. Thank you for all the support, patience, and affection that you have always given me,
I love you.

I would also like to thank Dr. Marcos Rodríguez Millán and Dr. Jacobo Antona-Makoshi for all the help and guidance that I have received in the development of this thesis.

CONTENTS

TABLE OF FIGURES

LIST OF TABLES

LIST OF ABBREVIATIONS

A3MS:	3 Ms Criterion
A5MS:	5 Ms Criterion
acc:	Acceleration
CEN:	European Committee for Standardization
CPSC:	Consumer Product Safety Commission
CT:	Computed Tomography
DAI:	Diffuse Axonal Injuries
DGT:	Dirección General de Tráfico
EN:	European Norm
EPS:	Expanded Polystyrene
EPS:	Expanded Polystyrene
FEA:	Finite Element Analysis
FEM:	Finite Element Methods
GSI:	Gadd Severity Index
HIC:	Head Injury Criterion
HPC:	Head Protection Criterion
MRI:	Magnetic Resonance Imaging
g:	Standard Earth Gravity
ICP:	Intracranial Pressure
PLA:	Peak Linear Acceleration
PU:	Polyurethane
TBI:	Traumatic Brain Injury
WSTC:	Wayne State University Cerebral Concussion Tolerance Curve

1. INTRODUCTION

This Bachelor's thesis was made collaboration with the Japan Automotive Research Institute (JARI), in order to assess the possible head injuries that might occur under the EN 1078 European helmet Standard testing conditions for bicycle helmets.

This thesis was developed with the relentless and masterful guidance of Dr. Marcos Rodríguez Millán and Dr. Jacobo Antona-Makoshi, to whom I am grateful for all the help that I have received.

The main hypothesis of this study is that the Finite Element Methods Simulation that is to be pursued will be able to assess the importance of bicycle helmets on the safety of cyclist and will be able to identify the possible head injuries that might happen while wearing a helmet under standard impact conditions.

An EN 1078 shock absorbing capacity test will be simulated and validated, using a CAD Design based on a helmet that is available on the market, and a validated FEA head provided by Dr. Antona-Makoshi.

The results will show the influence of wearing a helmet during an impact, and the resultant acceleration that the head still suffers during the impact. The energy absorbed by the helmet will also be determined; Thus, the effectiveness of the helmet will be tested.

The possible head injuries that might occur while wearing a helmet will also be assessed with different Head Injury Criteria; there are multiple methods of measuring head injuries; therefore, multiple criteria is to be tested to ensure a full analysis. The criteria used are shown below:

- Peak Linear Acceleration (PLA) which determines the probability of skull fracture and concussion based on the acceleration that the head suffers.
- Gadd Severity Index (GSI) based on the acceleration and impact duration on the head, and predicts serious internal head injuries.
- Head Injury Criterion (HIC_{15} and HIC_{36}) based on the acceleration and impact duration on the head, is one of the most widely used head injury criteria. It can determine multiple modes of head injuries (maximum, critical, minor…).
- Head Protection Criterion (HPC) which is similar to the Head Injury criterion and measures multiple modes of head injuries (severe, serious, moderate...).
- 3 Ms Criterion (A3MS) based on the maximum head acceleration on a time interval, which as an indicator of head injuries.
- Diffuse Axonal Injuries (DAI) are related to cases where comma or loss of consciousness has happened. The probability of suffering DAI is measured using the Intracranial Von-Misses Stress.
- Skull fracture probability under impacts is determined using a probability function developed by Philemon Chan [1].

The previous criteria serve as head injury indicators. For this thesis, multiple analyses are also made to assess the effectiveness of the helmet and the energy absorbing capabilities under multiple impact conditions. The following analyses are to be carried out:

- The influence of the EPS Foam on the maximum head acceleration, head acceleration-time curve, and HIC values are determined.
- The helmet has multiple elements, one of them is the PU Foam used to improve riders' comfort, and some authors state that it also absorbs part of the impact energy. Therefore, an analysis will be made to assess how much energy is absorbed by the PU Foam.
- The energy absorbed by the helmet during the impact will be assessed. This analysis will also be made at different impact speeds to determine at which speeds the energy absorbing capacities of the helmet are optimal.
- Curves to asses multiple head injuries (minor, severe, maximum…) will be developed. These curves will be based upon the Head Injury Criterion and the impact speed. Upon the finding of this curves, a maximum speed for bicycles will be proposed to increase rider safety.

There are multiple steps to develop the simulation from which all the necessary information will be obtained. To achieve the closest results to a real-life helmet impact, and to obtain accurate and representative data the following steps were made:

The first step, done in February, was choosing an appropriate bicycle helmet. A studio of the most appropriate helmet for the research was made. First of all, the helmet used had to comply with the European helmet standards (EN 1078) and had to be the right size and fit the head properly (S, M, L or XL). In this case it had to fit the FEM head provided. The helmet also had to be easily available to the general public.

Secondly, the helmet had to be replicated using a CAD program. The difficultness of this step, done in February, resides in the highly irregular shape of a bicycle helmet and the need to replicate the design as accurate as possible to obtain the best results in the FEM simulation. To tackle this challenge, the CAD program CATIA student version (V5-6R2017) was chosen as this program is commonly used in the aerospace industry, where highly non-homogeneous surfaces are commonly designed. Exactly what was needed in order to replicate the helmet shape.

Thirdly, in order to perform FEM simulations, done in March, an accurate meshing of the helmet was required. FEM programs such as ABAQUS, ANSYS or LS-DYNA have built-in meshing tools which are capable of producing meshes. Nevertheless, for this thesis, a highly irregular shape (helmet) had to be accurately meshed and therefore a specialized meshing program was needed. In this case, Hypermesh was chosen due to its outstanding Solid Map feature for 3D solids.

For the fourth step, done in April, and to obtain accurate simulation results, a complete set-up needs to be done in a FEM program. LS-DYNA is a program widely used in the Engineering industry and Academic World for impact simulations and it is consequently used for this thesis. In order to develop a correct analysis, the approach followed was to increase the difficultness of the simulation one step at a time. Firstly, the helmet was simulated by itself, then a simplified FEA head was used, and lastly the FEA head provided by Dr. Antona-Makoshi was included. The most critical part in this step will be setting up the contacts between solids and surfaces, defining the material properties, and

controlling the simulation boundaries such as initial speed, impact location, and other forces such as gravity that might have a significant outcome on the simulation.

The fifth step, done in May, would involve a comparison between the results obtained and previous real-case-scenario tests and simulations made in earlier studies. If the acceleration results in the flat anvil and curbstone anvil impacts agree, then the FEM simulations would be validated and could be used for further analyses.

The sixth and last step, done in June, was doing several tests with the FEA simulation introducing modifications such as speed, anvil type and contact surface. Then, analyses of these results were needed to assess whether any sort of head injury would occur and the influence that the helmet has to reduce the energy that is absorbed by the head during the impact.

It must also be noted that it is the intention of my directors and myself to publish the findings of this thesis as a JCR. It is also expected to do a real test with a helmet and a head dummy at Universidad Carlos III de Madrid during the summer period of 2019, at which point it is expected that the necessary helmet testing equipment becomes available in the University. The Procedure followed in the thesis can be seen in Figure 1 below:

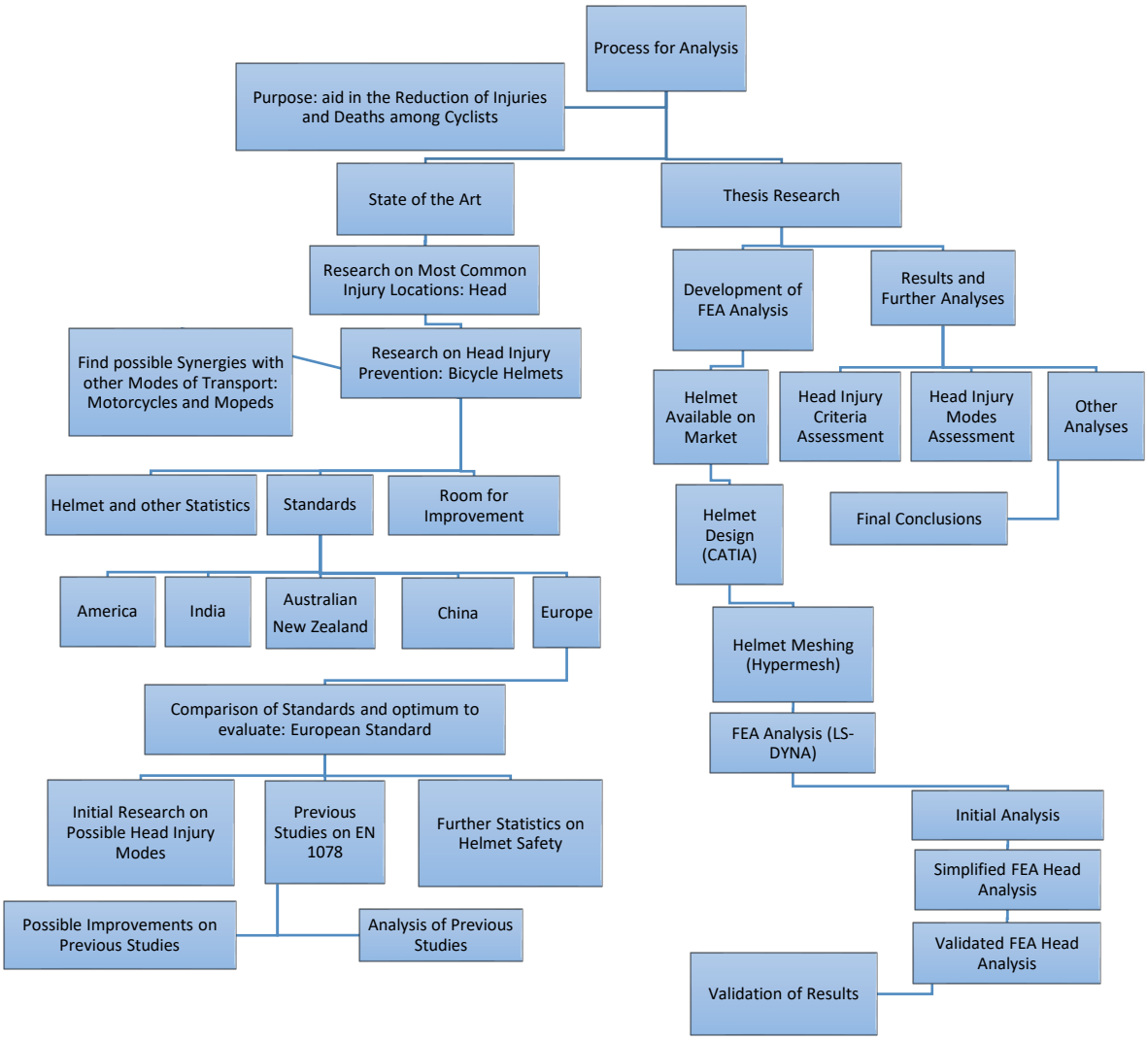

Figure 1: Schematics of Thesis Procedure.

2. MOTIVATION FOR THE THESIS

This thesis was chosen due to concern caused by the high number of bicycle accidents happening all around Europe. During 2018 a total of 2015 cyclists died in the European Union (recorded fatalities) and a total number of 67 in Spain [2].

The research performed on this thesis mainly uses data from the European Union, but it can also be applied to other countries that may have concerning problems with regards to the safety of their cyclists.

For example, in a developed country comparable to the European Union, the United States of America, a total of 840 pedal cyclist died in 2016, where the data also shows an increasing trend of pedal cyclist deaths since 2007 when 701 persons died [3].

Developing countries such as India also have the same problem with safety. During 2016 2.585 persons died while cycling in India [4].

The most frequent safety equipment used by the cyclists is the helmet, it is more common every day to see cyclist wearing them. This surge is due to the increase in awareness of their effectiveness, and the increasing regulations that oblige people to wear them.

Nevertheless, the use of bicycle helmets strongly varies depending on the country and even on the province within the same country. The wearing percentage is usually less than 50% [5,6].

There are also some groups that disagree with the helmet energy absorption capabilities, which leads to misinformation. Therefore, new research and findings on the helmet protection capabilities can help to further cement the status quo of the helmet in society and increase the wearing percentages among riders.

Hospital data recorded all around the European Union shows that the most common cycling injuries are related to the head, upper extremities and lower extremities as shown in Figure 2 below [2].

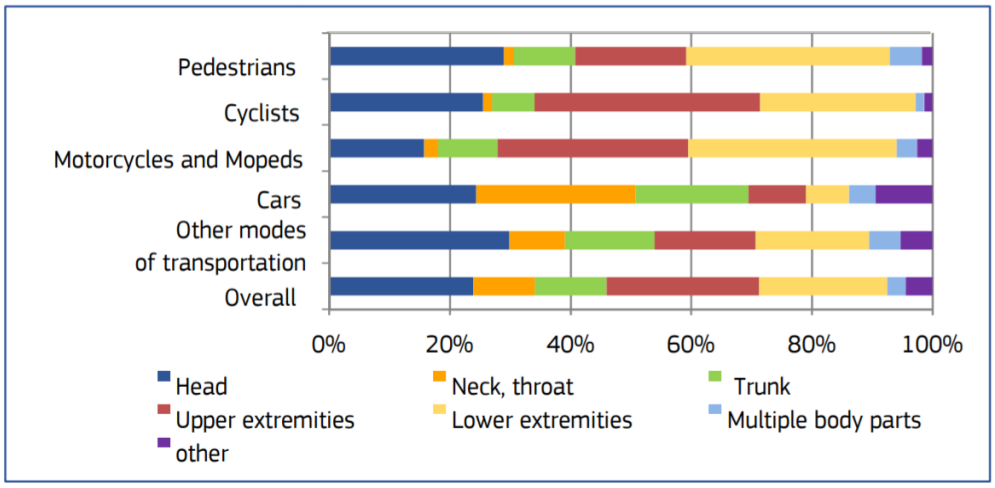

Figure 2: EU Injury Database with Transport and Injury Type Statistics *[2]*.

As shown in Figure 2, head related injuries are important on all major forms of transportation. Thus, the research performed in this thesis can be applied to other sorts of transportation were helmets are also used such as motorcycles and mopeds.

Since a head injury is one of the most common sorts of bicycle injuries, and due to the increase in helmet awareness, my supervisors and myself believe that new findings, research and improvements made to bicycle helmets can lead to a further reduction of head injuries, and in the most extreme impact scenarios, reducing the percentage of deaths.

In order to obtain new information, and improve the existing helmets, there is a need to conduct new research on them. The first step in this process is to cement the background of bicycle helmet and produce repeatable, representative and meaningful analyses of them. These analyses also need to be validated.

Currently, there are two options for this kind of research, the first one implies very expensive testing equipment using real impact analyses. The second one implies using Finite Element Analysis software.

Finite Element Analysis is a technique used to simulate real life situations on a computer. Its largest asset is the capability of reducing testing time and allowing the designers and engineers to make meaningful changes to the designs with a low economic input. Finite Element Analysis is a technique that everyday more engineering companies use to test their designs.

With relation to this thesis, using Finite Element Methods would allow my supervisors and myself to test the European Standard for bicycle Helmets, the EN 1078. It would also allow to obtain meaningful data on the head injuries that might occur during the EN 1078 and other impacts. Furthermore, it can serve as a basis to test the most adverse impact case scenarios, which could lead to a complete helmet redesign to optimize helmet safety in the most adverse impact scenarios.

Additional mentioning needs to be done to **Dr. Jacobo Antona-Makoshi**, who has kindly provided us with a validated FEA Head Model and to the **Japan Automobile Research Institute** who has helped in the process.

The FEA head that will be used has been validated by the Japan Automobile Research institute, which means that the data gathered in this head is perfectly applicable to real-life impacts. The head has all the key elements to assess head injuries, amongst which stand out the cerebellum, corpus callosum, neck, cerebrum, skin, skull, brainstem and spinal cord.

Regarding Finite Element Methods and bicycle helmet impacts, there has been some previous research, which can validate the results obtained in this thesis. Nevertheless, some of the previous research analyses lack some key elements (such as using a real human validated FEA head or helmet elements such as the chin straps) and do not extensively assess the possible head injuries.

In conclusion, my tutors and myself have chosen this thesis due to the outstanding impact that new research can have on bicycle helmet safety and the corresponding reduction of head injuries and fatalities.

3. STATE OF THE ART

3.1 State of the Art Worldwide

3.1.1. Introduction on Bicycle Helmet Parts

Most bicycle helmets share the following elements:

- EPS Foam: which absorbs most of the energy during the impact [7].
- Padding: A material which improves rider comfort and is also used to absorb energy [8].
- Retention System: used to keep the helmet attached to the head during impact; it comprises the chin strap which is worn under the jaw and the rear strap close to the neck [8] .
- Ventilation holes: which are used to improve rider's comfort.
- Shell: The out-most part of the helmet, which is in contact with the EPS Foam.

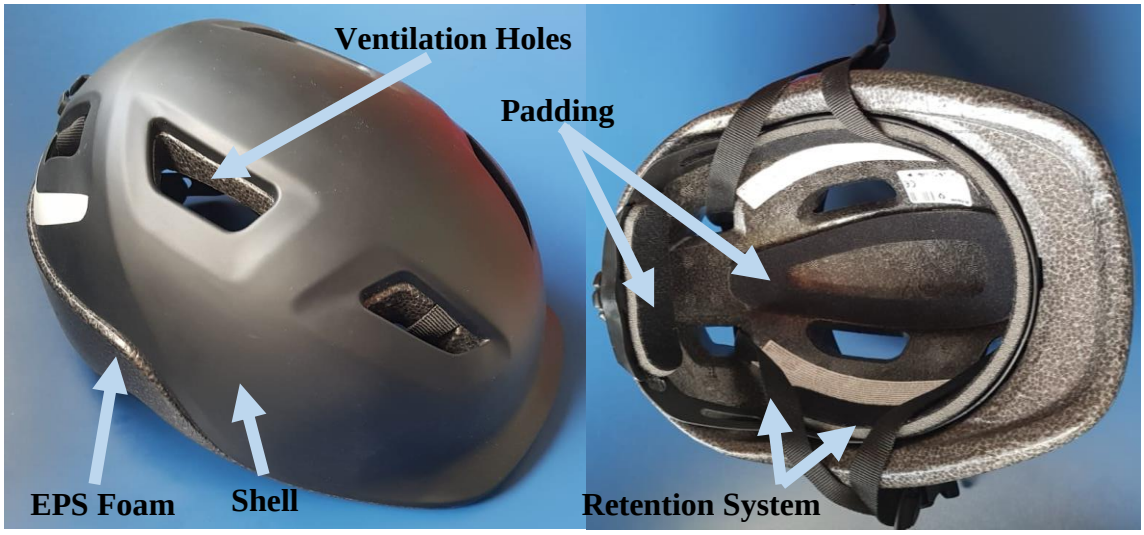

Figure 3: Example of Bicycle Helmet (used for this thesis).

Figure 3 shows a standard bicycle helmet. This helmet has the EN 1078 certification, which is the standard set by the European Union to increase safety in bicycle helmets. Different countries have different Standards.

3.1.2. Introduction on Bicycle Helmet History and How they Work

The bicycle helmet was first introduced in the 19th century, but it did not start to have real implementation until the late 20th Century. The bicycle helmet surge occurred after the 1960's when some companies such as BELL helmets introduced advances like the first hard shell helmet in 1975 [9]. The development of helmet standards that started in 1970 has led to numerous improvements in the safety of helmets. Moreover, now some countries such as Spain have made it mandatory to wear a helmet for some age groups, and in certain paths like interurban roads [10].

Bicycle helmets have three main purposes:

1. Providing a crushable foam (EPS Foam) which allows the helmet to absorb energy on the impact. Thus, reducing the energy that is transmitted into the head [11]. The helmet energy absorption capabilities reduce the risk of head injuries [12].
2. The helmet allows the impact stresses to be distributed through the helmet, thus providing a greater surface where the force is applied. This increased surface will distribute the stresses over the skin in a more homogeneous way, which prevents the stresses from being concentrated in a very small area [11].
3. The helmet also protects the wearer from coarse, sharp or uneven surfaces which may cause damage to the skin or skull including penetration [11].

The helmets usually meet the following requirements demanded by the users:

1. They must be wearable in multiple conditions such as rain or cold weather [12].
2. They must be comfortable for the rider to wear [12], which as a result, makes the rider more prone to wear the helmet.
3. The helmet must be ventilated [8], reason for which the ventilation holes are used.

3.1.3. Brief Description of Helmet Standards Around the World

3.1.3.1. History

The first standards that were introduced for safety regarding any sort of helmets dates back to 1952 when the Transport Research Laboratory in the United Kingdom published its research for racing motor cyclists (BS 1869:1952). This led to new standards for helmets such as the Snell 1959 for protective helmets. More standards were introduced for other helmet applications such as heavy duty works and motorcycles. It was not until 1970 when the first standard was introduced for pedal cyclists regarding Protective helmets, which was published as a British Standard (4544:1970) [12]. Some representative and meaningful helmet standards are the following:

3.1.3.2. European Standard [8]

Europe introduced this Standard for bicycle helmets in 1997, the "EN 1078: Helmets for pedal cyclists and users of skateboards and roller skates". The most important features of this standard are the following:

1. There are minimum requirements regarding rider's vision when worn [8].
2. Peak acceleration cannot exceed 250 g for an impact speed of 5.42m/s on a flat anvil and 4.57 m/s on a curbstone anvil [8].
3. The head form used must comply with the EN 960 [8].
4. High temperature conditioning, low temperature conditioning and artificial ageing must take place [8].
5. When impacted the helmet must remain on the head form, the retention system strength must be tested, and it must be at least 15mm wide [8].

3.1.3.3. American Standard (CPSC [13])

The United States introduced its Standard for bicycle helmets in 1999 the CPSC (16 CFR Part 1203 – Safety Standard for Bicycle helmets) which is only aimed at bicycle users, unlike the European Standard which targets a larger group of sports. This standard

concerns to the third largest population in the world [14]. The most important features of this norm are the following:

1. There are minimum requirements regarding rider's vision when worn [13].
2. High temperature conditioning, low temperature conditioning, and water immersion conditioning (helmets is kept at least 4 hours underwater) [13].
3. Peak acceleration cannot exceed 300g for an impact speed of 6.2m/s on a flat anvil and 4.8 m/s on a curbstone anvil [13].
4. The helmet must be tested with the smallest head form which lets a partially compressed pad hold the helmet in position [13].
5. The straps cannot stretch so that it allows the helmet to come off during an accident. Straps are tested for strength [13].

3.1.3.4. Indian Standard

To the author's knowledge there are no bicycle helmet standards that must be followed in India, which is the second most populated country in the world [14]. Therefore, standardizing bicycle helmets could increase safety. Nevertheless, it is conceivable that Indian helmets may follow standards from other countries in order to sell them there.

3.1.3.5. Australian/New Zealand Standard (AS/NZS 2063:2008) [15]

Australia and New Zealand introduced their latest Standard for bicycle helmets in 2008 the "AS/NZS 2063:2008 Australian New Zealand Standard Bicycle Helmets" which is only aimed at bicycle users, unlike the European Standard which targets a larger group of sports. This is one of the toughest standards. The most important features of this norm are the following:

1. When impacted, the helmet must remain on the head form. The retention system strength must be tested, and it must be at least 15mm wide [15].
2. All tests must be done without the Padding pads [15].
3. High temperature conditioning, low temperature conditioning, and water immersion conditioning [15].
4. The head form used must comply with the AS/NZS 2512.1. Sizes A, E, J, M and O must be used, and they have to be appropriate for the helmet size [15].
5. A maximum of 10% of the mass of the helmet can detach during impact [15].
6. There are minimum requirements regarding rider's vision when worn [15].
7. Peak acceleration cannot exceed 250g for an impact height of 1500mm on a flat anvil. Furthermore, the acceleration duration cannot be more than 3ms when the acceleration is 200g and it cannot be more than 6ms for an acceleration larger than 150g [15].
8. There are requirements regarding load distributions; When the helmet is dropped from 1000mm height it cannot exceed a 500N force over a smaller circular area of $100mm^2$.

3.1.3.6. Chinese Standard (GB 24429-2009) [16]

China introduced this Standard for bicycle helmets in 2009, the GB 24429: "Sports helmets-Safety requirements for sport helmets for cyclists and users of skateboards and roller skates". The most important features of this norm are the following:

1. There are minimum requirements regarding rider's vision when worn [16].
2. The straps cannot stretch so that it allows the helmet to come off during an accident. Straps are tested for strength and they must be at least 15mm wide [16].
3. Head forms are distinguished by the head circumference dimensions and there are four sizes that can be used for the tests [16].
4. Peak acceleration cannot exceed 300g for an impact speed of 6.2m/s on a flat anvil and 4.8 m/s on a curbstone anvil [16].
5. High Temperature Conditioning, Low Temperature conditioning, and Water Immersion Conditioning [16].

3.1.3.7. Comparison of Bike Helmet Standards

As shown, different standards are used on each country. Nevertheless, it can be seen that these standards are closely related. All of them ensure that the helmet stays attached to the head during impact. They also use various head forms to ensure that helmet sizes can adapt to all head dimensions. There are minimum requirements on rider's vision, which must not be obstructed, and is used in all the standards. Material conditioning is done in all the standards; Nevertheless, some of these conditionings differ from each other but they all replicate the effect that different weather and helmet storage can have on the material properties. Moreover, all of them have a closely related impact testing method; The difference between the methods is found in the maximum g (gravity) acceleration that the head can sustain, as shown in TABLE *1* below.

TABLE 1: STANDARD COMPARISON MAXIMUM G ACCELERATION AND SPEED.

Standard/ Region	Europe	United States	Australia/ New Zealand	China
Flat Anvil	Speed:5.42 m/s Max g acc:250	Speed:6.2 m/s Max g acc:300	Height: 1.5m Max g acc:250	Speed:6.2 m/s Max g acc:300
Curved Anvil	Speed:4.57 m/s Max g acc:250	Speed:4.8 m/s Max g acc:300	None	Speed:4.8 m/s Max g acc:300

The speed of the impact determines how much kinetic energy the helmet will have to absorb and is also related to the maximum head acceleration while absorbing that energy. Therefore, an analysis of this relationship is presented, with the hypothesis that the head form and helmet weight are the same for all tests, shown in equation 3.1 and equation 3.2:

$$Ec\ (J) = \frac{1}{2} * m(kg) * v^2 \left(\frac{m}{s}\right) \quad (eqn.\ 3.1)$$

$$Eag\left(\frac{J}{(\frac{m}{s^2})*kg}\right)=\frac{Ec(J)}{g_t(\frac{m}{s^2})*m(kg)} \quad (eqn.\,3.2)$$

Where

Ec is the Kinetic Energy (J)

Eag is the Energy absorbed per g acceleration and common weight(J/(kg*g))

M is the Mass of the helmet and head form (kg) (hypothesized equal for all tests)

v is the Speed at impact (m/s)

g_t is the maximum g acceleration of the test (m/s^2)

The calculation of energy absorbed per test are shown in TABLE 2 below.

TABLE 2: ENERGY ABSORBED PER G ACCELERATION STANDARDS (FOR SAME HEAD FORM AND HELMET WEIGHT).

Region/Test Type	Flat Anvil J/(100kg*g)	Curbstone Anvil J/(100kg*g)
Europe	5.88	4.17
America	6.40	3.84
Australia/New Zealand	5.88	Not Tested
China	6.40	3.84

TABLE *2* shows that all standards are closely related in terms of Energy per maximum g acceleration. For a flat anvil, the most thorough standards are the American and the Chinese, on the other hand, Europe has the most thorough standard when it comes to a curbstone Anvil. In order to see how much they differ a percentage difference was calculated and is shown on TABLE 3.

TABLE 3: PERCENTAGE DIFFERENCE ON ENERGY ABSORBED FOR STANDARDS (FOR SAME HEAD FORM AND HELMET).

Region/Test Type	Flat Anvil J/(100kg*g)	Curbstone Anvil J/(100kg*g)
Europe	-8.125%	0% (benchmark)
America	0% (benchmark)	-7.91%
Australia/New Zealand	-8.125%	Not Tested
China	0% (benchmark)	-7.91%

TABLE *3* shows that all standards are within 8.5% of difference on energy absorbed per maximum g acceleration. Thus, it can be concluded that even though these standards have different testing methods, they will all share a common grade of safety.

An external source (Department of Transport: London) also claims that there is limited evidence to suggest that some standards are better than others [11], which agrees with the previous calculations.

Since the helmet that will be studied in this thesis has been certified for the EN 1078 standards, and since the previous calculations and external evidence [11] proves that all standards show the same grade of protection (with less than 10% of margin difference), the standard chosen to test the helmet in this thesis is the EN 1078.

3.2 European Helmet Industry

3.2.1 Test for Bicycle Helmets in Europe; the European Standard

Helmets in Europe are standardized by the EN 1078 norm which tests the following properties of a helmet [8]:

- Capacity of absorbing energy (shock absorbing capacity).
- Construction and shape of the helmet.
- Properties of the retention system.
- Information and labels of the helmet.

In this thesis it is assumed that the helmet's construction, retention system and labelling information has been done accordingly to the EN 1078 norm.

The concern of this thesis is the injuries that a helmet can help prevent. Therefore, the capacity of absorbing energy is the property to be assessed. The EN 1078 norm has a specific test for this, described in the point 5.4 in the EN 1078 document "Determination of shock absorbing capacity" [8], the test layout can be observed in Figure 4.

These are the key points of the EN 1078 shock absorbing test:

1. The helmet must be stabilized in the head form with a 50 N load.
   1.1. This point is covered in the FEA analysis with pre-checks which ensure that the helmet is stabilized and has the normal wearer's position which allows the user to have the right vision field.
2. There is a specific area where the flat anvil impacts are done, and another specific area where the curbstone impacts are done.
   2.1. This point is covered in the FEA analysis since the exact position of the impact can be implemented into LS-DYNA. Therefore, the impact areas will be analyzed in the real helmet and then these impact areas will be tested in the software.
3. Low Temperature conditioning, High Temperature conditioning and artificial ageing.
   3.1. This can be implemented onto the FEA analysis by introducing helmet material properties that consider the ageing. These aged properties can be found from material research and testing or from previous FEA analysis made to helmets.
4. Several apparatuses are used for guidance and measurements of the acceleration (e.g. a free fall guidance system and an accelerometer output recorder).

4.1. These systems are already implemented in the FEA software; for example, the guidance system to avoid the helmet from changing the impact area is not needed since the FEA software allows to choose the desired impact area; the accelerometer is not needed either since the software also has tools that allow for a measurement of the accelerations in any node, part, and element of the system.

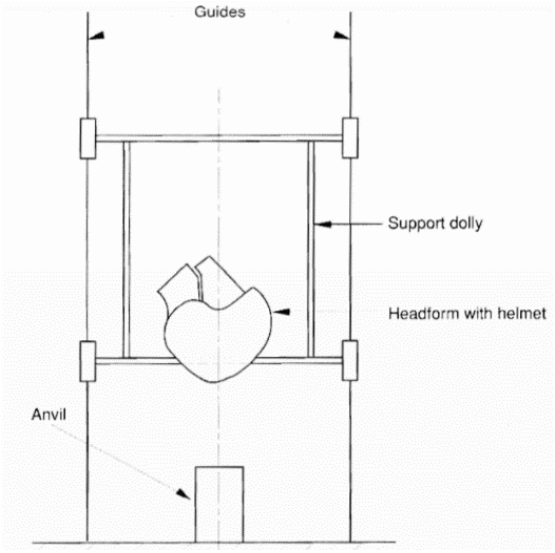

Figure 4: Apparatus to Determine Shock absorbing Capacity *[8]*.

5. The base of the test must be made of steel or concrete and must have a mass of 500kg.
   5.1. This is to prevent the ground in the test to be unstable. It can be simulated in the FEA software by introducing a base of steel that is large enough to weigh 500 kg or by assigning rigid properties to the anvil base.
6. A flat steel anvil must have a diameter of 130 mm.
   6.1. This is to ensure that in case of large deformation the helmet impacts against the anvil. It can be done by designing, meshing and simulating such a shape in the FEA analysis, or using a base that is large enough to cover all the impact area of the helmet.
7. A curbstone anvil must have two faces with an inclination of 52.5º each and a common edge of 15mm. The height has to be at least 50mm and the length 125mm at least.
   7.1. This can be done by designing, meshing and simulating such a shape in the FEA analysis.
8. The head form has to comply with the EN 960 standard.
   8.1. In this case, the simulation will be done with a real human FEA head provided by Dr. Antona-Makoshi and validated by the Japan Automotive Research Institute (JARI), which allows for a full assessment of head injuries .
9. Impact the helmet where the worst-case conditions happen.
   9.1. This can be performed by doing a visual examination on the helmet and then impacting it on the desired place, it is also possible to do multiple simulations on different impact points to assess which impact point causes the largest acceleration.

10. The helmet must be impacted at a speed of 5.42 m/s on a flat anvil and 4.57 m/s on a curbstone anvil (equivalent to 1497mm and 1064mm respectively for drop height).
    10.1. This is introduced within the simulation parameters of the FEA simulation.

Once the helmet has been tested using the previous set-up, the head form must not exceed a maximum acceleration of 250 g in order to be valid.

3.2.2 Legal Background on Bicycle Helmets

The EN 1078 (dated to 1997) norm [8] states that the following countries have to implement the previous standard:

Austria, Belgium, Denmark, Finland, France, Germany, Greece, Iceland, Ireland, Luxembourg, Netherlands, Norway, Portugal, Spain, Sweden, Switzerland and the UK.

According to the CEN (the European Committee of standardization) the standards are voluntary (i.e. legally there is no obligation to automatically follow them) but there may be laws that make it mandatory to comply with them [17] .

On the other hand, CEN states that the European Standards are important for the Single European Market because they facilitate trade and gives the manufacturers a goal to accomplish [17]. This statement, to the author's knowledge, is extremely important since all the helmets that the author has found or researched comply with some of the previously stated standards. Hence, standards provide the manufacturers a common platform to design their helmets and sell them in multiple countries, which in return means that these standards are followed, and rider's safety is increased.

3.2.3 Lethal Bicycle Accidents and their relationship with Helmets

A study published in 2018 by Michal Bíl et al. [18] collected data on 119 lethal bicycle accidents in a time span of 19 years. The report concludes that 37% of all deaths could have been prevented if a bicycle safety helmet had been worn. It remarks that one-vehicle crashes, cyclist hitting obstacles, and falling from the bike are the most preventable injury scenarios. It also outlines that death in the most energetic crashes such as impacts with trains or cars cannot be prevented. The outcome of the report was that helmets should be worn. Nevertheless, cyclist should also comprehend the dangers of high-impact crashes [18].

This study agrees with the theory that helmets increase safety in bicycle accidents and that they should be worn at all times. Therefore, research and development in the field of bicycle helmets can lead to an increase in safety and a decrease in head trauma and fatalities.

3.2.3.1 Percentage of Bicycle riders that wear Helmets

Two studies conducted by Ioana Popa et al. [5] and Pamela L. Ramage-Morin [6] have summarized key statistical studies around the world regarding bicycle helmet use, the results are the following:

TABLE 4: STUDIES REGARDING BICYCLE HELMET USE AROUND THE WORLD [5,6].

Country/Region	Percentage of users who wore helmets
Studies within the European Union	
Paris, France, Europe [5]	2% (1998 study)
United Kingdom, Europe [5]	27% (2000 study)
Florence, Tuscany, Italy, Europe [5]	37% (2008 study) 28.3% (2009 study)
Germany, Europe [5]	12% (2011 study)
Denmark, Europe [5]	12% (2017 study)
Studies Outside the European Union	
Montreal, Canada [5]	46% (2012 study)
New York City Bike Lanes, U.S.A [5]	50% (2014 study)
Quebec, Canada [6]	34.5% (2013-14 study)
Ontario, Canada [6]	38.2% (2013-14 study)
British Columbia, Canada [6]	65.3% (2013-14 study)
Nunavut, Canada [6]	9% (2013-14 study)
North Carolina, U.S.A [5]	25% (2015 study)

It is hard to determine the percentage of bicycle users who wear helmets within a safe confidence interval because they might use it or not depending on different scenarios such as the weather or their route. Nevertheless, the previous studies and reports shed some light on helmet use; as shown in the studies done by Ioana Poa et al. [5] and Pamela L. Ramage-Morin [6] most of the countries/regions have a wearing percentage lower than 50%.

Some countries such as Germany and Denmark have low wearing percentages (12%). On the other hand, Canada has achieved high wearing percentages in some of its Provinces such as British Columbia with a 65.3% percentage of users who wear helmets, but within the same country there are other provinces who have a much lower percentage such a Nunavut with 9%. Even though there is high variability on the helmet wearing data, the percentage of users who wear helmets worldwide and within Europe is very low (usually less than 50%).

Further analysis and evidence supporting the increase of safety that helmets provide might lead to new laws and regulations. It will also show the average user the benefits of wearing helmets which in return might lead to higher wearing percentages and as a result lower fatality and injury rates. This is one of the main reasons to perform this thesis.

3.2.3.2 Statistic within the European Union regarding Cyclist Fatalities

Europe had 2015 fatalities involving bicycle users in 2016, which is a 24.2% reduction from the year 2007 when 2660 people were killed. By country, Germany was the country with the highest number of fatalities in 2016 with 393 (4.8 per million of population). Meanwhile, in Spain 67 people died (1.4 per million of population).

The difference in the fatality rate can be attributed to multiple reasons, the most important one is the percentage of people that use the bicycle as a means of transport in each country.

TABLE 5: NUMBER OF CYCLIST FATALITIES BY COUNTRY, 2007-2016 *[2]*.

	2007	2008	2009	2010	2011	2012	2013	2014	2015	2016
BE	90	86	89	70	70	69	73	76	83	71
BG	-	35	29	27	17	32	31	29	29	-
CZ	116	93	84	80	63	78	74	68	84	53
DK	54	54	25	26	30	22	33	30	26	31
DE	425	456	462	381	399	406	354	396	383	393
EE	13	9	7	0	0	0	0	0	0	-
IE	15	13	7	5	9	8	5	13	-	-
EL	16	22	15	23	13	21	15	19	11	18
ES	90	59	57	67	48	74	70	75	58	67
FR	142	148	162	147	141	164	147	159	149	162
HR	28	47	29	28	28	21	23	19	34	27
IT	352	288	295	265	282	292	251	273	251	275
CY	3	6	2	2	2	1	2	1	1	0
LV	18	15	26	13	15	18	13	16	9	7
LT	-	-	-	-	-	-	18	19	22	-
LU	0	0	2	1	2	0	0	0	0	1
HU	158	109	103	92	85	84	68	98	83	73
MT	0	0	0	0	-	-	-	-	0	1
NL	147	145	138	119	144	145	112	118	107	101
AT	37	62	39	32	42	52	52	45	39	48
PL	498	433	371	280	314	300	306	286	300	271
PT	34	42	29	33	45	32	29	35	25	33
RO	179	179	157	182	140	154	161	151	162	176
SI	17	17	18	17	16	12	16	13	14	12
SK	61	46	22	27	-	-	-	-	-	-
FI	22	18	20	26	19	19	20	27	30	26
SE	33	30	20	21	21	28	14	33	17	22
UK	138	117	104	111	109	120	113	116	100	105
EU	2.660	2.483	2.289	2.048	2.054	2.152	1.982	2.096	2.008	2.015
Yearly Change		-6,6%	-7,8%	-10,5%	0,3%	4,7%	-7,9%	5,7%	-4,2%	0,3%

The data shown in TABLE 5 also shows a decrease in the number of fatalities each year, with some exceptions such as 2014 when the fatalities incremented 5.7 %.

The report made by the European Road Safety Observatory also includes a distinguishable fact in fatalities; Males account for 80% of all bicycle fatalities, and regarding age groups, the most vulnerable one is the 65+ age group which gathers 45% of all fatalities [2]. By Road type, approximately 41% of all fatalities occurred outside urban areas, 58% inside urban areas, and a small percentage (1%) occurred in a Motorway. Nonetheless, this statistic varies depending on the country; for example, in Malta all the fatalities occurred outside urban areas.

3.2.3.3 Increase/Decrease of Severe/Fatal accidents when Helmet Regulations are Introduced

There is some evidence supporting both sides, but multiple studies suggest that introducing helmet legislation leads to a decrease in injuries and fatalities; which supports the theory that wearing a bicycle helmet increases safety.

A study by the Department of transport of London gathered data regarding the introduction of bicycle helmets in some regions, shown in TABLE *6* below for reference [11].

TABLE 6: REGULATIONS OF BICYCLE HELMETS AND ITS OUTCOME *[11]*.

Country (Region)	Regulation	Results
Australia (Victoria)	Obligation to wear helmets introduced in 1990	48% less head injury admissions in hospitals in 1990-1991; 70% less in 1991-1992 Helmets worn increased from 5% in 1982-1983 to 75% in 1991
New Zealand (Statewide)	Obligation to wear helmets introduced in 1994	30% less head injuries Helmet wearing rate is 95% across the country
Australia (South Australian State)	Obligation to wear helmets introduced in 1991	Admissions decreased 24.7% in hospitals Helmets worn increased from 15% to 90% in cyclist older than 15 years.

From these studies, although disputed by some, it can be concluded that the introduction of bicycle helmet laws and the increase in helmet use leads to a decrease in head injuries.

3.2.3.4 Statistics Conclusions

The previously mentioned statistics outline the high number of fatalities in Europe. The statistics in the use of helmets showed that there is low usage (usually less than 50% of the population) with room for improvement. When laws where introduced regarding helmet safety, the number of head injuries and hospital admissions were reduced.

Thus, it can be concluded that using helmets increases the safety of cyclists. There is also a need to keep reducing the fatality rate of cyclists in Europe. Therefore, if the helmets are safer, then the number of fatalities will decrease even further.

The previous statistics show the importance of doing research and development in the helmet field, which includes the study of FEA helmets. Finite Element Analyses of helmets will determine their effectiveness and will allow for a faster development of safer helmets.

3.3 Current Approaches, Designs, Meshes and Simulations for Bicycle Helmets

3.3.1 Previous Studies

The papers that have been analyzed in search of previous FEA analyses on bicycle helmets are summarized in TABLE *7*.

TABLE 7: FEA STUDIES ANALYZED BASED ON FEA BICYCLE HELMETS.

Name	Principal Author	Year	Shortening
Finite-element analysis of bicycle helmet oblique impacts [19]	N.J. Mills et al.	2007	Studio 1
A transient finite element study reveals the importance of the bicycle helmet material properties on head protection during an impact [20]	Asiminei Ag et al.	2009	Studio 2
Development and validation of finite element model of helmet impact test [21]	Tso-Liang Teng et al.	2012	Studio 3
Development and validation of a bicycle helmet: assessment of head injury risk under standard impact conditions [22]	G. Milne et al.	2012	Studio 4
Bicycle helmet modelling and validation under linear and tangential impacts [23]	G. Milne et al..	2014	Studio 5
Finite element bicycle helmet models development [24]	Helmy Mustafa et al.	2015	Studio 6
The protective effect of a helmet in three bicycle accidents-A finite element study [25]	Madelen Fahlstedt et al.	2016	Studio 7
A computational study of the EN 1078 impact test for bicycle helmets using a realistic subject-specific finite element head model [7]	Michael Sandberg et al.	2018	Studio 8

The key aspects of the previous studies have been summarized in TABLE *8* below. Each analysis has used different helmet properties, helmet generation methods, helmet meshing techniques, elements of the helmet and different impact speed and locations.

TABLE 8: PROPERTIES OF EACH FEA BICYCLE HELMET ANALYSIS.

Studio	Helmet Inspiration	3D Making	Elements modelled	Mesh Properties	Impacts and Speeds
Studio 1	Specialized S1 Simplified Design	Scanned Shape of helmet	Chin Straps EPS Foam Shell	Tetrahedral Solid Triangular Shell Triangular Membrane	0, 5, 10m/s Front 90º Right 70º Back Crown Side
Studio 2	No data + Simplified Design	Provided .stl File	Shell EPS	Tetrahedral solid (6mm) Shell(not specified)	5.23 m/s (1.5 m fall) Vertical Impact
Studio 3	Author's Design	Not Described	Shell EPS Foam Padding Foam Chin Strap	Tetrahedral Solid Shell(not specified)	3.6 m/s tangential 4.5 m/s normal Left 70º Front 70º
Studio 4	Helmet Available on Market	Digitalized real Helmet	EPS Foam Shell	Tetrahedral Solid Trias Shell	EN 1078
Studio 5	Helmet Available on Market	Digitalized real Helmet	EPS Foam Shell	Tetrahedral Solid Trias Shell	EN 1078
Studio 6	MET Kaos MET Crossover Netti Lightning	Scanned Shape of helmet	EPS Foam Shell Chin Straps	Triangular Shells Tetrahedral Solids	5.44 m/s (1.5 m fall) Top Side Front
Studio 7	Helmet Available on Market	Not Described	EPS Foam Shell Rear Straps	Tetrahedral Solid Triangular Shells	4.3-7.2 m/s Front Left perp. Left 45º
Studio 8	Author's Design	Author's Design	EPS Foam Shell Chin/Rear Straps Padding	Tetrahedral Solid Triangular Shells	5.42 m/s (1.5 m fall) Vertical Impact

3.3.2 Helmet Designs of Previous Studies

Most of the designs of the previous studies are obtained from helmets that are available on the market. Their conversion into 3D shapes was mainly done by scanning or digitalizing these helmets with very advanced equipment such as with the Flexscan 3D Scanner [24].

However, for this thesis, the author did not have the means or tools to use one of these scanners; therefore, the helmet CAD design was created in three-dimensions using CATIA by a three-dimensional approach that will be explained in the following sections.

3.3.3 Meshes of the Previous Designs

All the previous studies use tetrahedral shapes for the solid elements and triangular shapes for the shells. Presumably, because they are easier and faster to mesh than hexahedral elements.

Even though using hexahedral and quadrilateral elements will mean a longer time necessary for meshing, it is expected that using these elements will reduce computational time, convergence time, and they will also increase the accuracy of the results. Therefore, hexahedral and quadrilateral elements will be used for this thesis.

3.3.4 Speed and Impact Locations of Previous studies

Mostly, all the previous studies have impacts within the same range of speeds (0-10 m/s) and they are based upon the EN 1078 standard against a flat anvil. Nevertheless, some of these studies replicate documented accidents [25].

Regarding impact locations, the main impact location is a vertical impact. The results of these previous studies correlate with their expected results (real-life experiments).

Since the previous studies mainly use the EN 1078 test, they will serve to compare them with the results obtained in this thesis and validate the results.

3.3.5 Results from Previous Experiments

Some of these studies have compared the simulations and real-life experiments; for example, the study made by G. Milne at. Al [23] which shows that they both correlate, as seen in Figure 5. Here it can be seen that the simulation and the real-life impact both have close running times (approx. 10ms). They also have related loading and unloading curves, with only a difference in the loading curve, when at 3ms the acceleration in the simulation decreases.

The difference in the loading curve can be due to the lack of padding and straps in the simulation, which may affect the output. Nevertheless, the maximum resultant linear acceleration in both models is very close (within 7 g, or less than 10% difference) and since this is the most important aspect of the simulation, it can be concluded that it this model was validated.

A comparison between the helmet that is simulated in this thesis and the results of the previous EN 1078 studies will serve for validation purposes.

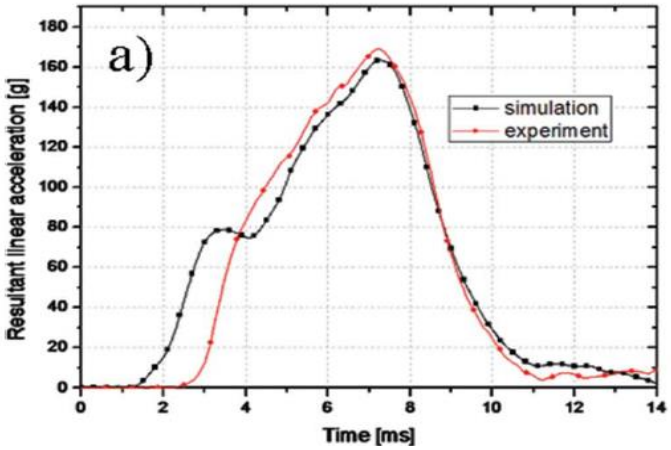

Figure 5: Simulation and Real-Life Impact Comparison made by G. Milne et al. *[23]*.

3.3.6 Head Injury Assessment on Previous Experiments

One of the key parts of this thesis is assessing the impact that the helmet has on the rider's safety. The most precise way of measuring this safety improvement is by determining whether the impact will cause any sort of head injury.

From the previous analysis there are only three studios that assess head injuries, the rest focus on the maximum g acceleration that the head suffers. The advanced studios have the following analyses:

- The studio made by G. Milne et al. in 2012 [22] uses a finite element model of the anatomic human head and it measures Intracranial Von-Misses stress (calculates Diffuse Axonal Injuries). This studio is missing some elements that may have a large impact in the results of the simulation: it does not simulate the helmet Padding that can lower the maximum g acceleration and makes the head properly fit the helmet and the chin straps that keep the helmet completely attached to the head at all times.
- The studio made by Fahlstedt et al. in 2016 [25] evaluates the risk of skull fracture and concussion by means of the Von-Misses stress measured in the skull bone and the first principal strain of the brain tissue. This studio is missing some elements that may have a large impact in the results of the simulation: it does not simulate the helmet Padding that can lower the maximum g acceleration and makes the head properly fit the helmet. It also lacks the chin straps that keep the helmet completely attached to the head at all times.
- The studio made by Michael Sandberg et al. in 2018 [7] uses a FE human head model and it measures Diffuse Axonal Injuries with the maximum principal strains. It measures Intracranial Pressure, to asses brain injuries and also measures skull stress to calculate a failure. The main deficiency of this study is that this helmet is not based on a helmet available on the market and some of its features have been added to the author's discretion (for example, the ventilation holes), which may affect the final results.

3.3.7 Differences between this Thesis and Previous Studies

Apart from simulating a helmet that to the author's knowledge has not been simulated before, and assessing its individual safety, this study also introduces new aspects:

All the previous bicycle helmet studies, to the author's knowledge, have used tetrahedral elements. In this thesis the elements will be comprised of hexahedral elements, which will reduce convergence efforts and may also aid to obtain more accurate results.

To the author's knowledge, there is no previous simulation that considers all the following elements at the same time:

- EPS Foam.
- Padding.
- Chin Strap.
- Rear Strap.
- Shell.
- Validated FEA head (including brain tissue, brainstem, cerebellum….).
- The Helmet that is simulated is also available on the market.

A key aspect of this study is using a detailed FEA head that has been validated by the Japan Automobile Research Institute which, for example, includes a skin, cerebrum, vertebrae, ligaments, neck, cortical bones. Such a precise FEA head will be able to provide significant data on head injuries.

The most important head injury criteria and head injuries assessed are the following:

- Peak Linear Acceleration (PLA).
- Gadd Severity Index (GSI).
- Head Injury Criterion (HIC_{15} and HIC_{36}).
- Head Protection Criterion (HPC).
- 3 Ms Criterion (A3MS).
- 5 Ms Criterion (A5MS).
- Diffuse Axonal Injuries.
- Skull Fracture Probability.

This thesis also introduces several additional analyses such as:

- The percentage of energy absorbed by the helmet in the impact.
- The importance of the EPS Foam density.
- The energy absorbed by the PU Foam during the impact.
- Curves were developed to assess the probability of multiple injury types based on the impact speed.

4. DEVELOPMENT OF A HELMET FOR FINITE ELEMENT ANALYSIS

4.1 Sequence for Helmet Development and Analysis

Multiple steps and iterations were needed in order to develop the FEA analysis of the bicycle helmet, all the steps taken were correlated with each other. A small summary of the approach followed is shown in Figure *6* below.

The first step was obtaining the measurements from the real helmet (and FEA head) which is available on the market.

The second step was designing the helmet in CATIA using the previous measurements (a simplified FEA head was also designed with CATIA based on Antona's design).

The third step was exporting the FEA head onto Hypermesh. To do so, a program was needed to translate the .igs files given by CATIA (student version) to the format that Hypermesh (desktop 13.0) recognizes .step files. The program used was FreeCad.

The fourth step was meshing the helmet using Hypermesh, at this step many simplifications and adaptations were needed in order to obtain a proper mesh; hence, in some occasions a step back was taken, and a new design iteration was made in CATIA (the same design procedure was done for the FEA head).

The fifth step was conducting the FEA analysis on the helmet. For this purpose, LS-DYNA software was used. Throughout the simulations many possibilities of improving them were found; consequently, in some iterations a step back was taken, sometimes a new design was made in CATIA and sometimes improved meshing was done in Hypermesh, as shown in Figure *6*.

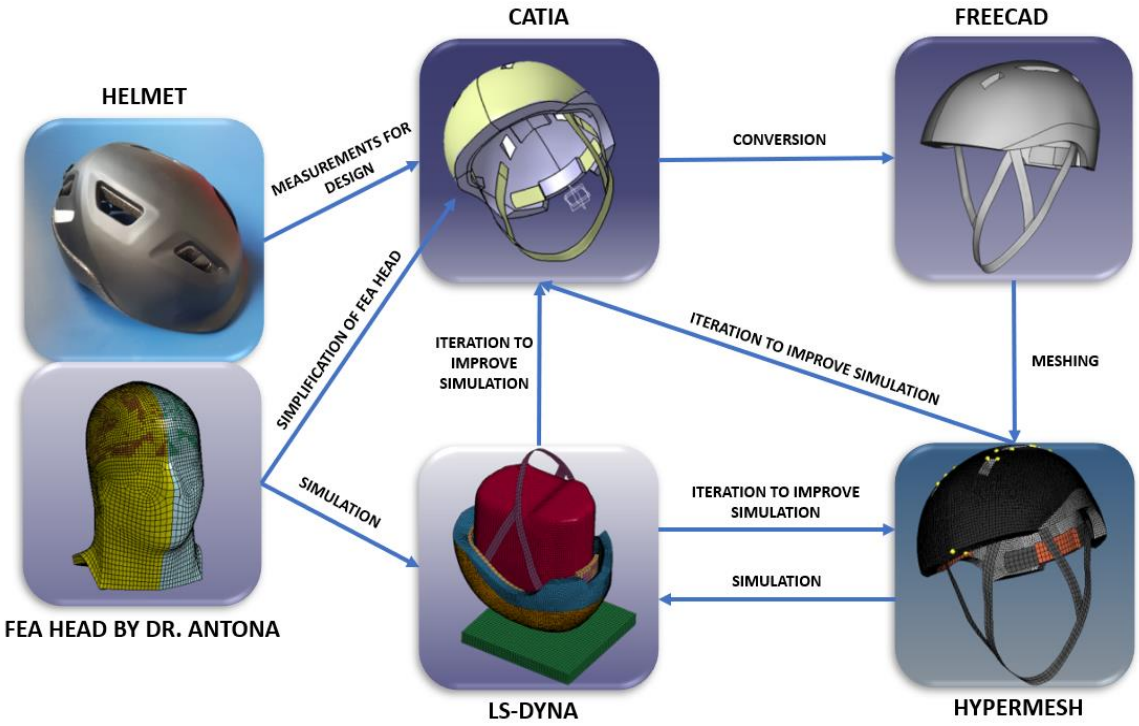

Figure 6: Process for Simulation.

4.1.1 Background on the Chosen Bicycle Helmet

The bicycle helmet that has been chosen for this thesis is widely available on the market. It is an entry level bicycle helmet available in one of the largest sport stores in Spain. The size of the bicycle helmet was based on FEA head provided by Dr. Antona-Makoshi. The basic layout of the helmet can be seen in Figure *3*.

The most important characteristic of this helmet is that it complies with the EN 1078 European Standard. Thus, it can be tested replicating the conditions of this standard and it should have an acceleration lower than 250 g for a 5.42 m/s impact on a Flat Anvil and 4.5 m/s on a curbstone anvil.

The helmet is comprised by an outer shell, a chin strap, a rear strap, and a three-zone Padding (Upper Padding, Side Padding, and Rear Padding), and lastly an EPS Foam.

The key characteristics from the specifications label that can be found on the helmet are the following:

EPS foam: 100% Expanded Polystyrene

Shell: 100% Polycarbonate

Straps: 100% Polypropylene

4.1.2 3D Positioning System for Coordinates

As previously stated, almost all previous bicycle FEA studies generated the helmet elements by a 3D scanning of a helmet. For this thesis there was no scanning or digitalizing way available for the author; therefore, the generation of the helmet had to be made manually.

The shape of the helmet is highly irregular, so, using a regular XYZ coordinate system was not possible. The helmet has one plane of symmetry (in the ZX plane referenced in *Figure 8*); consequently, only half of the helmet had to be measured. In order to locate any point in the helmet, three coordinates are needed.

The 3D coordinate system was implemented by choosing one angular coordinate (δ as shown *Figure 8* which would generate a plane (α plane in *Figure 8*). Then using a radial and angular coordinate system (ϱ radially and θ for the angular coordinate, shown in *Figure 8*) inside the α angular plane which means that a spherical coordinate system was used.

Four δ angular coordinates were used to obtain α planes: 0^{o}, 30^{o}, 60^{o} and 90^{o}. Inside each α plane multiple radial and angular coordinate were used to locate the key points of the system.

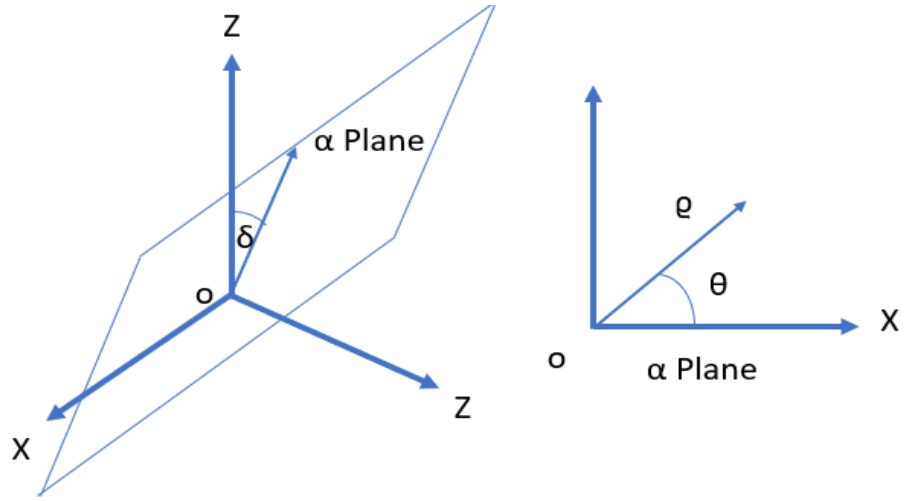

Figure 8: 3D Positioning System used to obtain Helmet Coordinates.

In order to implement the coordinate system shown in *Figure 8* the real helmet had to be cut at 0º, 30º,60º and 90º with respect to the angle δ. This process was made with two hand saws, shown in *Figure 7*. The larger saw was used in the initial cut, when the helmet had better structural integrity and was harder to cut. The smaller saw was used for the final cuts, where the larger saw did not fit.

Figure 7: Handsaws used to cut the Helmet at 30º, 60º and 90º.

The cuts made to the helmet with the saws in *Figure 7*, can be seen in Figure *9*.

Figure 9: Cuts made to Helmet with Handsaw, 30º Left Picture, 60º Middle Picture, 90º Right Picture.

The cuts made in Figure *9* correspond to the α plane in *Figure 8*. Then, once these cuts were made, a radial measuring system was used for each point. This was made by projecting the coordinates into a flat surface and then measuring the angle and the radial distance, as can be seen in Figure *10*.

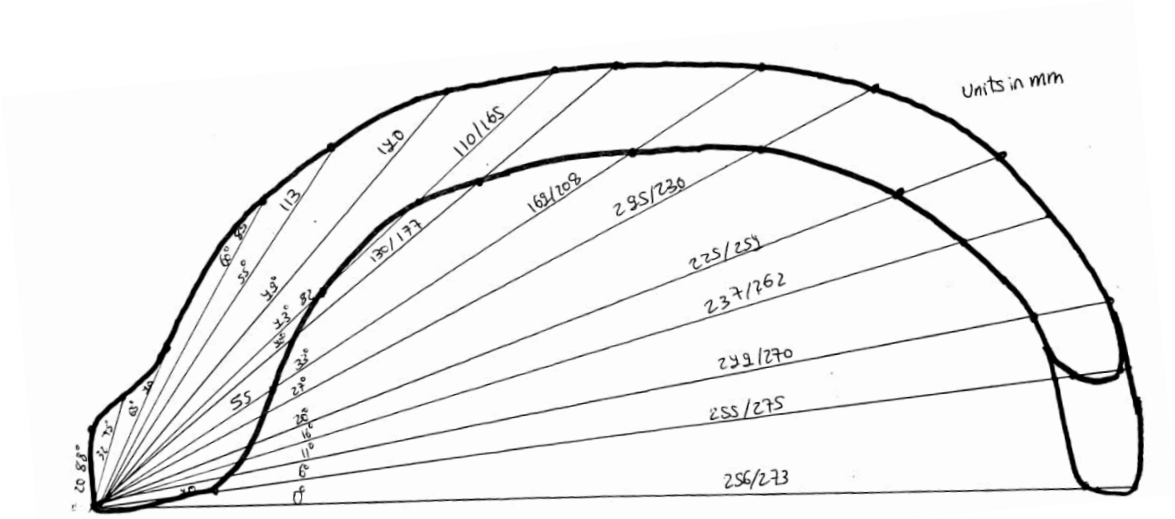

Figure 10: Radial Coordinate System implemented inside α Plane to find the Coordinates of each Point.

Figure *10* shows the 30º cut measurements, the same procedure was made to measure the 0º, 60º, and 90º cuts. A total of 268 three-dimensional points were used to generate the surfaces of the helmet.

4.1.3 Detailed Helmet Structure Explanation

4.1.3.1 EPS Foam

The EPS Foam is the element that will absorb most of the energy during the impact. Depending on the position, the EPS foam thickness varies, as can be seen in the cut of Figure *11*. The EPS Foam of this helmet has six ventilation holes. The EPS Foam is the main structural element where all the other elements are attached.

Figure 11: EPS Foam Cut.

4.1.3.2 Shell

The shell of the helmet is on the outer surface of the EPS Foam, and it is the first part of contact if an impact were to happen. The shell by default is very thin (less than 0.7 mm). It helps to prevent the penetration of sharp objects into the EPS Foam.

Figure 12: Shell Cut.

Figure *12* shows a cut made to the shell. The shell by itself has no structural integrity and would not be able to absorb the energy of the impacts.

4.1.3.3 Padding

The Padding of a helmet has two main purposes, one of them is rider comfort, and it also helps the helmet to properly adapt to the head which helps to absorb impact energy. In this case, this helmet has three main Padding areas, as shown in Figure *13*.

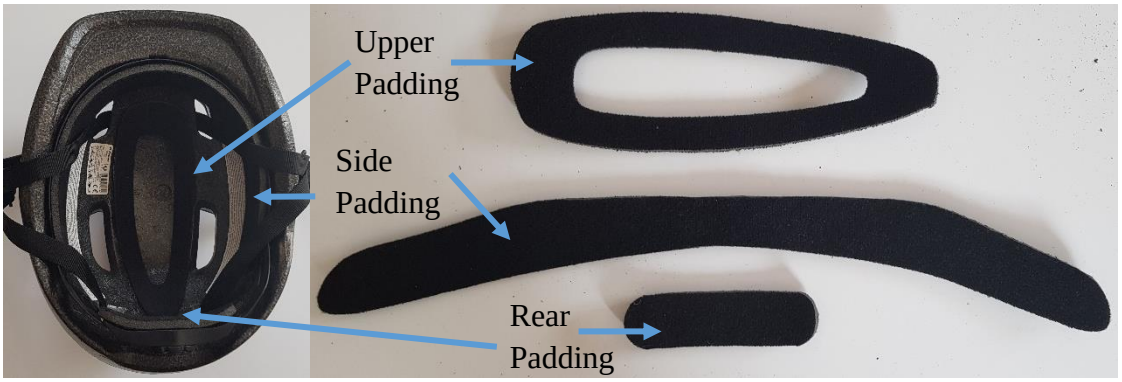

Figure 13: Helmet Padding, Upper, Side and Rear Padding.

4.1.3.4 Straps

The straps in the helmet have two main purposes in the helmet, one of them is keeping the head attached to the helmet at all times, and the rear padding also aids for a correct positioning of the head in the helmet. In this helmet the rear strap can move depending on the head size. Since the measurements of the head are known, for the CAD design, meshing and simulations, the rear strap will be simplified so that it has a fixed length. The chin and rear straps can be observed in Figure *14*.

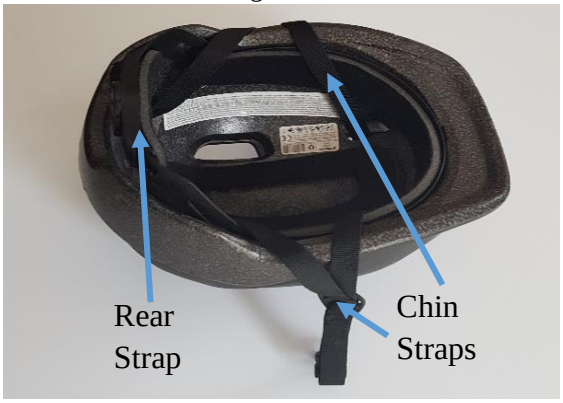

Figure 14: Chin and Rear Straps of the Helmet.

4.2 Helmet CAD Design with CATIA

4.2.1 Helmet Design in CAD, Initial Layout

The program used to generate the CAD Design is CATIA (CATIA V5-6R2017 student version). CATIA is a program widely used in the Aerospace Industry due to its outstanding features to produce irregular shapes. Since all the surfaces on the helmet are highly irregular, CATIA was the program chosen.

Within CATIA there are two main tools that were used: Mechanical Design (Part Design) and Shape (Generative Shape Design). Using the features that these two tools have all the parts of the helmet were generated.

Many iterations were made in order to generate the helmet shape.

The first iterations consisted on generating an extremely simplified helmet. Then, once the main commands to be used were known, the design was re-made adding all the complex shapes found within the helmet which led to obtaining a "very detailed" design.

The "very detailed" design was complicated to mesh using the "Solid Map" command in HyperMesh (meshing will be explained in the following sections). Consequently, the "very detailed design" was simplified to the benefit of the meshing section. The difference between the "very detailed" design and the final design can be seen below in Figure *15*.

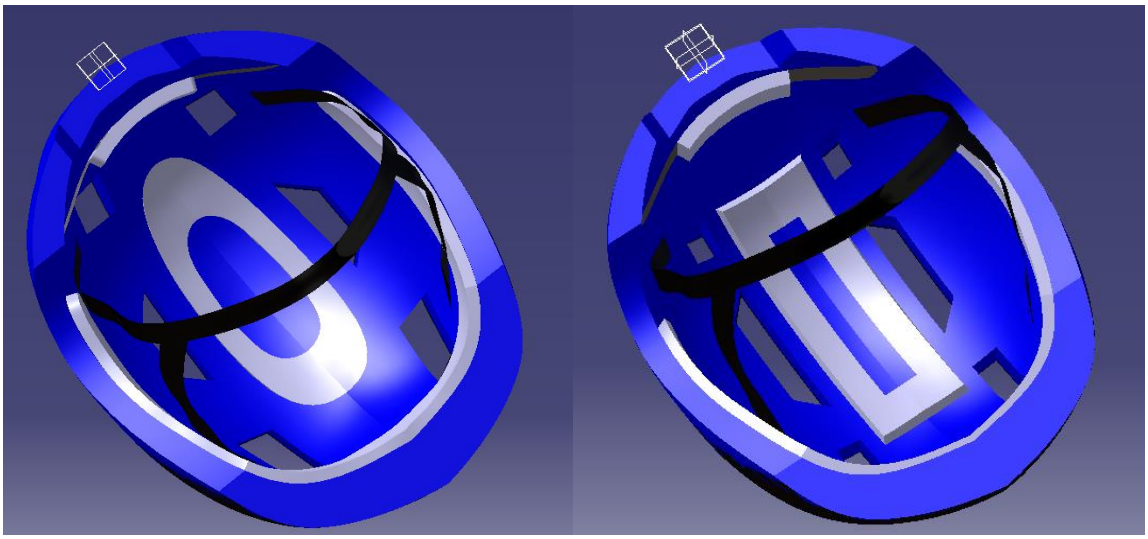

Figure 15: "Very Detailed" Design on Left Picture, "Simplified" and Final Design on Right Picture.

Figure *15* shows that the simplification in the design has been mainly done to the paddings, which now have a more "squared shape". The rounded edges of the "very detailed" design were eliminated to enhance meshing. The geometry of the ventilation holes has also been simplified.

A total of 32 design iterations were made in order to generate the final design that can be seen in Figure *15*. The design of each helmet element is explained in the following sections.

4.2.1.1 EPS Foam Design

In order to generate the EPS Foam a total of 46 commands had to be used in CATIA. The EPS Foam is the "base" of the helmet because the rest of the components of the helmet are attached to it. Hence, this was the first part of the three-dimensional design that was made. This part was mainly generated inside the Generative Shape Design Toolbar.

Using the coordinates that were obtained with the measurement method of *Figure 8* the surfaces were generated as follows: first, four planes at 0º,30º,60º and 90º degrees were generated. Inside those planes a spline was made using the radial coordinate (ϱ) and angular coordinate(θ), as shown in Figure *16*.

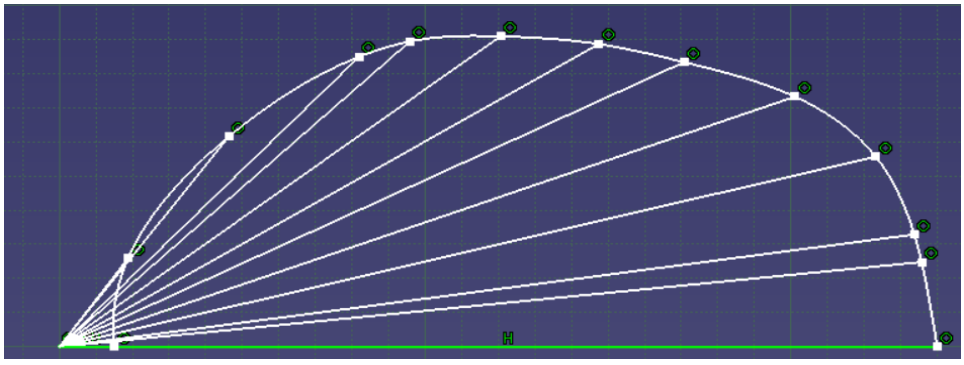

Figure 16: Radial Measurement System inserted into CATIA.

Figure *16* shows an α plane of the exterior surface. Four of these planes were generated for the exterior surface. A surface was then generated, using the four previously generated splines as can be seen in Figure *17*.

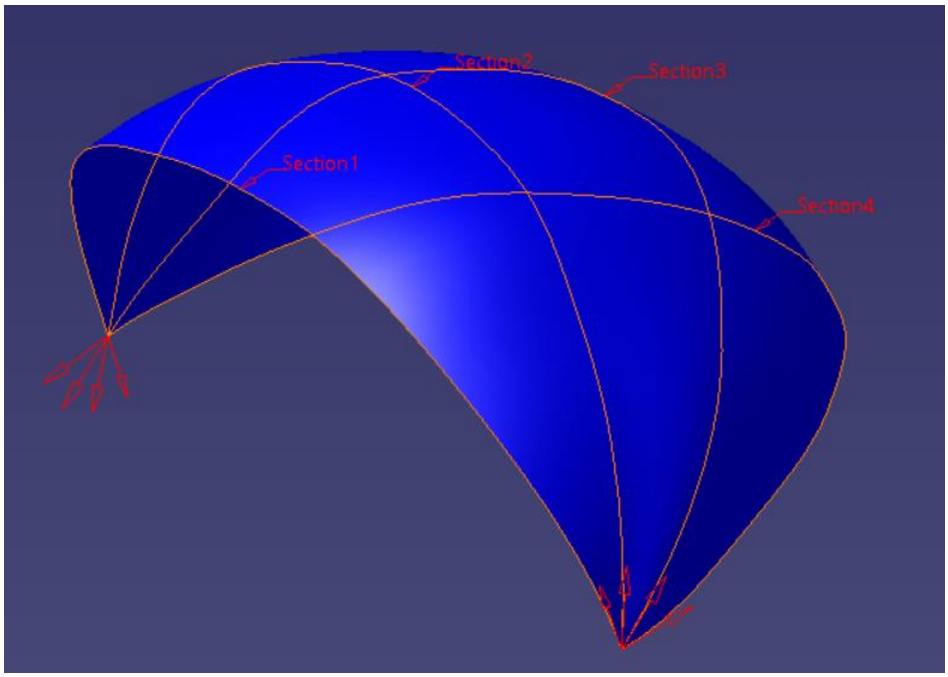

Figure 17: Exterior Surface Generation.

Once the exterior surface in Figure *17* was generated, the same procedure was made for the inner surface of the EPS Liner. Since the EPS Liner has ventilation holes and some other features such as the "space" for the ears (as can be seen in Figure *14*) more sketches had to

be generated to extract such areas. In this thesis, the procedure to extract the ventilation holes will be explained, but the same procedure (with different sketch layouts) was made to generate the rest of the additional features of the EPS Foam.

For the ventilation holes, a sketch with the geometry of the ventilation holes was generated, as can be seen in Figure *18*.

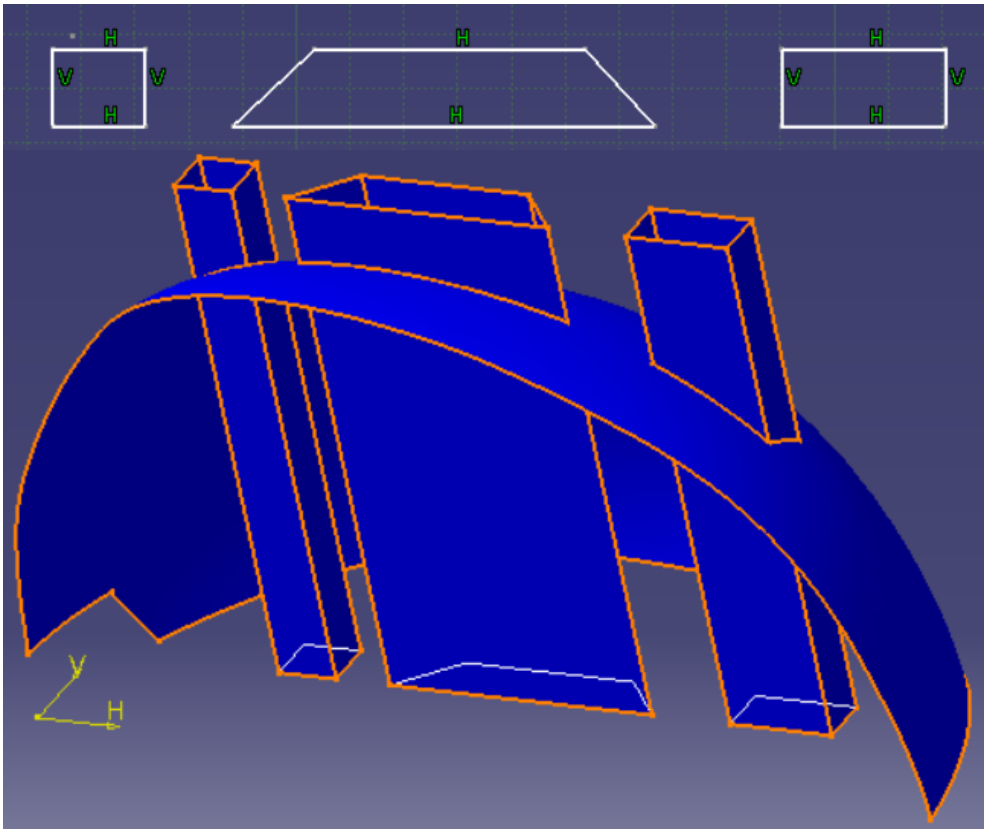

Figure 18: Top picture: a) Sketch for the Generation of the Ventilation Holes.
Bottom picture: b) "Extrude" Command within CATIA.

The Features in Figure *18* a) were then expanded using the "extrude" command, which generated an intersection with the previously generated surface, as shown in Figure *18* b). These intersections were then separated using the "split" command, which generated the ventilation holes as can be seen in Figure *15*. In Figure *18* b) a geometrical feature that was generated using the "extrude" command can also be seen on the rear of the helmet.

The next step in the generation of the EPS Liner was generating symmetrical surfaces to those previously generated (the helmet is symmetrical with respect to the ZX plane as can be seen in *Figure 8*) using the "symmetry" command.

Then, all the surfaces were joined together, firstly using the "healing" command that evens out some roughness that may have been generated between surfaces, and then, the "join" command was used to joint all the surfaces.

All the previously generated surfaces were made with the "generative shape design" command; thus, no solid surface was generated. The design will be meshed in Hypermesh

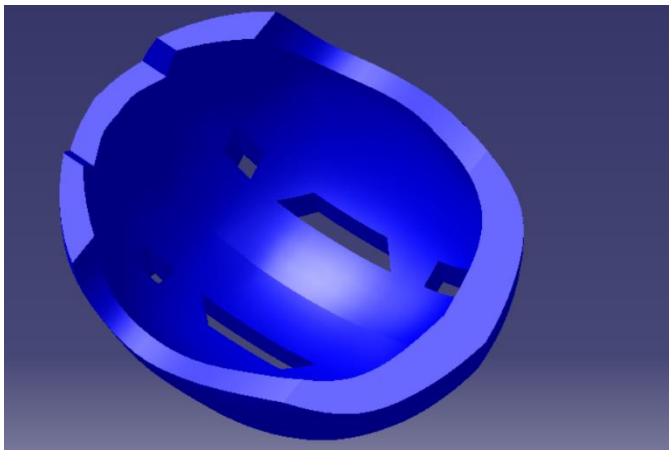

Figure 19: EPS Foam Final Solid Volume Generation.

using 3D solid elements; Therefore, using the "close surface" command in the Mechanical Design (part design) toolbar, the solid volume seen in Figure *19* was generated.

4.2.1.2 Adjusting the FEA Head provided by Dr. Antona-Makoshi

Once the EPS Foam was generated, the head provided by Dr. Antona-Makoshi was adjusted to the rider's position. This adjustment was made by comparing the normal position of the helmet on a real person and then, the same position was given to the three-dimensional head, as can be seen in Figure *20*.

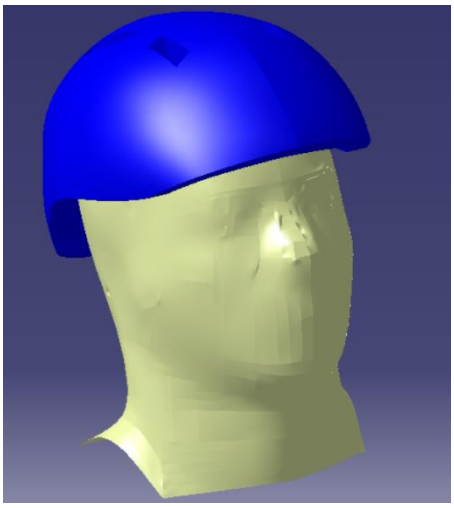

Figure 20: Positioning of FEA Head with respect to the EPS Liner.

The adjustment of the head in CATIA seen in Figure *20* was made inside the Generative Shape Design Toolbar, with the "translate" and "rotate" command, which allowed the head skin surface to be properly fitted to the EPS Foam.

The positioning of the FEA head is needed in order to generate the rear and chin straps.

4.2.1.3 Chin Straps Design

The chin strap avoids the helmet from being detached from the head. In a real-case scenario, the straps are in contact at all points with the Skin. Nevertheless, this way of generating the straps was tested in one of the iterations and it generated many penetration errors in Hypermesh. Therefore, it was decided to generate the straps with a distance of

less than 3mm from the skin. The first step to create them was generating four planes, in the desired locations. These planes will then be intersected with the FEA head using the "intersect" command, which generates four lines, as shown in Figure *21*.

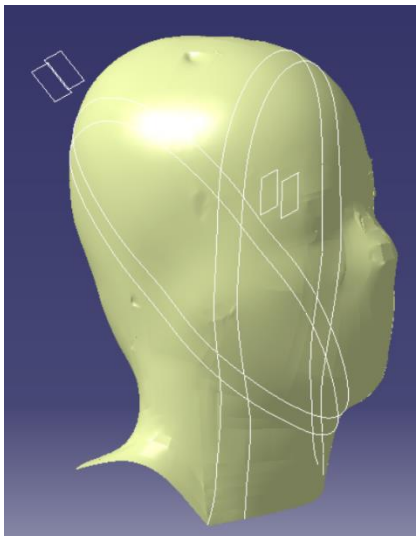

Figure 21: Generating the Chin Straps with Planes and "Intersect" Command.

Figure 21 shows the four planes used and the four generated lines. Using the four lines, a spline was generated inside a sketch with a maximum distance of 3 mm to the head (to avoid penetration in Hypermesh). Afterwards, these four generated splines are enclosed together using three-dimensional Lines. Later, these lines (two for each side of the strap) generated a surface using the "fill" command.

Then, the intersection with the EPS Liner is made using the "split" command, which will generate a surface that touches the surface of the EPS Liner without penetration.

In total, nine surfaces were created using the "fill" command, these were joined together using the "healing" command to even out some roughness that may have been generated between the surfaces, and then using the "join" command was used to join the nine surfaces. The result of all these steps can be seen in Figure *22*.

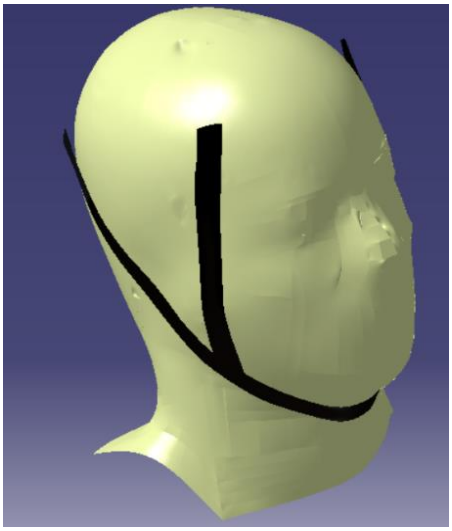

Figure 22: Final Chin Strap Generation.

The straps will be meshed with 2D elements in Hypermesh; therefore, they do not need to be converted into a Solid Element.

4.2.1.4 Rear Straps Design

The design of the rear straps follows the same pattern as previously seen in the chin straps design. The only difference is the number of necessary planes, which now is two, and also the distance to the head which now is a 7 mm maximum. This element will also be meshed with 2D elements in Hypermesh; therefore, it does not need to be converted into a Solid Element.

Figure 23: Rear Strap Final Design.

The distance of this Strap to the head is larger than the chin strap because the rear strap also has a cushion on it (as can be seen in Figure *13*, Figure *14*, and Figure *15*), the greater distance to the head can be seen in Figure *23*.

4.2.1.5 Upper Padding Design

The paddings of the helmet were modelled directly attached to the EPS Foam, from measurements made to the real paddings. They were created in the Generative Shape Design module within CATIA. The measurements were implemented into a sketch with the shape of the padding, as shown in Figure *24* (simplified design).

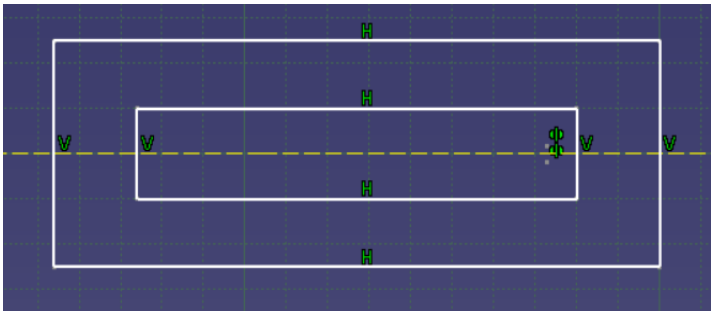

Figure 24: Simplified Design of the Upper Padding.

Afterwards, the inner surface of the EPS Liner was extracted using the "multiple extract" command. Then, the sketch shown in Figure *24* was projected onto the "Multiple Extract" Surface with the "project" command, which generated the shape of Figure *24* with the curvature of the EPS Foam as can be seen in *Figure 25*.

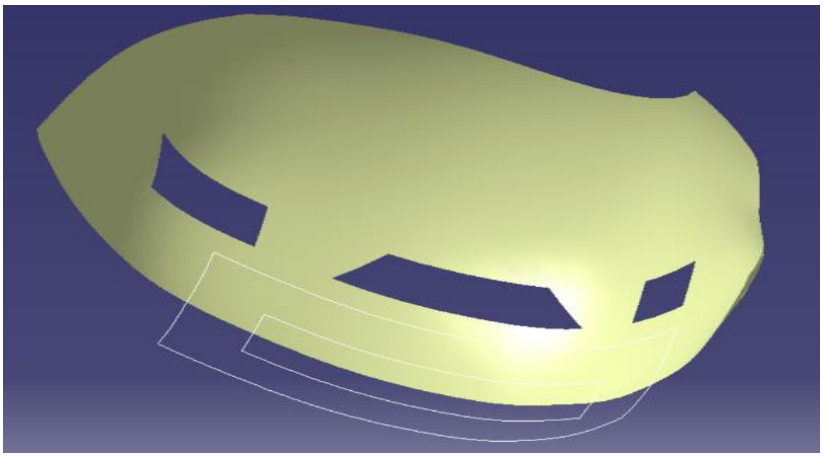

Figure 25: Projection of Cushion Shape into the Curvature of the EPS Liner.

Figure 25 shows the projected cushion shape, which is then converted into a surface by splitting the "Multiple Extract" surface using the "split" command.

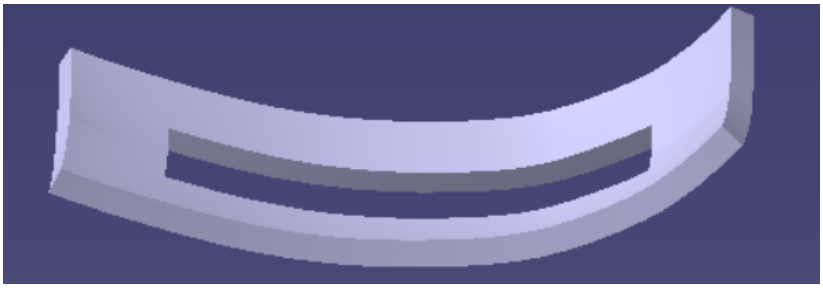

Figure 26: Final Design of Upper Cushion.

Once the Surface is generated, the last step is to convert it into a solid. The solid is created using the "thick surface" command and then adding the thickness of the cushion, the result is shown in Figure *26*.

4.2.1.6 Side Padding Design

The design of the side padding follows the same pattern as previously seen in the upper padding design until the surface of the cushion is created. From there on, the process is different to accommodate the complex shape (the "thick surface" command did not work with this design).

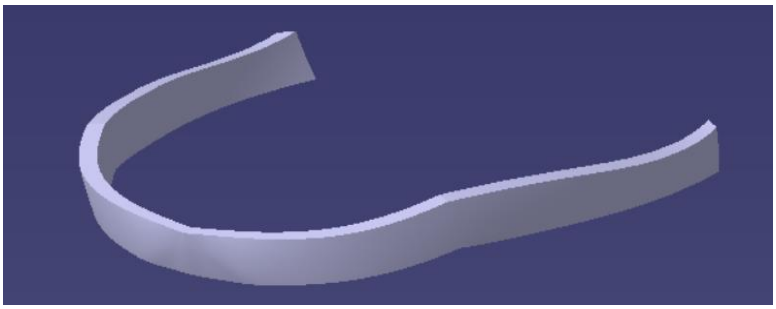

Figure 27: Side Padding Final Design.

Once the Surface of the cushion is generated, an extrusion is generated using the "extrude" command, which creates an unfilled surface, not a solid. Therefore, the last step will be generating the solid using the "close surface" command, which generates the shape shown in Figure *27*.

4.2.1.7 Rear Padding Design

The rear padding design follows the same design structure as the upper padding (same procedures), the only difference is the shape of the padding and the fact that the projection rather than doing it into the EPS Foam is made to the rear strap (previously created). The final design structure of the rear padding can be seen in Figure *28*.

Figure 28: Final Rear Padding Design.

4.2.1.8 Shell Design

The last helmet component to be modelled is the shell, which is directly in contact with the EPS Foam. In order to generate the shell, the following steps were followed:

First of all, the command "multiple extract" within CATIA was used to obtain the outer surface of the helmet. As can be seen in Figure *3*, the shell does not cover the entire outer surface of the Helmet; therefore, a part of the outer surface must be eliminated. To do so, a sketch was generated, this sketch would then be extruded onto the Surface, as can be seen in Figure *29*.

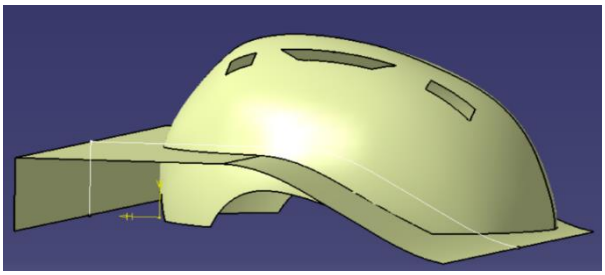

Figure 29: Generation of the Outer Shell.

After extruding the two surfaces, the shell is obtained with the command "split", which generates the outer shell design, as can be seen in Figure *30*. Since this is a surface, it will be modelled with a two-dimensional mesh, and therefore it is not converted to a Solid.

Figure 30: Final Outer Shell Design.

4.2.1.9 Complete Helmet Design and Possibility of Future Adaptations

All the components were designed inside a "Product Feature" within CATIA, which allowed each element to be independent from each other, but it also allowed them to search and retrieve data from the other components.

One of the key aspects of this "Product" structure in CATIA is the adaptability of the helmet design. This allows the helmet design to be easily adapted and redesigned with new coordinates and features (for example varying the thickness of the EPS Foam, the location of the ventilation holes…) with very low input time.

In order to implement these new features and changes only three steps need to be made to the current helmet design:

1. Updating or introducing the new geometrical measurements (e.g. ventilation holes, EPS Foam Thickness, length or width of the helmet, thickness of the straps, number and location of the padded areas…).
2. Reselecting the surfaces that have dependencies in other elements and that have been changed (i.e. if the thickness of the helmet is changed, the outer surface of the helmet needs to be reselected in the elements that are dependent such as the Shell).
3. Updating all the elements in the "Product" Structure (using the "Update All" feature inside CATIA).

This "nimble modification" feature can be implemented in further helmet studies to choose the optimal place and measurements of features such as the ventilation holes and the thickness of the EPS Foam. This can lead to an improvement in the energy absorption capability of the helmet; therefore, increasing bicycle helmet safety.

The helmet design used in the final simulation is shown in Figure *31* below:

Figure 31: Final CAD Design of the Helmet (with head provided by Dr. Antona-Makoshi).

4.3 Helmet Meshing using HyperMesh

4.3.1 Meshing Preview

The program chosen for meshing was Hypermesh (Hypermesh Desktop 13.0). First, the most important commands used are explained in the following section, then the individual meshing of each element will be explained.

4.3.1.1 Meshing 2D Geometries, Automesh Command

The command "automesh" within the 2D toolbar was chosen to mesh two-dimensional elements such as the straps. This command allows the user to choose a surface to mesh and it has multiple options to choose from.

The command that was mostly used for this thesis was the "size and bias" option, which allows the user to choose the size of the elements and the areas were the mesh should include more or less elements to improve dimensioning. It also allows to choose a mesh type (quads, trias, mixed, R-trias and quads only). Since one of the main goals of this mesh was to use quadrilateral elements, the option quads only was chosen, as can be observed in Figure *32*.

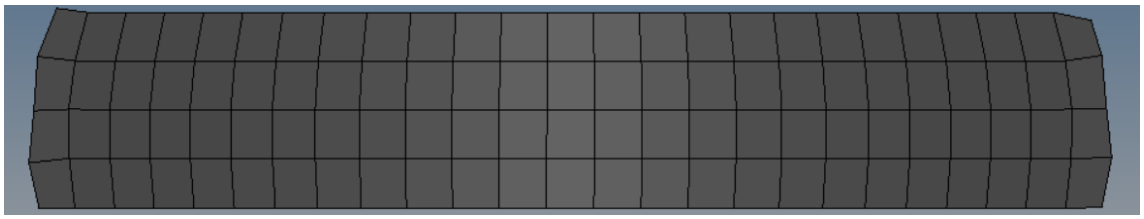

Figure 32: Two-Dimensional Mesh using the "Automesh" Command.

Figure *32* shows the two-dimensional mesh of one of the straps, set to an element size of six, biased equally along the top and bottom lines, using the quads only option.

4.3.1.2 Shrink Wrap Command, Lower 3D Fidelity.

The three-dimensional meshes of the EPS Foam, Paddings, and initial head had a high complexity and some of the commands such as "solid edit" did not work properly without prior adaptations.

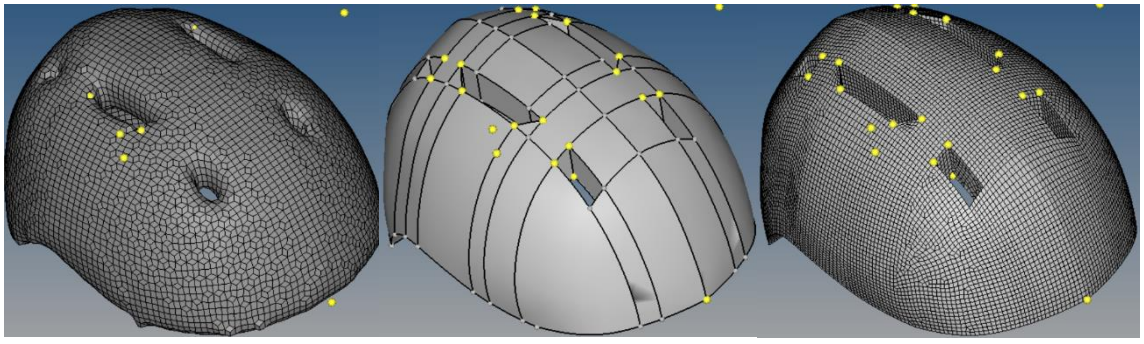

Figure 33: "Shrink Wrap" Command vs a more thorough Meshing (Shrink Wrap on the Left, Ideal Element on the Middle and Thorough Meshing on the Right).

Therefore, one of the initial commands used for the mesh was "shrink wrap" which allowed to create a mesh that simplified the topology and gave a mesh with the required size and element type, as seen in Figure *33*.

Figure *33* shows the difference between shrink wrap and a more thorough way of meshing. On the left, the "shrink wrap" command generates only hexahedral elements, but if compared to the element on the middle it can be appreciated that there is a significant change in some of the areas and the topology of the element. On the right, the more thorough meshing shows that it is closer to the "ideal" element.

Even though "shrink wrap" has a lower fidelity than a more thorough meshing, it is a much faster way of meshing and it can also mesh very hard topology with hexahedral elements. Therefore, this meshing command is used in some initial simulations for example in the initial FEA head, in order to assess if the results that are being obtained are within reasonable parameters.

4.3.1.3 Tetramesh Command

Even though this command was discarded after the initial simulations were made, it is important to mention that it is possible to generate a three-dimensional tetramesh easily in Hypermesh using the "tetramesh" command in the 3D tool bar. Selecting the "volume tetra" option and then the element size.

This generates a mesh within a reasonable time, and it adapts accordingly to the geometry. Even though tetrahedral elements are easier to generate, they take a longer time to converge in the simulation and sometimes they do not converge; therefore, this sort of meshing was discarded after the initial trials were made.

4.3.1.4 Solid Map Command for 3D Hexahedral Meshing

Hexahedral elements are the ideal type for this simulation due to their convergence properties. This can be achieved in three-dimensional elements using the "solid map" command within the 3D toolbar. As previously mentioned, this command needs very simple topology so that each part is mappable, this can be achieved using the "solid edit" command, explained later in this section.

Once the solid is mappable (a mappable solid can be observed in Figure *34*), there are multiple ways of obtaining an hexahedral mesh, the most relevant to this thesis were the "line drag" command and the "one volume" command.

"Line drag" expands a 2D mesh (meshed with the "automesh" command previously explained) along chosen lines, which creates a 3D mesh with the template of a 2D mesh, this command was used in the mainly in the Paddings. The only input needed is the element size desired.

The "one volume" command creates a 3D mesh directly from solids (mappable solids) and the only additional input needed is the element size. Even though this command seems simple, it is very hard to obtain mappable geometry in a complex shape such as the one found in the EPS Foam. Figure *34* shows a Solid Mapping section of the EPS Foam (which has been previously modified with the "solid edit" command to make it mappable).

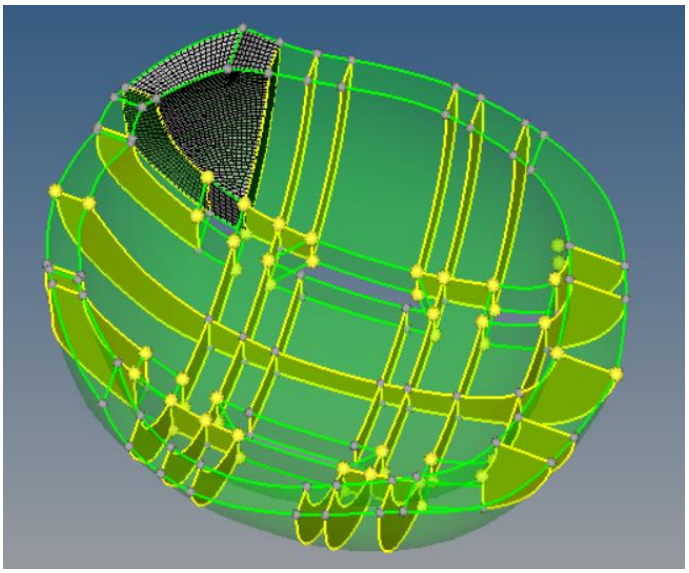

Figure 34: Solid Map Feature.

Figure *34* shows that the "solid map" feature is an effective way of generating hexahedral meshes and it adapts to the exact measurements of the desired geometry. The next step after Figure *34* would be to continue using the "solid map" feature in the rest of the parts of the solid, which would generate the geometry shown in Figure *35*.

4.3.1.5 Nodes Command

In order to implement multiple commands within Hypermesh, it is necessary to use nodes in the structure. There are multiple ways of obtaining the necessary nodes, the one that was used the most for this thesis was "nodes" within the Geometry tab in Hypermesh, then the "nodes on geometry" command was selected, which allowed to select some key points in the structure such as corners, surface separations, surfaces, and lines, as shown in Figure *35*.

Figure *35* shows some of the nodes that were selected within the EPS Foam. These nodes, later on, were used for multiple purposes, the most important one was "slicing" the EPS Foam into different sections for a more precise meshing using the "solid edit" command.

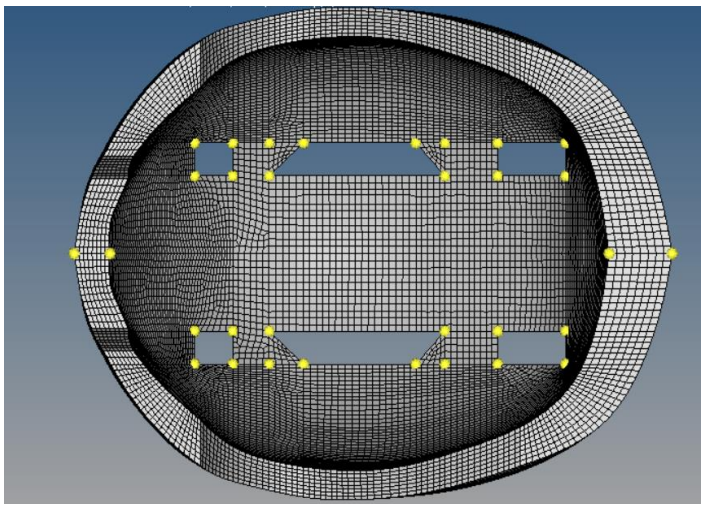

Figure 35: Obtaining Nodes within Hypermesh.

4.3.1.6 Solid Edit Command

When trying to use the “solid map” feature in Hypermesh, the solid must have an easy topology for the program to be able to generate the meshing. Most of the time, while doing the meshing of the EPS Foam, the command “solid map” was generating an error. Therefore, the solution implemented was to simplify the geometry of the EPS Foam.

To do so, the “solid edit” command in the geometry tab was used. This allowed to “slice” the geometry into a more simplified structure. Within this command there are multiple ways of slicing/trimming the EPS Foam. For this thesis the “trim with plane/surface” command was used. This was done by selecting multiple nodes which created a surface.

There were infinite ways of slicing the EPS Foam, multiple of those configurations were tried and there was only one way of slicing the EPS Foam which later gave the right output using the “solid map” feature, as shown in Figure *39*.

4.3.1.7 Edge Find Command

In order to have all the different elements properly connected in the mesh an “equivalence from node to node” is needed. This means that the nodes of all the elements must be connected. This allows for a better distribution of loads in the simulation. Therefore, yielding more accurate results.

In order to do so, the command used is “edge” within the tool menu in Hypermesh. The elements that are to be connected must be selected. Then, a tolerance for the contact is set. This means that the nodes that are closer than that tolerance will be joined together. For example, in Figure *36* a tolerance of 2.5 is set for the EPS Foam and the Padding, which selects the nodes seen in Figure *36*.

Figure *36* shows the nodes that will be connected after the “edge find” command is used, as shown in Figure *37*. In this case, the equivalence is set to happen to the Padding; meaning that the Padding elements will deform and adapt to the EPS Foam. The EPS Foam will keep almost all its nodes intact due to the fact that in the analysis, the most important part is the EPS Foam because it will absorb most of the energy of the impact.

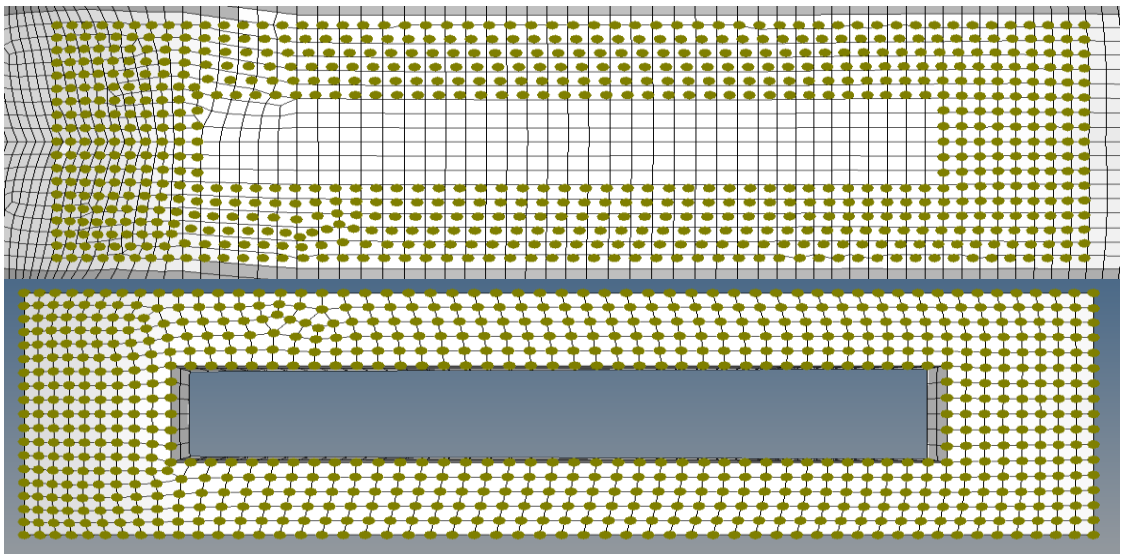

Figure 36: Edge Find tool in EPS Foam and Padding for "Connected" Mesh.

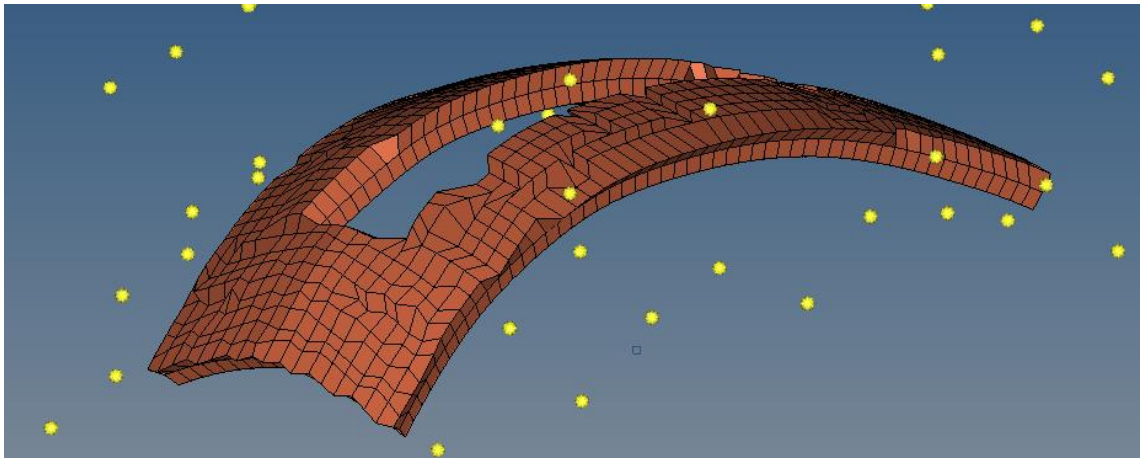

Figure 37: Result of “Edge Find” Command.

Figure *37* shows a deformed mesh in the padding, whose nodes are fully in contact with those found in the helmet, that can be seen in Figure *36*. After this node re-arrangement some penetrations/intersections can happen between the EPS Foam and the Padding; therefore, the command “penetration” found within the tool menu in Hypermesh is used. This command is later explained. The final result of using the “edge” command can be seen in Figure *38*.

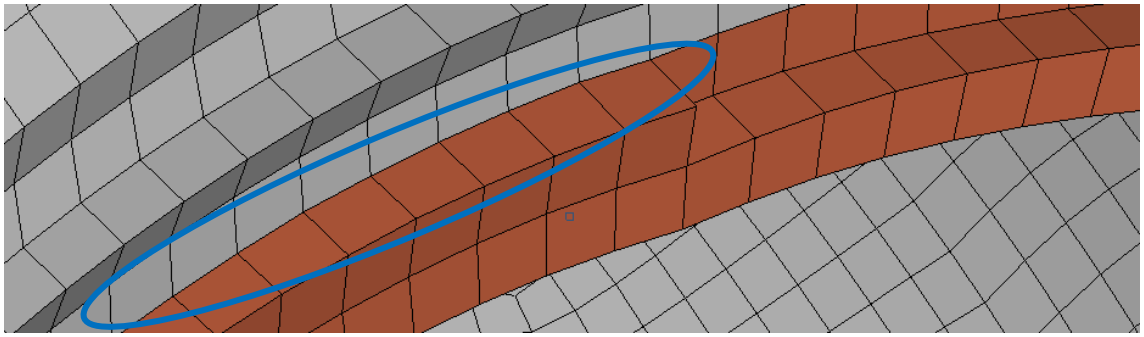

Figure 38: "Edge Command" Results.

Figure *38* shows that the mesh in the EPS Foam and the Padding are completely coincident after using the “edge” command.

4.3.1.8 Offset Command

After meshing the elements of the helmet, the initial penetration and intersections were checked, it was found that some elements had very large number of penetrations, this could not be solved by using the “penetration” command. Therefore, the mesh had to be separated from each other. The most prominent problem was in the Shell-EPS Foam contact, where almost all the elements of the shell penetrated the EPS Foam.

To solve this problem an offset was given to the shell using the “element offset” command in the 2D toolbar; then, selecting “shell offset” command and giving as input the offset measurement. The shell was displaced perpendicular to the previous surface, which eliminated the problem of the mesh intersection.

This offset does not change the output of the LS-DYNA analyses because there is a command in LS-DYNA that is capable of attaching (generating a contact between) two elements that have an offset from each other (explained in following sections).

4.3.1.9 Penetration/Intersection Fix Command

Once all the commands have been used for meshing, there is a final step that must take place in order to ensure that there is no penetration or intersection between mesh elements. The "penetration" command in the tool toolbar allows to check if there are any penetrations between two-dimensional and three-dimensional elements, it is also possible to define a thickness for the two-dimensional elements if none has been given to them yet.

After this tool has been used, Hypermesh shows the number of penetrations/intersections and their depth. Then there are two ways of eliminating them, using the manual fix tools and the automatic penetration/intersection tools. Depending on the difficultness of eliminating those penetrations, the automatic tool may not work, and that is when the manual fix tools are to be used.

4.3.2 Meshing of the Bicycle Helmet

In this section, an explanation of how each element was meshed is given. The only difference between the meshes explained in this section and the mesh used in the final simulation is the element size. The final mesh element layout is detailed in TABLE 9.

4.3.2.1 EPS Foam Meshing

4.3.2.1.1 EPS Foam Initial Mesh trials

The EPS meshing was the most difficult, due to its complicated shape. Many options were tried in order to mesh it correctly; for example, using the "shrink wrap" command and the "tetramesh" command. Nevertheless, these commands did not give the accuracy or the element types that were desired for this thesis. Therefore, it was necessary to use another command that was capable of producing hexahedral meshes and an element size between 1 and 6.

4.3.2.1.2EPS Foam Final Mesh

After many attempts, a way was found to produce a correct meshing in the EPS Foam, this way involved a multiple-step method, using the commands previously explained, as follows:

The first step of the process was obtaining key nodes from the EPS Foam, using the "nodes" command within Hypermesh; then, the EPS Foam was "sliced" into different parts using the "solid edit" command and using the previously obtained nodes to create the planes that would be used to slice it.

Choosing the nodes and the slicing planes to be used took a several iterations, since not all of them generated mappable parts. The final layout used is shown in Figure 39.

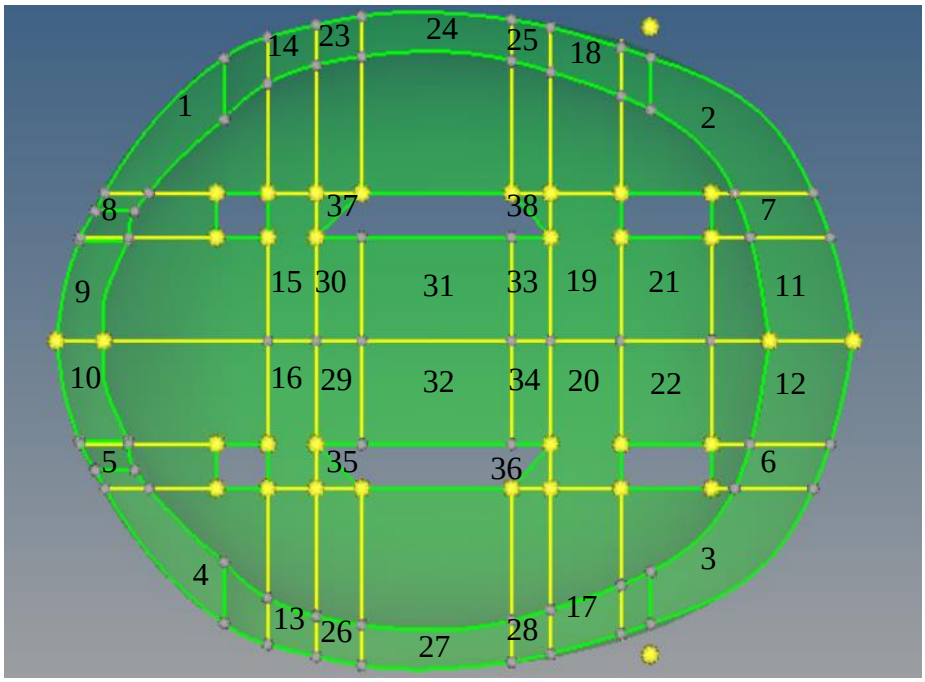

Figure 39: Meshing the EPS Foam.

Figure *39* shows the chosen layout for the slices. After these slices were made, the "solid map" command ("one volume") was used. Then, each part had to be meshed individually.

Depending on the order chosen for the meshing, the mesh could or could not be generated. Therefore, after several iterations a correct order for the meshing was found and is shown in Figure *39*.

The result of this meshing method can be seen in Figure *35*; in this case an element size of 3mm was chosen, generating 84064 hexahedral elements.

4.3.3 Simplified FEA Head

The simplified FEA head was to be meshed with hexahedral elements for convergence purposes. Due to its complicated shape, the "solid map" command (one volume) did not work properly.

A possible option would have been to slice element into simpler parts and then mesh those parts individually (as was done in the EPS Foam). Nevertheless, **this initial trial with the simplified head was only a first approach to ensure that all the contacts, boundary conditions and materials in the initial simulation were correct.**

Therefore, a simplified head geometry was generated with the "shrink wrap" command. This geometry can be observed in Figure *40*, which shows the simplified head used for the initial simulation.

The main change that was introduced between the initial simulations was the element size. The element type used was always hexahedral.

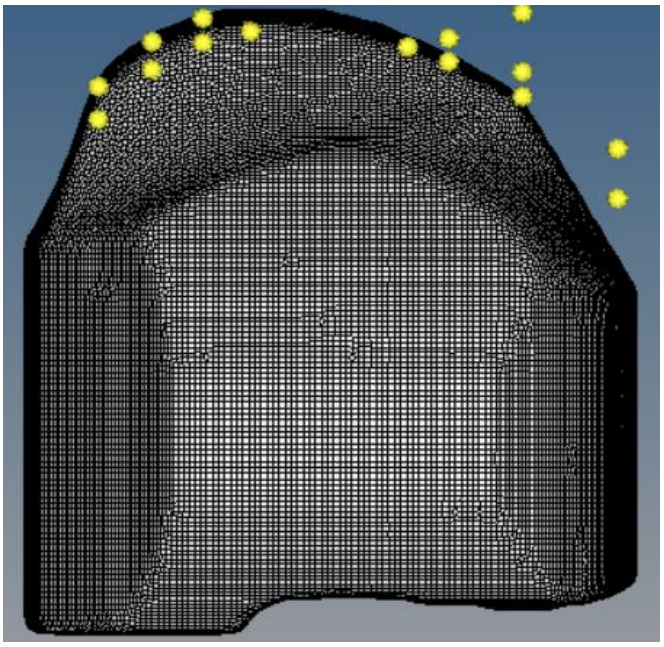

Figure 40: Initial FEA Head using the Shrink Wrap Command.

4.3.3.1 Padding Meshing

In order to mesh the three padding elements of the helmet (upper, side and rear paddings) the same method is used.

First, the external side of the Padding is meshed using the 2D "automesh" command; then it is expanded into a 3D mesh using the "line drag" command that can be found within the "solid map" feature. In order for this command to work the two-dimensional mesh has to be chosen, and then, the lines along which the padding is to be expanded.

After the 3D geometry is created, the "edge" command is used to ensure that the upper and lower padding mesh is coincident with the EPS Foam, and that the rear padding is coincident with the rear strap. An example of these meshes can be seen in Figure *41*.

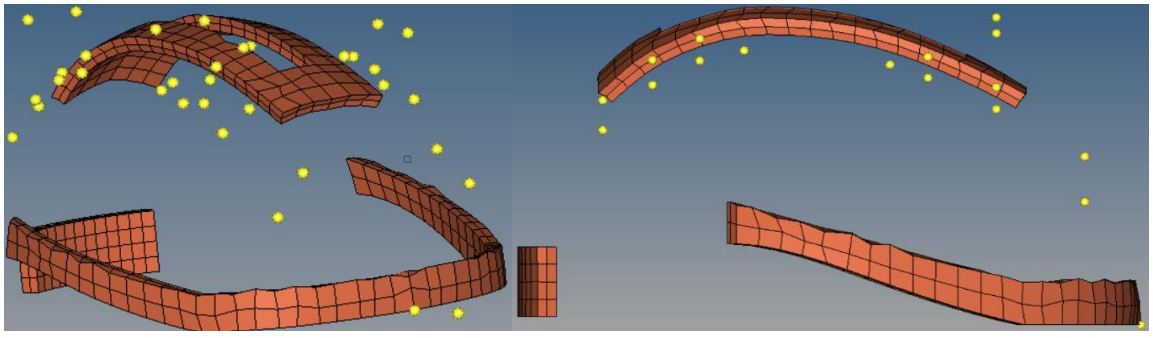

Figure 41: Isometric and Left View of Padding Meshing.

Figure *41* shows the Padding mesh after using the "edge" command. The Padding will be between the EPS Foam/rear strap and the FEA head and will have to sustain large deformations. Therefore, it must be ensured that the element size properly adapts to both elements. This initial mesh has an element size of 6.5mm, which means that the three Paddings have a total of 472 elements. For the final mesh the element size is decreased to increase the accuracy, this is detailed in TABLE *9*.

4.3.3.2 Strap Meshing

The main goal of the straps is to keep the head attached to the helmet, it will not absorb the main energy of the impact; therefore, to save computational time, two-dimensional elements will be used for the straps.

Hypermesh will only generate the mesh shape, the thickness of the straps will be set afterwards in the simulation program (LS-DYNA).

There are two straps in the helmet (rear and chin straps). The rear straps prevent the head from having forward/backwards movement. The chin strap keeps the helmet attached to the head at all times. In this case, the straps were generated using the "automesh" command in the 2D toolbar, using quads. This generated, the layout seen in Figure *42*.

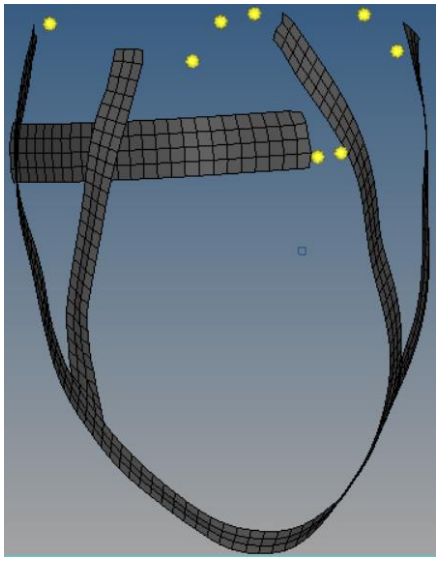

Figure 42: Rear and Chin Strap Meshing.

Figure *42* shows a homogenous 2D mesh. After using automesh, the "edge" command was used to ensure that the end nodes in the straps that are in contact with the EPS Foam are also coincident with the EPS Foam nodes.

Using the "edge" command generates penetration between the two meshes; therefore, the "penetration" command is used afterwards to get rid of the penetrations and intersections.

4.3.3.3 Shell Meshing

The shell will be the point of contact between the EPS Foam and the anvil in the simulation. The real shell has less than 1mm in thickness; consequently, a 2D mesh will be generated for the shell using the "automesh" command, with quadrilateral elements.

The shell will distribute some of the impact stresses throughout the EPS Foam; thus, the meshing needs to be precise. The element size chosen for the initial mesh is 4mm, which generated the mesh shown in Figure *43*.

When the "automesh" command was used, and penetration was checked, all the elements in the shell mesh had penetration with the EPS Foam. Therefore, using the "penetration" command did not solve the problem.

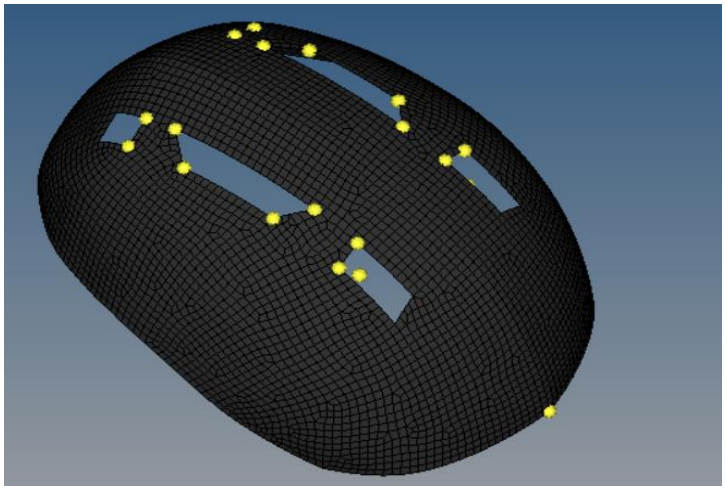

Figure 43: Shell 2D Meshing.

Using the "offset" command, the shell was separated 0.4 mm from the EPS Foam, which avoided all the penetrations and intersections that were previously happening, the result is shown in Figure *43*.

4.3.4 Total Number of Elements and Element Shape

Many meshes were generated to improve the simulations of this thesis; the most important meshes used are for the initial simulation using the simplified FEA head and the final simulation using the validated FEA head, the layout of these two meshes is shown in TABLE *9*. The initial helmet mesh with all the elements from the simulation can be seen in Figure *44*, and the element types an number of elements used can be seen in TABLE *9*.

Figure 44: Mesh used for the Initial Simulation.

TABLE 9: INITIAL AND FINAL MESH CONFIGURATION FOR THE SIMULATIONS.

Element	Type of Geometry/ Element	Number of Elements in Initial Simulation	Number of Nodes in Initial Simulation	Number of Elements in Final Simulation	Number of Nodes in Final Simulation
EPS Foam	Solid/Hexahedral	84064	96875	84064	96875
Straps	Shell/Quadrilateral	548	729	548	729
Shell	Shell/Quadrilateral	4622	4802	4622	4802
Flat Anvil	Solid/Hexahedral	31122	36640	31122	36640
Curbstone Anvil	Solid/Hexahedral	Not Used	Not Used	107300	115544
Padding	Solid/Hexahedral	1312	2307	3559	5994
Initial FEA Head	Solid/Hexahedral	532400	554477	Not Used	Not Used
Final FEA head	Solid Elements	Not Used	Not Used	291948	175404
Final FEA head	Shell Elements	Not Used	Not Used	53609	43355

From TABLE 9, it can be observed that the all the components of the helmet in the initial and final simulations have a total of 90546 and 92793 elements respectively, which is a reasonable number of elements in order to obtain a simulation within a practical Computing Time.

The final simulation has a total of 469472 elements for the flat anvil case and 545650 elements for the curbstone anvil including the FEA head, which means that the helmet accounts for 19.8 % and 17% of the elements used for the simulation. It is a reasonable number due to helmet size and the precision that will be needed in order to determine the amount of energy that is absorbed, while keeping the simulation under a reasonable computing time.

4.4 LS-DYNA Initial Setup

4.4.1 Initial Summary of Approach to Solve Simulation

4.4.1.1 Initial helmet Set-up without FEA head Flat Anvil EN 1078 Test

LS-DYNA was used with a VPN connected to UC3M and a license provided by Dr. Marcos Rodríguez Millán, the program ran on a personal computer, with limited storage and processing power (this is a key part in the solution approach due to the limitations of the computer).

In order to perform such a complex analysis, the approach to understand LS-DYNA and to solve the simulation was increasing the difficultness of the simulation one step at a time. A summary of the steps followed in shown below:

1. The first step was importing the mesh from Hypermesh. Since the thickness of the straps and the shell was not defined in Hypermesh, LS-DYNA did not recognize neither of them in its native format (.k). This led to do a research of the possible importable extensions that could be used in LS-DYNA. It was found that if the straps and shells were exported as NASTRAN Files (.bdf) from Hypermesh, LS-DYNA was able of recognizing the format.
   The solid mesh (hexahedral elements) was directly importable from Hypermesh using the LS-DYNA exporting format (.k). The result of all the imported files in LS-DYNA is shown in Figure *45*.

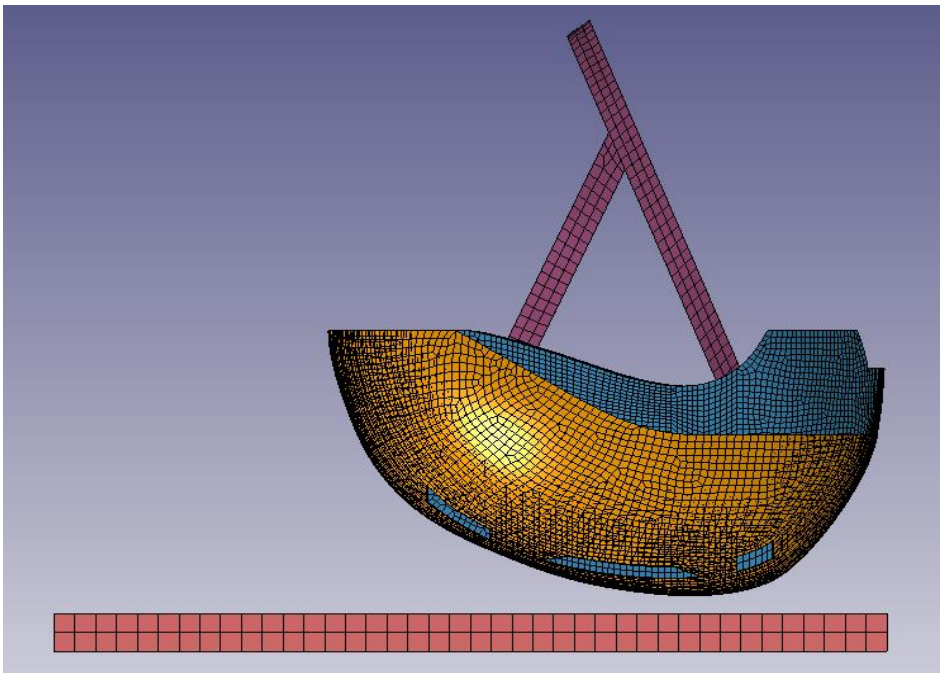

Figure 45: Initial LS-DYNA Files Imported.

2. LS-DYNA, by default, is a unitless FEA solver. This meant that a homogeneous system of units had to be defined. A system of units based on the International SI but more adequate to the type of analysis that was being conducted was used:
   - The units of length were set as mm (equal to 10^{-3}m in the SI) since the analysis was done in a small object; as an example, in some of the meshes the length of the side was 5mm.
   - The units of time were set to ms (equal to 10^{-3}s in the SI) since the analysis was done in an impact that was expected to last a maximum of 20 milliseconds.
   - The units of mass were set to kg (equal to the SI) since the analysis was made to a helmet and a head; for example, the head was expected to weight between 4 and 5 kg, which made this unit of measurement appropriate.
   - From the units previously set, the rest of units could be derived; for example, the Stress was set to GPa, the force to KN, the speed to mm/ms, and the acceleration to mm/(ms)^2.

3. The third step was to perform a basic analysis of the different parts of the designs to assess their validity. In order to reduce the complexity and computation time, the materials were set with very basic properties and basic contact conditions in this initial step. The FEA analysis structure was to start with a small number of elements in the simulation and build complexity on each iteration, as follows:
    - The EPS Foam and the anvil were simulated in a very basic impact which gave some initial results on the acceleration of the helmet.
    - The EPS Foam and the padding were simulated together.
    - The EPS Foam and the padding were simulated together in an impact with the anvil.
    - The EPS Foam and padding were simulated adding the straps to the simulation.
    - The EPS Foam, padding and straps were simulated together in an impact with the anvil.
    - The EPS Foam, padding, and straps were simulated, adding the outer shell to the simulation.
    - The EPS Foam, Padding, straps, and outer shell were simulated in an impact with the anvil, which started to yield more accurate results as shown in Figure *46* where the initial impact sequence is shown.

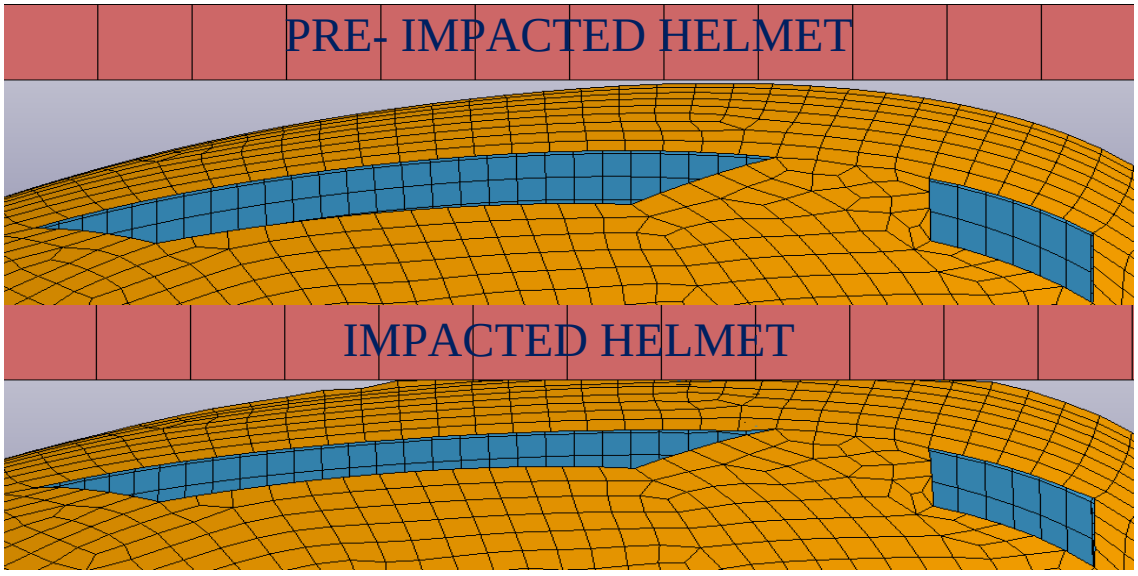

Figure 46: Initial FEA Analysis, Pre-impacted and Impacted helmet.

On each of the previous simulations, multiple adaptations had to be made in order to avoid terminal errors in the simulation. Each of these improvements was made in multiple iterations, were the properties, contacts, and boundary conditions were improved once at a time. Some iterations and its corresponding improvement will be excluded from this explanation in order to keep the thesis within a reasonable length. Nevertheless, the most important and meaningful changes will be explained.

At this stage in the simulation process, a data-check was needed to ensure that the simulation parameters were giving results with reasonable values. To do so, the acceleration of the EPS Foam was measured, as shown in Figure *47*.

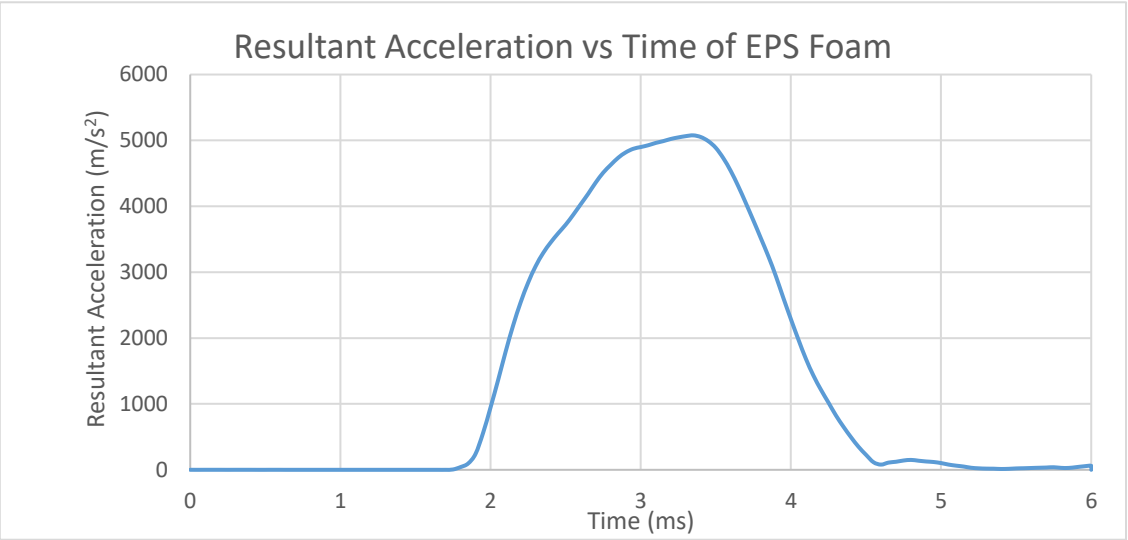

Figure 47: Resultant Rigid Body Acceleration of the EPS Foam.

Therefore, from Figure *47*, it is concluded that the EPS Foam has a maximum acceleration of 5076 m/s and 518g.

Because this was an initial analysis, the contacts and materials are approximations in order to reduce computational time and complexity. The result is within reasonable parameters when compared to the previous studies and acceleration values, as can be seen in Figure *5*.

It is concluded that the initial approach for the simulation is heading in the right direction. The next step for the FEA simulations will be attaching a simplified FEA head to obtain more accurate results.

4.4.1.2 Initial Helmet Set-Up with FEA Head Flat Anvil EN 1078 Test

The FEA head provided by Dr. Antona Makoshi was discarded for the initial analysis because the head has such a depth in detail that the computational time and difficulty for the simulation increased exponentially.

Since this approach to the simulation was only an initial estimation, an extremely simplified FEA head model with simplified material properties as shown in Figure *48* was used to keep building the complexity and fidelity of the analysis.

The simplified FEA head was designed in CATIA using some measurements of the FEA head provided by Dr. Antona Makoshi, other measurements were simplified for the analysis; for example, the neck has been excluded to reduce computational power (by reducing the number of elements).

Afterwards, the head was exported onto Hypermesh, and then using the "shrink wrap" command the mesh was done. In this case the "shrink wrap" command was set as a "tight wrap" and five element sizes of 1, 5, 10, 15 and 20 millimeters were tested. The result of this simulation tests are explained below:

- In the simulations, using the 10, 15 and 20 mm element size for the head produced multiple errors. In this case, the head did not stop when it contacted

the EPS Foam because the element size of the FEA head was much larger than the helmet; therefore, this element size was discarded.

- Using a 1 mm element size, meant that a total of 3978163 elements composed the FEA head and the computational time increased exponentially. A simulation was tested it to see if it increased the fidelity of the results. A time step of 0.01ms took more than 30 minutes to compute. Therefore, it was expected that a 12 ms simulation would last 10 hours. As this was an initial approximation for the simulation this option was discarded due to the computational time required.
- Using a 5mm element size in the simulation produced more accurate results. Therefore, this element size was chosen to perform further analyses.

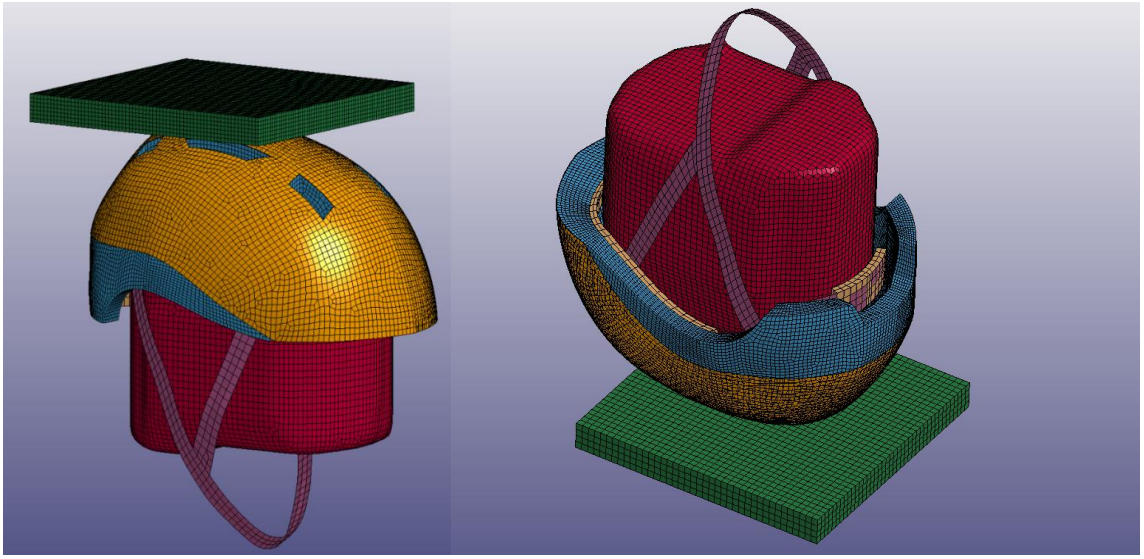

Figure 48: Initial FEA Head Approximation Included in Simulation.

Figure *48* shows the first flat anvil EN 1078 simulation that was made including a FEA head with a 5mm element size. Initial errors were found, which meant that some adjustments had to be made until the right set-up was found.

An error involving the necessary memory to run the simulation was found, also an error involving the volume of the EPS, which at some point reached a negative volume making the simulation stop. Another error regarding penetration happening in the anvil, EPS Foam, and the padding was found, as shown in Figure *50* halfway through the simulation (approximately at 5ms), this was the most prominent error.

Multiple solutions were implemented in order to solve the initial penetration and negative volume issues. The one that had the biggest impact was refining the helmet material properties, contacts, and meshing the anvil with a smaller element size.

Refining material properties for this simulation yielded more accurate results, but it still did not include the complexity of the materials implemented in the final simulation.

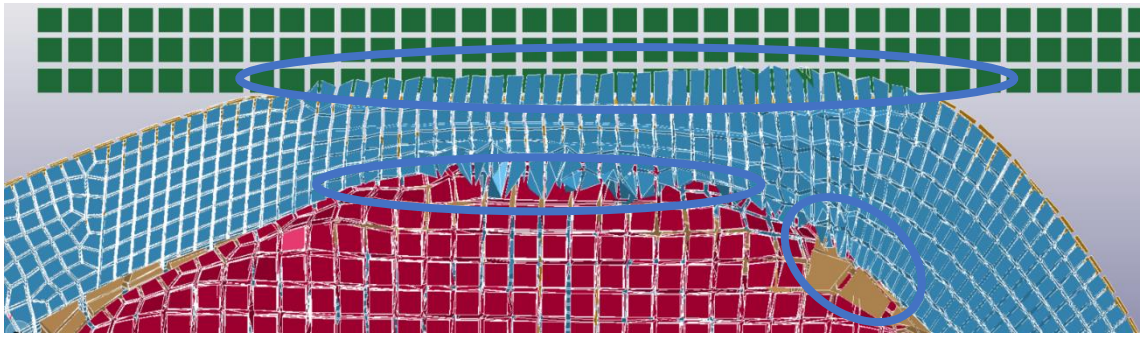

Figure 50: Penetration Issues in Initial FEA Analyses (EPS Foam, Padding and Anvil Penetration).

Figure 50 shows penetration, the biggest issue in the initial analyses. Nevertheless, the rest of the simulation seemed to yield correct results. Therefore, an initial comparison between the acceleration of the FEA head and other studies was made. The results are shown in Figure 49 and Figure 5.

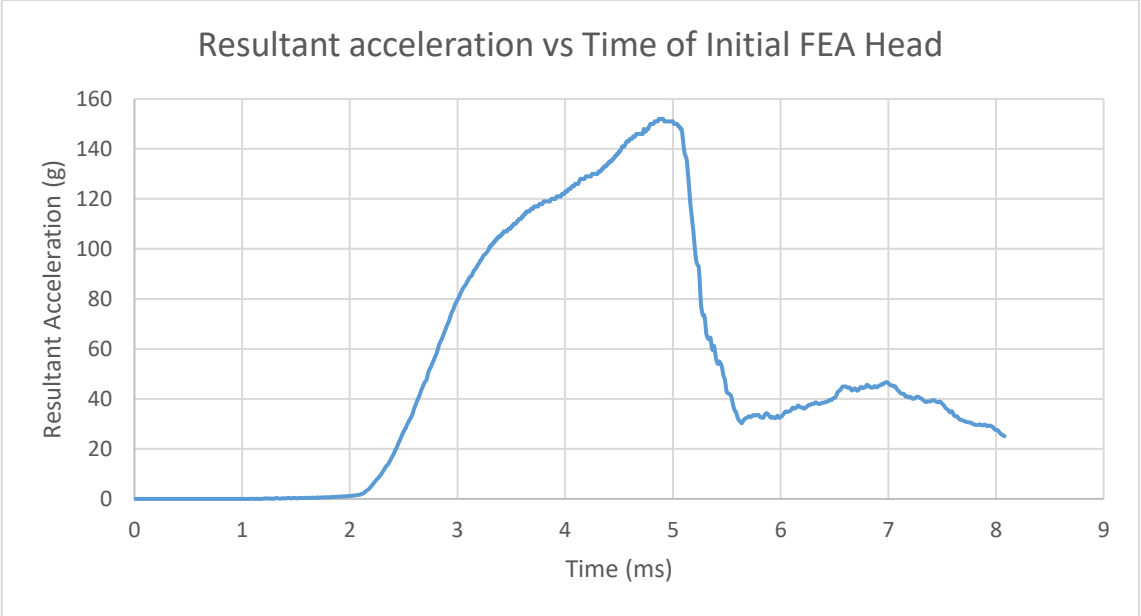

Figure 49: Initial FEA analysis Rigid Body Acceleration (measured in g).

The graph in Figure *49* shows that the initial FEA head has a maximum acceleration of 152 g. Figure 5 is from a FEA study made to a FEA head with a helmet by G Milne et al. [23]. This study shows that the maximum acceleration achieved is 170 g.

It can be concluded that the simulation is heading in the right direction because both results are within the same order of magnitude. The initial increasing "slope" matches on both studies (until the maximum g acceleration is reached). Nevertheless, it does not match on the "downwards side".

The mismatch was expected because at this point is when penetration error seen in Figure *50* starts to happen (penetration happens in the anvil, EPS foam and padding). Therefore, in further analyses the issue of penetration needs to be solved.

Reasons for penetration to happen are contact properties, material properties and mesh element size. Multiple solutions for these problems will be tested in later analyses.

4.4.1.3 Computational Time and Storage Check

At this stage in the process, the simulation was increasing in computational time and storage needed due to the complexity of the analysis. These issues are influenced by the output timing in the database (BINARY_D3PLOT).

In order to perform a comparison analysis changing the BINARY_D3PLOT output, three restrictive limitations were set to the analysis:

- A maximum computational time of 1 hour.
- A maximum simulation time of 7.3ms.
- A maximum memory storage of 35 Gb.

Three output timings were tested: 0.25, 0.01 and 0.005ms respectively. The result of the analysis is shown in Figure *51* below.

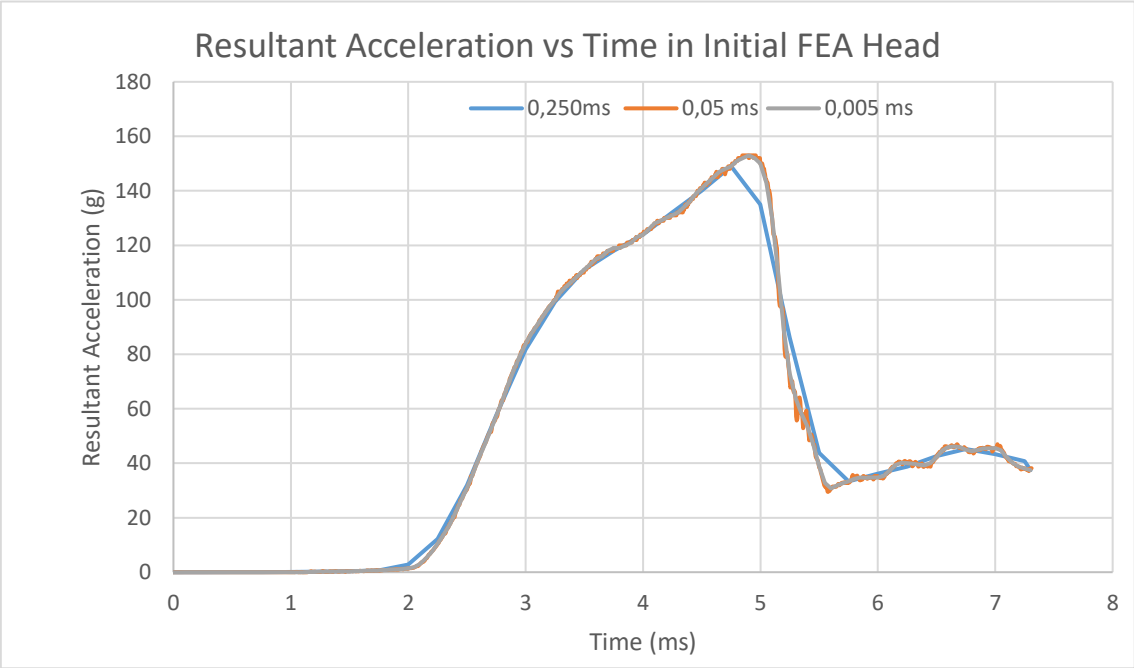

Figure 51: Initial Analysis, Computational Time Check (0.25ms, 0.050ms and.0.005ms output).

From Figure *51* it is observed that when the output time is reduced the data obtained is more precise. Overall, all the graphs have the same layout and could be considered to yield close results.

Nevertheless, an improvement is seen when the output time is 0.05 ms or less; for example, the maximum acceleration for 0.005 and 0.05 ms is 153 g, meanwhile, for the 0.25ms it is 149g. This is a noticeable difference and should be considered.

The comparison between the computational time, storage and fidelity of the results is shown in TABLE *10* below.

TABLE 10: COMPARISON IN COMPUTATIONAL TIME, SIMULATION TIME AND STORAGE WHEN THE BINARY_D3PLOT OUTPUT CHANGES.

Analysis/ Data Output	Computational Time (minutes : seconds)	Max. Simulation Time (ms)	Storage Usage (GB)	Data Points
0.005ms	19:01	7.3	29.1	1463
0.050ms	25:07	7.3	3.18	148
0.250ms	21:32	7.3	0.578	31

Using an output of 0.25ms is discarded due to Figure *51* as the results have a lower fidelity when compared to more accurate results.

From TABLE *10* it is seen that in computational time the 0.05 and 0.005ms options is close and the number of data points for both options is acceptable. Nevertheless, it is observed that the space needed to store the 0.005ms simulation is 9.3 times more than the 0.05ms simulation.

It is concluded that the BINARY_D3PLOT has to be set in a value close to 0.05ms to yield correct results and at the same time reduce the storage space needed.

4.4.1.4 Solving Initial Penetration

In the initial simulation penetration occurs at three important spots: the contact anvil-EPS-Foam, EPS-Foam-head and head-padding as it can be seen in Figure *50*. In order to solve this issue multiple configurations and modifications in the simulation were tested.

4.4.1.4.1 Anvil-Eps Foam Penetration Solving

For this iteration, the simulation was made without the padding, it will be included in later simulations. The exclusion of the Padding in this simulation is to reduce the level of complexity which allows for a faster recognition of the elements that are failing within the simulation.

Solving the penetration on the Anvil was mainly done including new contacts and adjusting the existing contact parameters in the simulation. The most important contacts that have relevance when avoiding penetration are shown in TABLE *11* and the improvement can be physically seen in Figure *52*.

TABLE 11: CONTACT SET-UP IMPROVEMENT.

LS-DYNA Contact Type	Part 1 in Contact	Part 2 in Contact	Dynamic/Static Friction Coefficient
AUTOMATIC_SURFACE_TO_SURFACE	Shell	Anvil	0.2/0.1
AUTOMATIC_SURFACE_TO_SURFACE	Head	Padding	0.2/0.1
AUTOMATIC_SURFACE_TO_SURFACE	EPS-Foam	Head	0.2/0.1
AUTOMATIC_SURFACE_TO_SURFACE	EPS-Foam	Anvil	0.2/0.1
TIED_SHELL_EDGE_TO_SURFACE_OFFSET	Shell	EPS-Foam	TIED

The result of this new contact set up provides the output shown in Figure *52*.

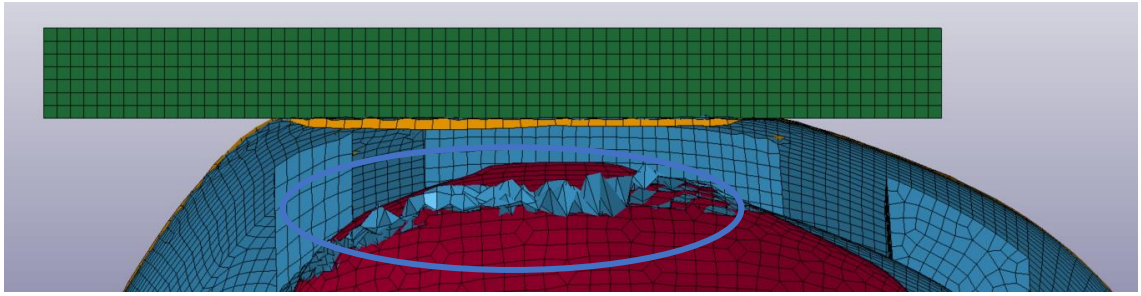

Figure 52: Solving Initial Penetration in Anvil, there is still Penetration in the Head-EPS Foam Contact.

Figure *52* shows that the anvil is no longer penetrated by the EPS Foam, due to the new contact set-up. This provides a slight change in the results regarding acceleration in the head; now, the maximum acceleration happens 0.1ms before than the acceleration in the previous study which is shown in Figure *51*.

4.4.1.4.2EPS Foam-Head Penetration Solving

For this iteration, the simulation was made without the padding, which will be included in later simulations. The exclusion of the padding in this simulation is to reduce the level of complexity which allows for a faster recognition of the elements that are failing.

In order to solve the EPS Foam-head penetration issue many possibilities were tested. From the dynamic view of the simulation it was concluded that at 4.9ms the mesh element size in the head was too large, and it penetrated the EPS-Foam because the AUTOMATIC_SURFACE_TO_SURFACE contact was not recognizing the surfaces in contact as some nodes could penetrate each other's surface.

This disparity in element size led to a change the element size of the mesh. The best results were obtained when the head was re-meshed with smaller elements. This

remeshing was done in Hypermesh, using the "shrink wrap" command. This time, the element size was set to 2mm.

Since the command to generate the mesh was "shrink wrap", the element size varies slightly depending on the position where it is located. This mesh had a maximum element size length of 3.44mm and a minimum size of 0.21mm. The result on penetration of this change in the mesh can be observed in Figure *53*.

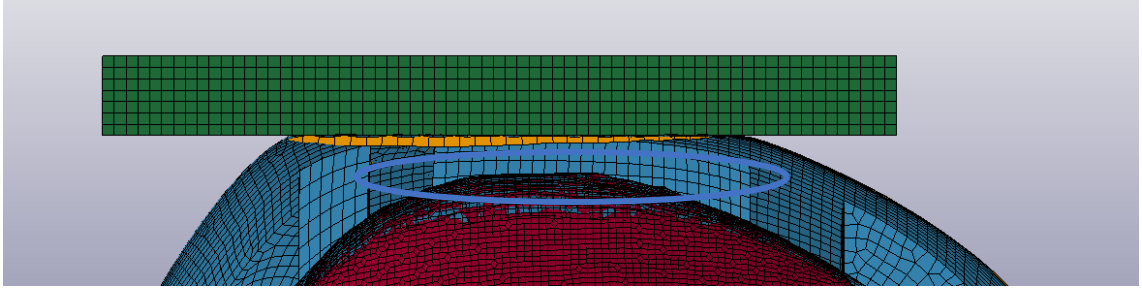

Figure 53: Solving Initial Penetration in the Head-EPS Foam Interface.

Figure *53* clearly shows that the penetration issue is solved by producing a finer mesh in the head, which allows the AUTOMATIC_SURFACE_TO_SURFACE to recognize both surfaces (and all the nodes). Consequently, the EPS Foam - head penetration issue was solved.

The penetration was causing several problems in the maximum acceleration output on previous LS-DYNA Analyses. As it can be seen in Figure *49* and Figure *51*, when the head started to penetrate the EPS-Anvil (approx. at 5ms) the EPS Foam was not opposing the movement of the head. Therefore, when the penetration started the velocity of the head was not lowered, which in the Figure *49* and Figure *51* graphics caused the acceleration to suddenly drop, yielding incorrect acceleration results.

By solving the head penetration, the newly generated acceleration graphic yields results that are closer to the previous studies, as seen in Figure *54*.

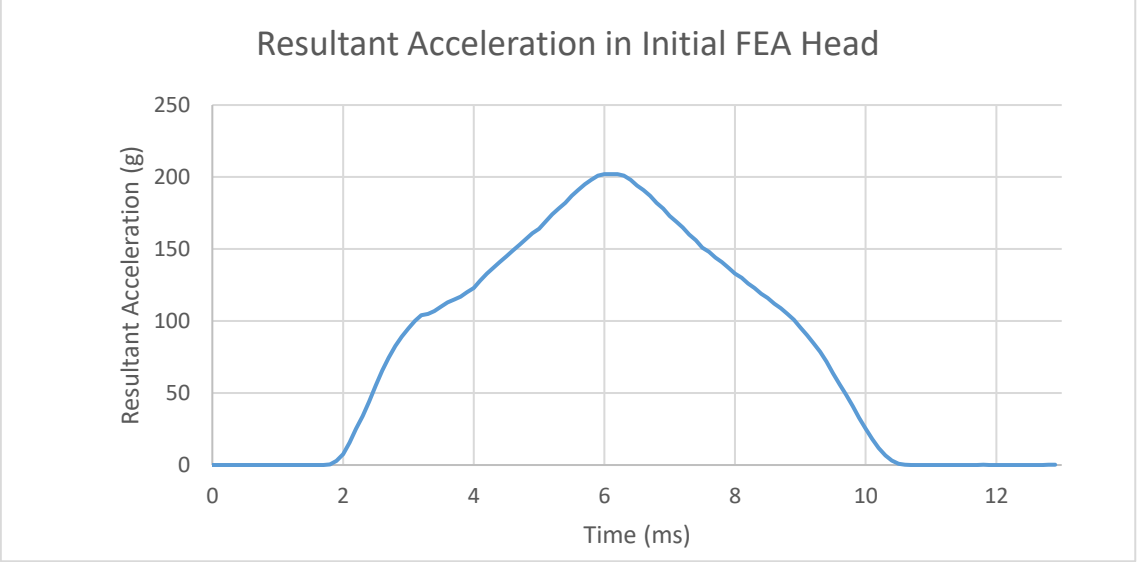

Figure 54: Improved FEA Acceleration Measurement.

Figure *54* shows a great variation with respect to Figure *49* and Figure *51*. The maximum head acceleration increases from 153 g to 202 g. This variation is due to the fact that the EPS Foam is capable of "stopping the head acceleration" for a longer period. Now, the maximum acceleration happens at 6.1ms (4.35 ms if measurement starts when the head has contact with the EPS-Foam).

The simulation impact time has also increased up to 10.5ms (8.75ms if measurement starts when the head has contact with the EPS-Foam). This correlates better with the previous studies that have been analyzed in this thesis.

4.4.1.4.3 Padding-Head Penetration Solving

For this simulation iteration the padding was included. In order to solve the padding-head penetration many changes were tested, the ones that yielded the best results were improving element size and the material properties of the padding.

The padding was re-meshed with 3 mm elements. This set-up was tested, and it prevented the penetration for a longer time than the previous set-up. Nevertheless, penetration still occurred, and further refinement was needed.

A further improvement was made using the "edge" command between the EPS Foam and the padding which made the meshes of these two elements be coincident. This simulation also prevented the penetration for a longer time than the previous ones. Nevertheless, penetration was still happening.

The next important change was using more refined material properties for the Padding. It was concluded, after examination of the dynamic results of the previous simulations that the padding kept deforming indefinitely.

Therefore, the padding properties were improved, the most important improvement was defining a maximum deformation, which would mean that once that maximum deformation is reached, the volume of the padding would not change and would remain the same until the pressure stopped.

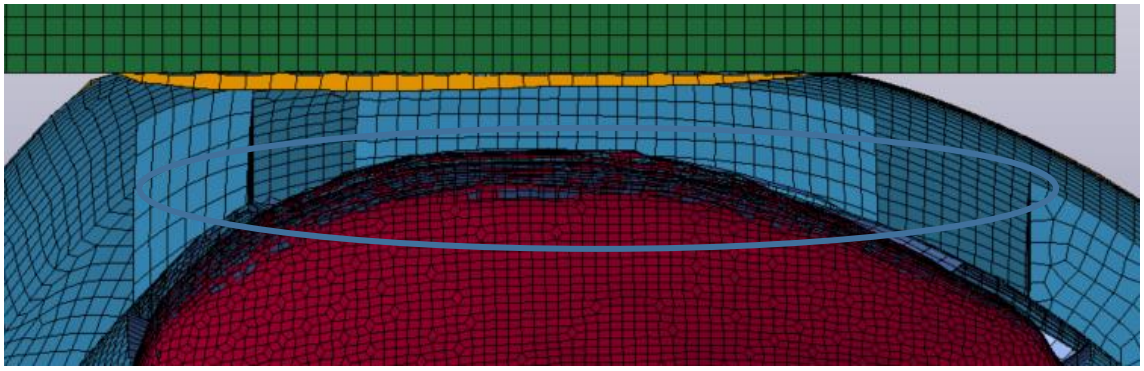

Figure 55: Solving the Penetration between the Padding and the FEA Head in the Initial Analysis.

This improvement joined together with a more refined mesh and using the "edge" command prevented the penetration of the padding into the head, as shown in Figure *55*.

In this figure it can also be appreciated that the penetration issues between the EPS Foam-Anvil and FEA Head-EPS Foam are not happening either.

This simulation also yielded small changes in the acceleration compared to the one that has no Paddings, seen in Figure *54*. The paddings are expected to give a small change in the maximum g acceleration because they will "adapt" to the head and will make the initial impact contact smoother and will absorb a certain percentage of energy. The results of adding the paddings to the simulation can be seen in Figure *56* where the EN 1078 impact test at 5.42 m/s in a flat anvil is tested.

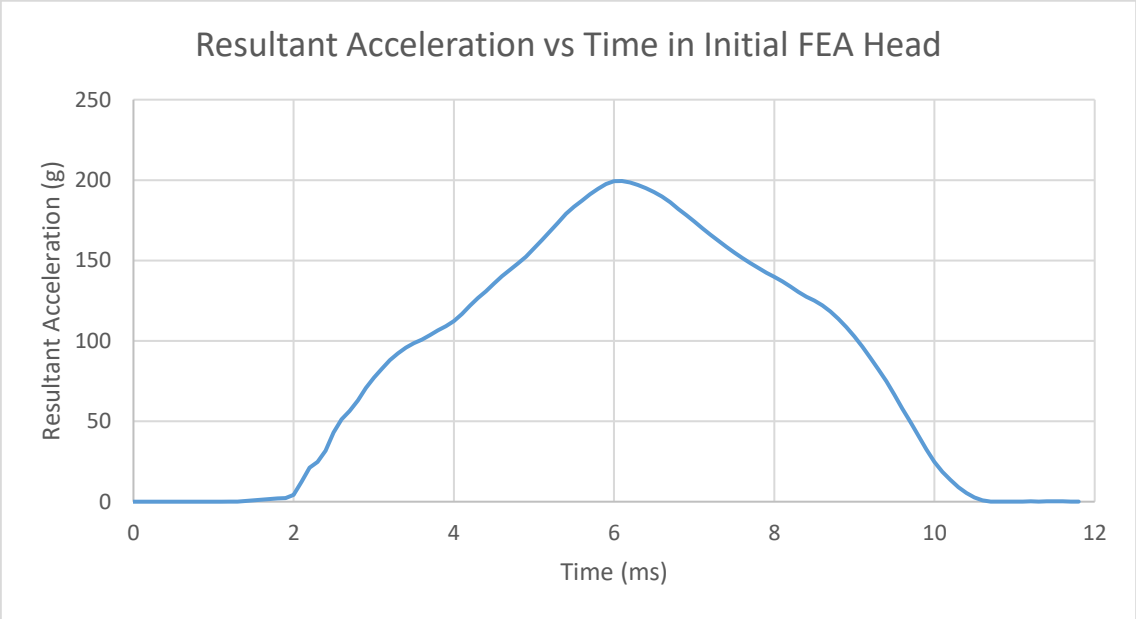

Figure 56: Initial Simulation, with the Final Acceleration Results.

Figure 56 shows that adding the paddings to the simulation introduces a change in the maximum g acceleration of the head, in this case the acceleration is reduced 3 g with respect to the previous simulation, as expected due to the "cushioning" effect of the Padding.

The duration of the simulation is the same, and the maximum g acceleration happens at the same timeframe (6.1 ms). The unloading curve is the same for both simulations. Nevertheless, the loading curve introduces some changes, as expected due to the "cushioning effects" of the padding; for example, at 3ms the previous simulation had a 90 g acceleration, the latest simulation has 75 g.

4.4.1.5 Additional Analyses with Initial FEA Head to ensure Adaptability

In order to ensure that the previous simulation is adaptable to more scenarios and impact types, and before the validated FEA head is used, two additional simulations with different anvils and impact positions were tested. These simulations take approximately three-and-a-half hours to compute. The detailed FEA Head provided by Dr. Antona-Makoshi will increase computing time exponentially and therefore shall only be used in the final simulations once everything prior has been tested and proven correct.

The previous simulation was done in a flat anvil, the following ones will be done in a curbstone anvil (according to EN 1078 specifications). The impact speed will be 4.57 m/s, and the maximum acceleration needs to be lower than 250 g so that the helmet complies with the EN 1078 specifications. The curbstone anvil has a "triangular" shape, which will lead all the stresses and deformation to be concentrated over a very small area.

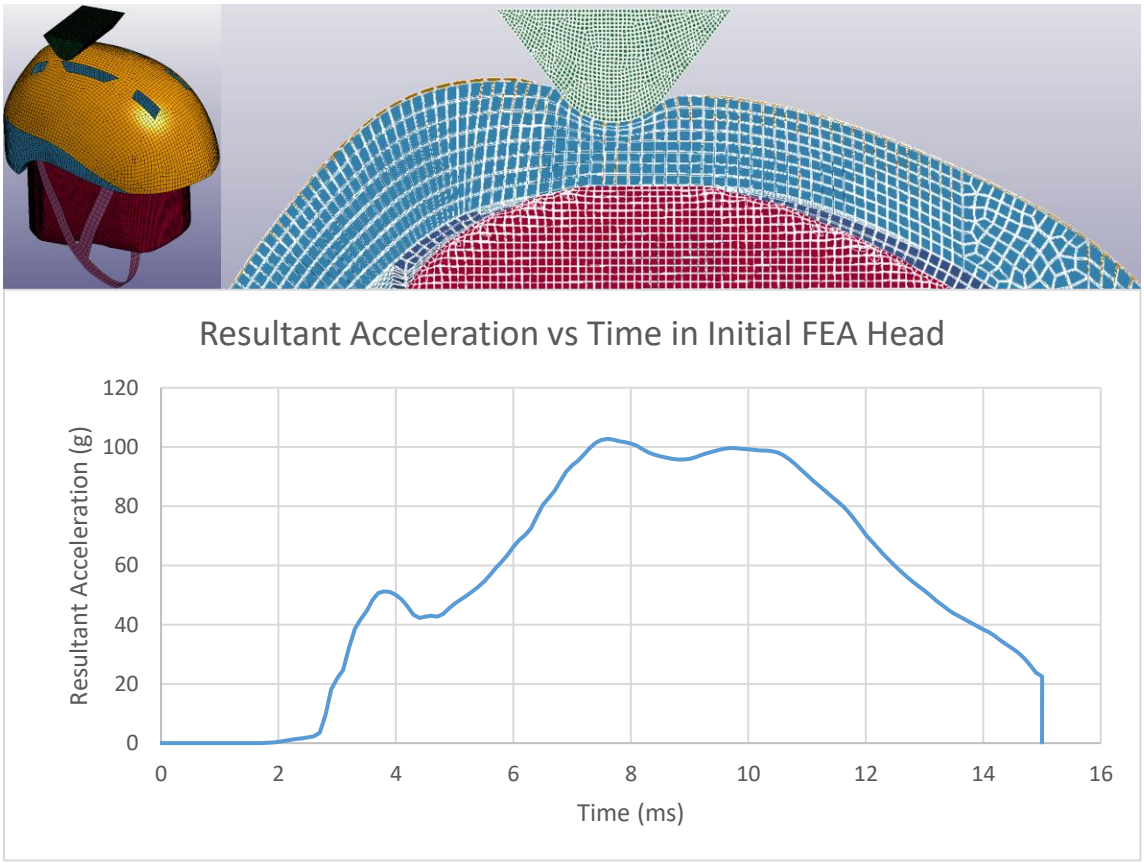

Figure 57: Curbstone Anvil Location and Acceleration Results.

The first additional simulation is made locating the anvil on the rear of the helmet, sideways, as shown in Figure *57*. This simulation had a time limit of 15ms, later it was seen that the simulation would have needed additional time to completely reach zero g acceleration in the unloading curve, it also took 3 hours and 38 minutes to compute.

In Figure *57* it can be observed that now the impact duration time has increased to more than 14ms, this is to be expected because now all the deformations in the helmet are located in the same area. Therefore, this area will deform more and longer time period than the previous simulations; thus, increasing impact time.

On the other hand, since the helmet deforms longer and for a longer time and the impact speed is lower, the head suffers less "g acceleration". Now, the maximum acceleration is 102.7 g, but it sustains that maximum acceleration for a longer time. Even though the maximum "g" acceleration is lower, the increased impact time can also lead to multiple Head Injuries due to the sustained acceleration. Once the head by Dr. Antona-Makoshi is implemented in this same test, the risk of this sustained g acceleration will be assessed.

The next test is also done on a curbstone anvil, but now the Anvil is rotated 90º from the previous simulation and has been given an offset from the center of the helmet, as can be seen in Figure 58. This simulation took four hours and two minutes to compute.

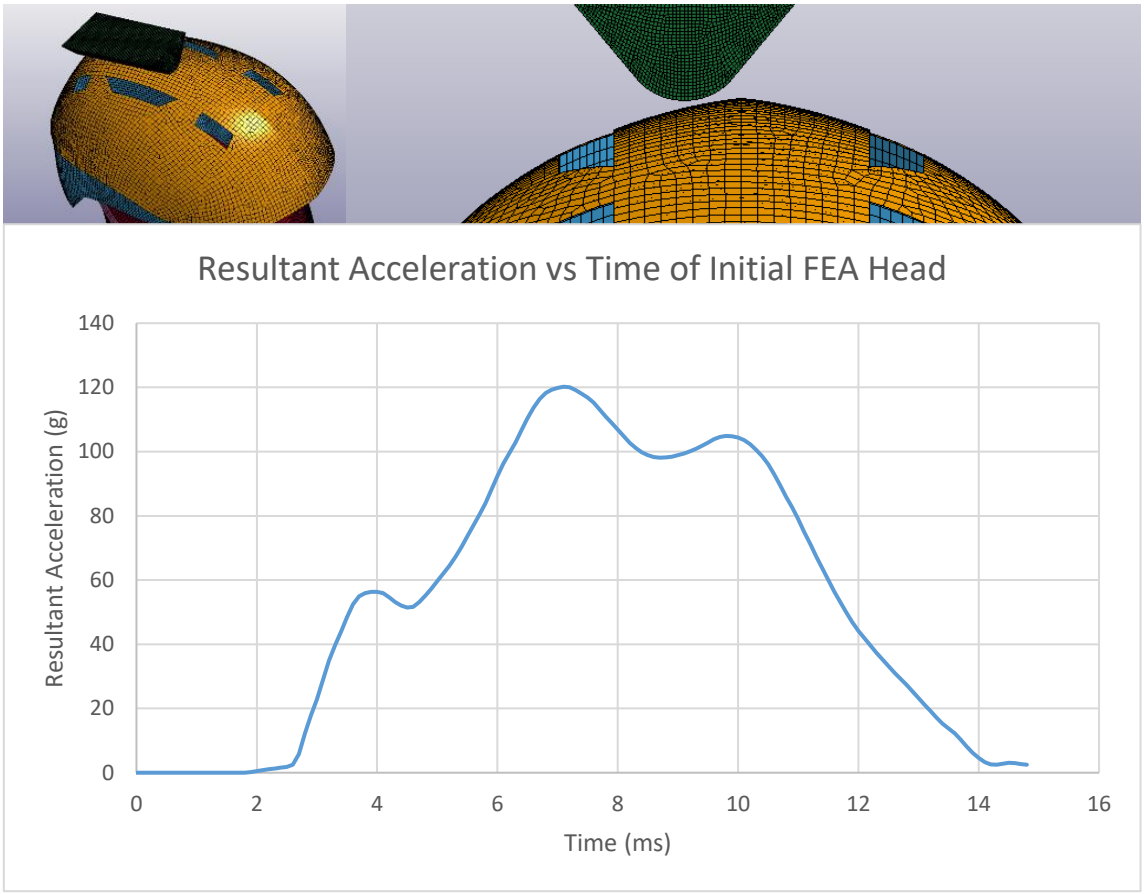

Figure 58: Curbstone Anvil Impact Position Number 2.

Figure 58 shows that the impact duration is 11.5ms approximately (3.5 ms more than the flat anvil simulation). As in the first curbstone impact, this impact also has a low "g acceleration" but sustains it for a longer time. The maximum acceleration is 120 g.

It is observed that the maximum acceleration of the FEA Head depends on the position of the anvil since there is a 16.8% difference in the maximum head acceleration between this and the previous simulation. When the head by Dr. Antona-Makoshi is tested with the same test, the risk of this sustained g acceleration will be assessed.

4.4.2 Validation of the Initial Helmet Set-up

In order to validate the results of the initial simulation, a comparison is made against the results of previous studies. This comparison will show whether the results that are being obtained are correct.

The most widely tested and simulated case from the previously mentioned studies is the EN 1078 test against a flat anvil, which is shown in Figure *56* for this study. Therefore, a comparison between this result and the other studies used for validation purposes is shown in Figure 59 below.

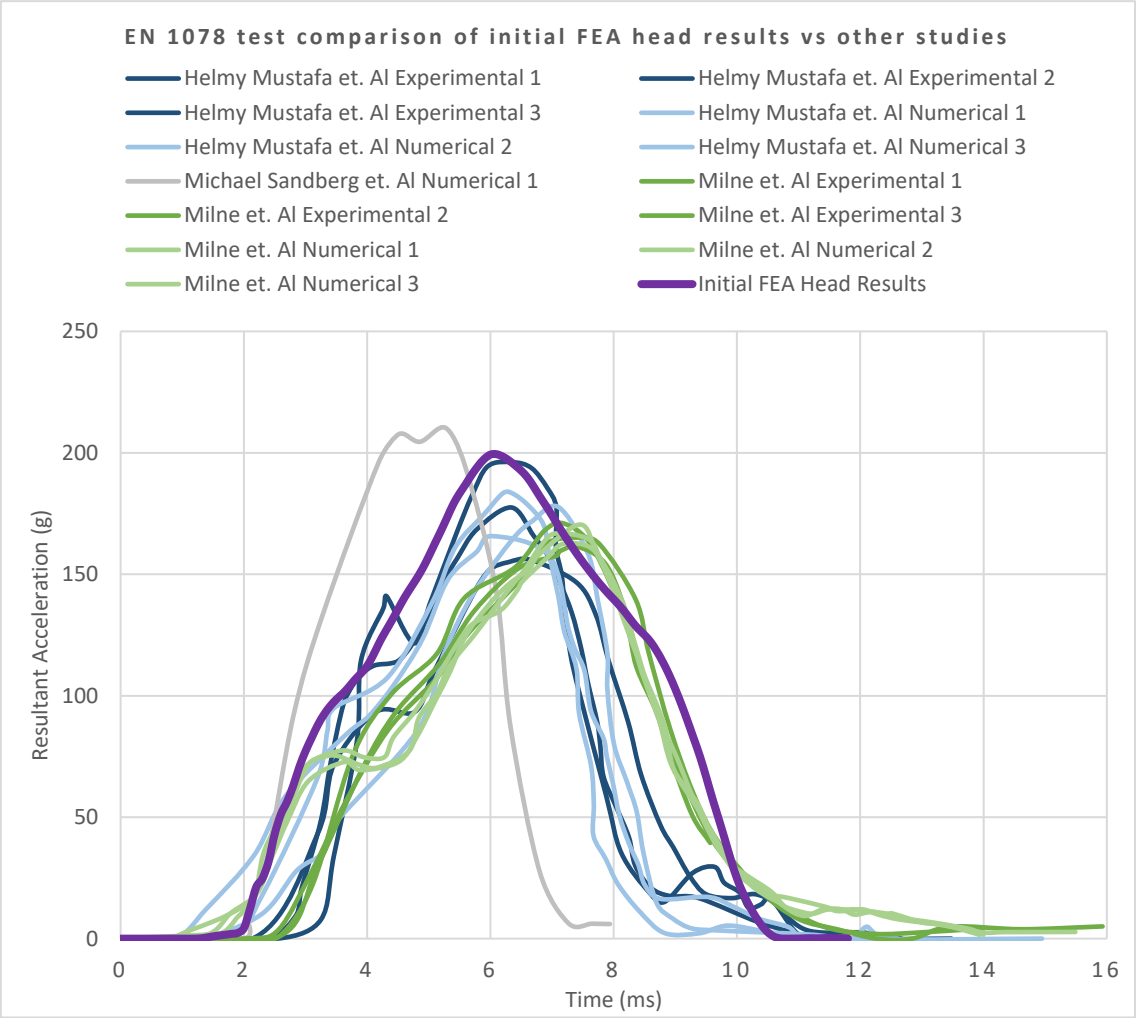

Figure 59: Initial Validation of Helmet Impact with Initial FEA Head.

Figure *59* shows that the initial helmet set-up is closely related in terms of maximum resultant acceleration and impact time duration. The loading and unloading curves are also related. Thus, it can be concluded that the helmet Set-up used for this scenario has been validated.

In conclusion, after solving the penetration issues, using more accurate materials and contacts, using all the elements of the helmet, using multiple impact positions and multiple anvils, it can be concluded that the set-up used for this simulation is adequate and the simulation that will be made with the head provided by Dr. Antona-Makoshi will be based upon this initial simulation (contacts, boundary conditions, speeds, meshing, etc..).

The key aspect that will have to be detailed and improved in further simulations are the helmet material properties which may lead to more accurate results.

4.5 LS-DYNA Final Set-up

4.5.1 LS-DYNA Validated FEA Head by Dr. Antona Makoshi

Dr. Antona-Makoshi and the Japan Automotive Research institute provided a FEA head for this thesis in order to asses possible head injuries during bicycle impacts.

The Head is based upon CT (Computed Tomography) and MRI (Magnetic Resonance Imaging). This head was provided with properties in the SI System (m, s, kg, and N).

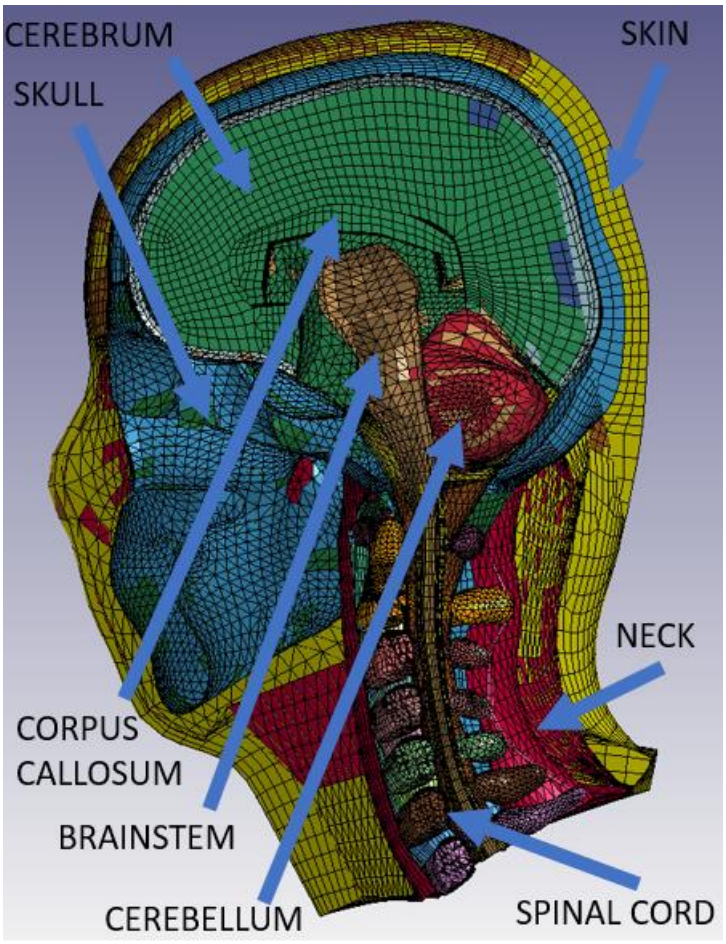

Figure 60: Validated FEA Head.

The head has 291948 solid elements, 53609 shells and a total of 342838 elements, it is very detailed and has been validated by the Japan Automotive Research Institute (JARI).

Among other parts, the head has Skin, Neck, Cerebrum, Cerebellum, Brainstem, Ligaments, Spinal Cord, Cortical Bones, and Corpus Callosum.

Some relevant parts for the analysis made in this thesis are shown in Figure *60*. These parts have been assigned detailed properties, which will allow, later on, for a full assessment of the possible head injuries.

4.5.2 LS-DYNA Set-up of Helmet and Detailed FEA Head

In order to use the provided head multiple adjustments had to be done to the Set-up previously made, the most important two are the following:

The first adjustment was the system of units. Since the initial helmet unit system was in mm, kg, and ms and the head system was in m, s, and kg one of the systems had to be adjusted. It was decided to adjust the system of units used in the helmet Set-up.

The second adjustment was the positioning of the FEA head and the helmet. Initially, each part was designed using different coordinate axis. This means that if both were joined without any prior adjustment the helmet would not be positioned in the correct position with respect to the head. Therefore, the helmet was adjusted using translational and rotational procedures, the coordinate axis of these translations can be observed in Figure 61. The adjustments can be seen in TABLE *12* below.

TABLE 12: AXIS ADJUSTMENT FOR CORRECT POSITIONING OF HEAD AND HELMET.

Rotation/Translation Axis	Angle (Degrees)	Distance(m)
X	0	0.022
Y	-80	-0.0002
Z	180	0.132

Once all the necessary adjustments had been done, the head was correctly located, as shown in Figure *61*.

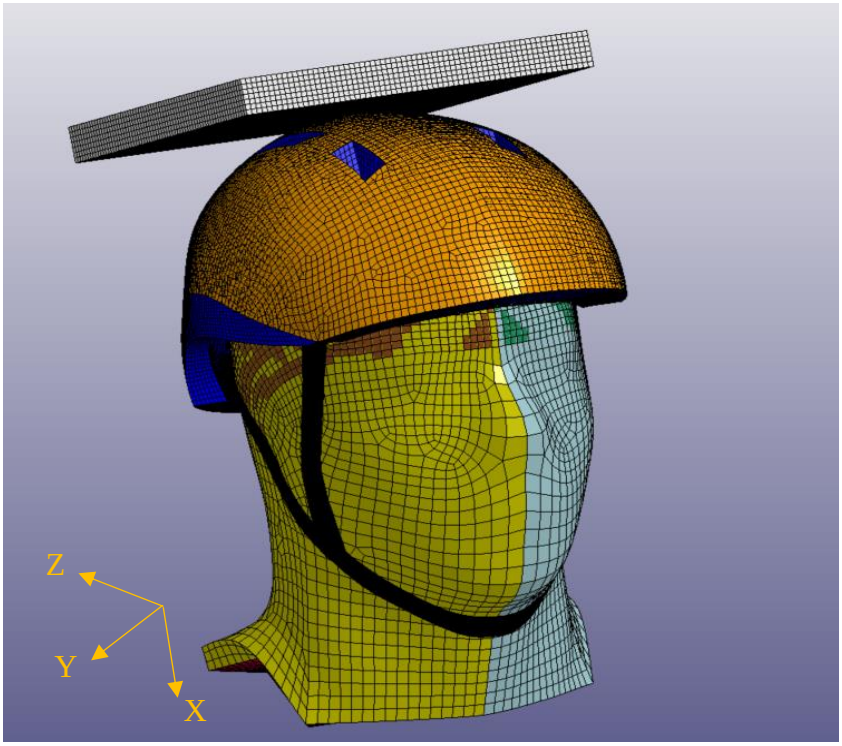

Figure 61: Helmet Impact Layout with Validated FEA Head.

The next step was to correctly define the material properties, contacts, boundary conditions and other characteristics such as gravity. For further analyses, some characteristics such as the anvil type and positioning will also be altered to obtain multiple results on the different impact conditions.

4.5.3 Material Assignment

The materials used for the helmet in this thesis were assigned based on the materials of the helmet and previous studies, which are shown in TABLE *13*.

The EPS Foam needs special mentioning, since this is the most critical material in terms of energy absorption. There are multiple EPS Foams in the market, and each one has very different properties. They are distinguished from each other based on their density; therefore, the density of the EPS Foam of the helmet was measured.

Two squared elements were cut from the helmet as can be seen in Figure *62*. The dimensions of these samples were:

$7.3cm * 2.2cm * 2.2cm = 35.33cm^3$ and $5.25cm * 2cm * 2.3cm = 24.15cm^3$

Together both samples weigh 5.0g, which means that the EPS Foam has a density of 84.05 kg/ m^3.

Figure 62: EPS Foam Samples from Helmet to Measure Density.

Knowing the real EPS density, a previous study was found that had the properties of foams with 14.8 Kg/ m^3, 31.2 kg/ m^3, 50.6 kg/ m^3 and 86.8 kg/ m^3. Thus, the foam used for the simulation was 86.8 kg/ m^3.

The curves of this study were digitized using the program Plot Digitizer. This same study has the properties of the PU Foam that belongs to the padding. The stress-strain curve of the foams are important to model since these materials can sustain large deformations without failure while absorbing impact energy. These curves are implemented in the material model within LS-DYNA.

The materials used for the simulation are shown below.

TABLE 13: MATERIAL PROPERTIES USED IN FINAL SIMULATION OF EN 1078 TEST.

Properties/ Element	Material Model in LS-DYNA	Material Properties	Stress/Strain Curve	Source
EPS Foam (86.8 kg/ m^3)	MAT_LOW_ DENSITY_FOA M_57	ϱ= 86 kg/m^3 E=22.4MPa	Curve 1	[21] & [26]
Straps	MAT_PIECE WISE_LINEA R_PLASTICIT Y_24	ϱ=1400 kg/m^3 υ=0.44 E=1000 MPa	None	[21] & [26]
Shell	MAT_PIECE WISE_LINEA R_PLASTICIT Y_24	ϱ=2080 kg/m^3 υ=0.325 E=8.54 GPa	None	[26] & [27]
Steel Anvil	MAT_RIGID _20	ϱ=7800 kg/m^3 υ=0.3 E=200 GPa	None	[23]
PU Foam Padding	MAT_LOW_ DENSITY_FOA M_57	ϱ=32kg/m^3 E=0.47 MPa	Curve 2	[21] & [26]

The EPS Foam and PU Foam curves used for this model are shown below in Figure *63* and Figure *64*. It is noticeable how both deform approximately the same amount, but the EPS Foam is capable of sustaining much larger stresses while it deforms.

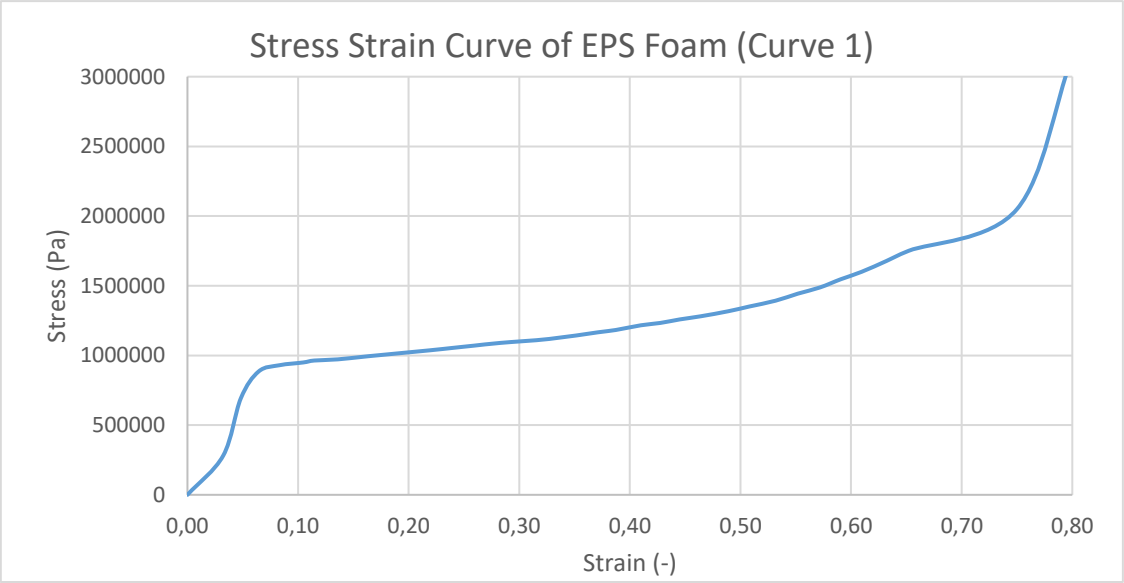

Figure 63: Curve of EPS Foam modelled in Final Simulation with 86.8 kg/m^3 density *[26]*.

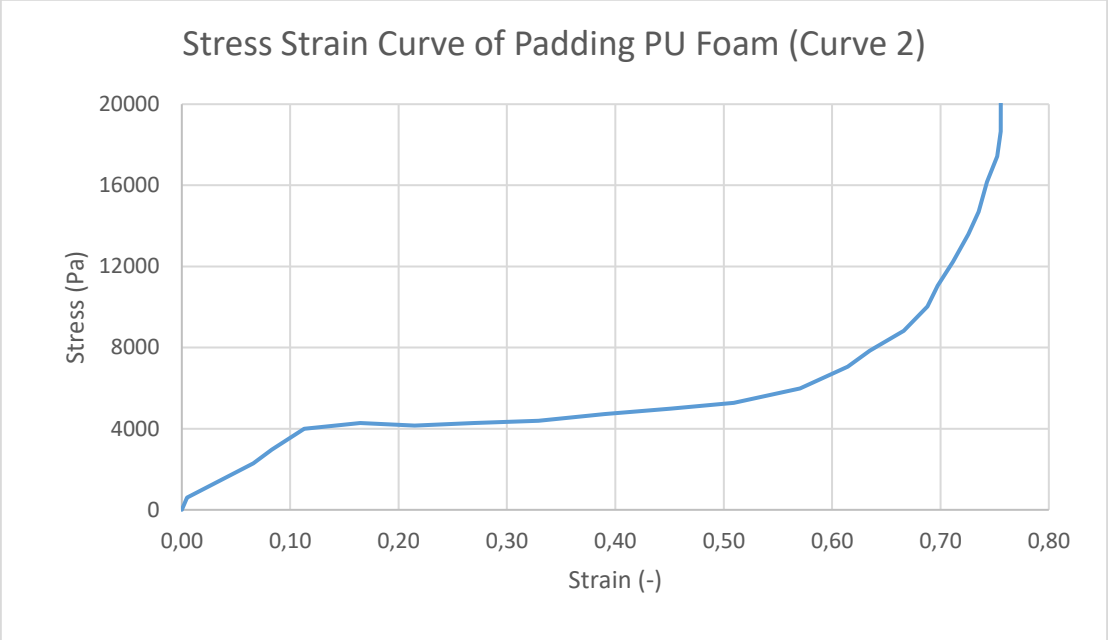

Figure 64: Curve of PU Foam modelled in Final Simulation *[26]*.

The properties assigned to the FEA head are referenced in the thesis of Jacobo Antona-Makoshi "Traumatic Brain Injuries: Animal Experiments and Numerical Simulations to Support the Development of a Brain Injury Criterion" [28].

4.5.4 Helmet and Head Contact Assignments

The contact assignments between the different parts of the simulation are important since they will determine how each part will behave with respect to each other; four contact conditions were used for the simulation, a summary simplification of how each contact works is shown below for reference, and the type of contact used for each element can be seen in TABLE *14*.

The CONTACT_AUTOMATIC_SURFACE_TO_SURFACE is a two-way approach that checks for penetration on both elements which are in contact, it is recommended for crash analysis. It allows the elements to separate and slide with respect to each other. In this type of contact a static coefficient of friction and a dynamic coefficient of frictions can be set [29].

The CONTACT_TIED_SHELL_EDGE_TO_SURFACE is a contact which ties both elements that are in contact in translational and rotational movement, in this case a surface and a shell [29].

The CONTACT_TIED_SHELL_EDGE_TO_SURFACE_OFFSET is a contact which ties both elements that are in contact in translational and rotational movement, in this case a surface and a shell that have an offset distance (i.e. not in direct contact) [29].

The CONTACT_TIED_SURFACE_TO_SURFACE is a contact where both elements are set to move with each other. In this case two surfaces are constrained to move with each other [29].

TABLE 14: BOUNDARY CONDITIONS USED IN FINAL SIMULATION OF EN 1078 TEST.

Element A	Element B	Type of Contact	Dynamic/Static Friction Coeff.
Shell	Anvil	Contact_automatic_surface_to_surface	0.2/0.2
Straps	EPS Foam	Contact_automatic_surface_to_surface	0.2/0.2
EPS Foam	Anvil	Contact_automatic_surface_to_surface	0.2/0.2
Straps	Head	Contact_automatic_surface_to_surface	0.2/0.2
Padding	Head	Contact_automatic_surface_to_surface	0.2/0.2
Padding	Straps	Contact_automatic_surface_to_surface	0.2/0.2
Head	EPS Foam	Contact_automatic_surface_to_surface	0.2/0.2
Straps	EPS Foam	Contact_tied_shell_edge_to_surface	TIED
Shell	EPS Foam	Contact_tied_shell_edge_to_surface_offset	TIED
Padding	Rear Strap	Contact_tied_shell_edge_to_surface_offset	TIED
Padding	EPS Foam	Contact_tied_surface_to_surface	TIED

The contacts between the elements within the FEA Head are referenced in the thesis of Jacobo Antona-Makoshi “Traumatic Brain Injuries: Animal Experiments and Numerical Simulations to Support the Development of a Brain Injury Criterion” [28].

4.5.5 Helmet and Head Boundary Conditions

Apart from the previous material properties and contact conditions, some other boundaries that are used have a noticeable influence in the results and are shown below:

- In order to keep the anvil on a fixed position, the lower nodes of the anvil that are not in contact with the helmet in the impact (i.e. in Figure *61* the nodes that located on area of the negative X direction) are fixed, which means that all translational and rotational degrees-of-freedom have been constrained.

- The termination time is set to 15ms to simulations with a flat anvil and 25 ms for simulations that use a curbstone anvil.
- The main output of data is obtained from the BINARY_D3PLOT database, with a time interval between outputs of 10^{-4} s.
- Gravity is included for the simulation, in this case acting in the negative X direction, which can be seen in Figure *61*.
- An initial speed is given to the head, 5.42 m/s for the flat anvil case as specified by the EN 1078 norm and 4.57 m/s on the curbstone anvil.

4.5.6 LS-DYNA Analyses

As previously mentioned, two studied are to be made in order to assess the head injuries that may occur during a head impact while wearing a bicycle helmet.

The first studio performed in this thesis is the EN 1078 flat anvil test with a head speed of 5.42 m/s in the negative X direction, this set-up can be observed in Figure 61.

The second studio performed is the EN 1078 curbstone anvil with a speed of 4.57 m/s in the negative X direction, the setup and location of the anvil can be seen in Figure *65*.

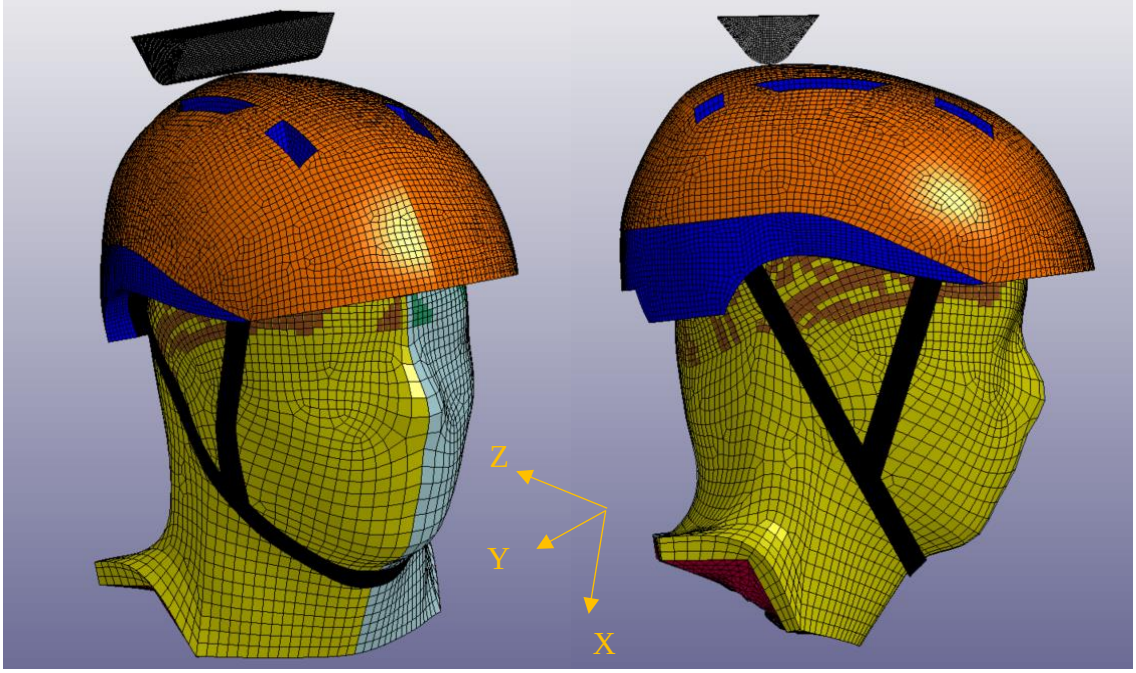

Figure 65: Set-Up for Final Simulation of EN 1078 Test with a Curbstone Anvil.

The results of these two tests will be the ones upon which the head Injury Criteria in the impact will be assessed.

4.6 LS-DYNA Result Validation

In order to validate the previous se-up for the analyses, a comparison between the results of this simulation and the results of previous studies is made. This shows whether the results that are being obtained are yielding correct results.

The most widely tested and simulated case from the previously mentioned studies is the EN 1078 test against a flat anvil, which is shown in Figure *61* and Figure *56* in this study. Therefore, a comparison between this result and the previous flat anvil studies is shown in Figure *66* below and is used for validation purposes.

Regarding the curbstone anvil impacts, to the author's knowledge, there has only been one previous EN 1078 FEA study which assess the head accelerations in curbstone impacts. Thus, this impact will not be used for strict validation purposes since not enough data is available, but it will be able to assess the correctness of the set-up used for this thesis.

4.6.1 EN 1078 Flat Anvil Validation

There are three key points that can be used to validate the Flat Anvil impacts analyses:

1. Impact Duration: the duration of the impact should be within a reasonable value when compared to the previous studies. It is observed from the previous studies that the average impact duration is 10.5ms, the maximum impact duration is 13.95ms and the minimum impact duration is 5.89ms.
2. Maximum head acceleration (measured in g): the maximum acceleration should be within a reasonable range of values when comparing it to the previous studies. It is observed from the previous studies that the average of the maximum head acceleration is 174.1 g, the maximum head acceleration is 210.31 g, the minimum head acceleration is 155.83 g`s ms.
3. Loading and Unloading Curves: the layout of the loading and unloading curve shall follow the same pattern as the one found in previous studies. The derivative of the function shall be in close terms to the previous functions, it shall not tend to zero or infinite, and it shall reach the maximum value approximately half-way throughout the impact period in order to agree with the previous results.

The results for the head acceleration that were obtained from the average of the accelerations of the Cerebrum, Corpus Callosum, Brainstem, and Cerebellum in the flat anvil test are shown in Figure *66*.

The effective impact starts at 1ms and finishes at 12ms. The maximum acceleration of the head is 150.61 g, as shown in Figure *66*.

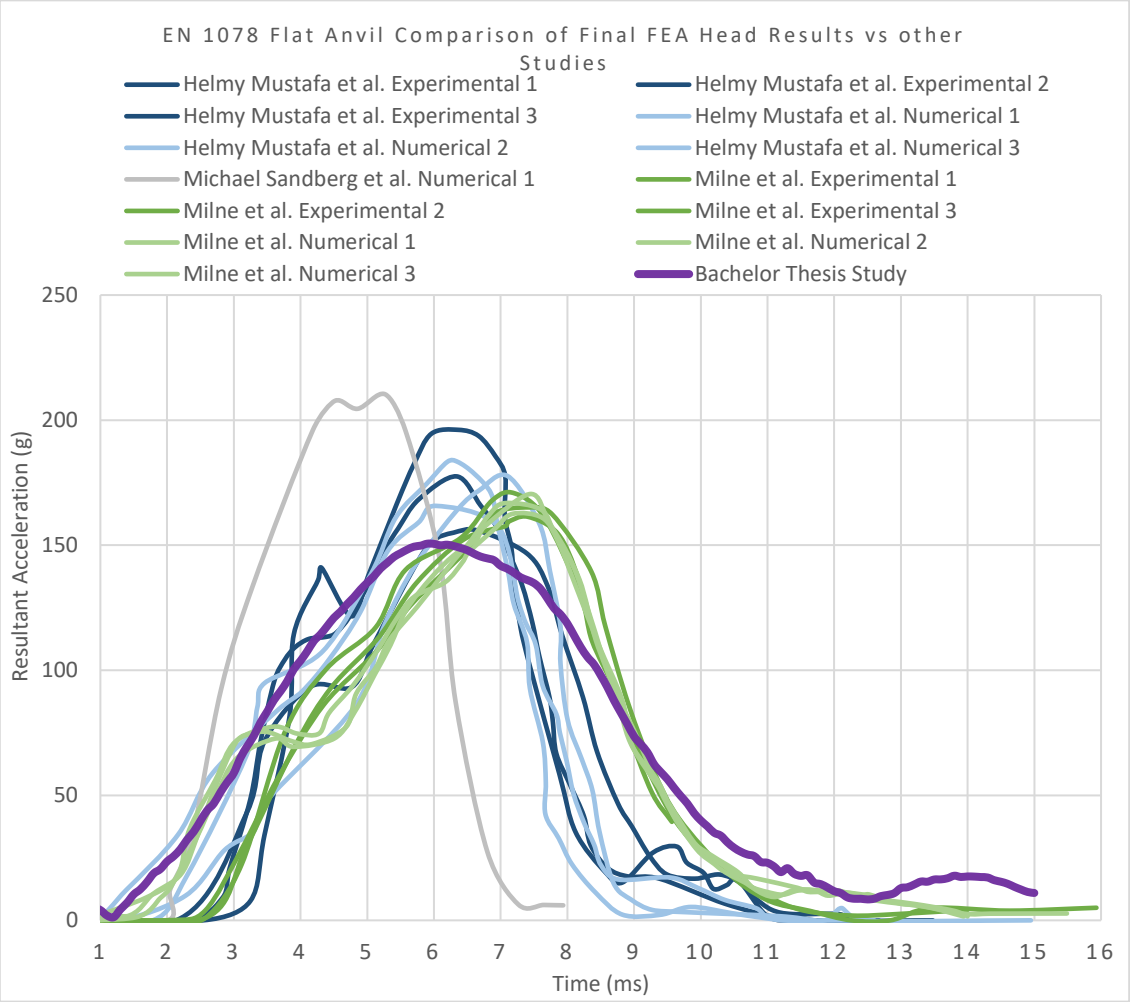

Figure 66: EN 1078 Test Results on Flat Anvil Comparison with Previous Studies.

Comparing the loading and unloading curve of this study with the previous studies it can be observed that they follow similar patterns on both. The maximum value is also reached halfway through the impact period, as seen in previous studies.

The average value of maximum head acceleration in the previous studies is 174.1 g. The result obtained in this simulation is close to those of the previous studies and has a 15.6% difference with the mean value of the previous studies, which is reasonable due to the many differences of these studies (mainly seen in helmet model, and FEA head used).

The average impact duration of previous studies is 10.5 ms, the simulation has an impact duration of 11 ms which is between the minimum and maximum values of the previous studies and has a 4.5% difference with the average value of the previous studies.

4.6.2 Helmet-Head Validation Conclusions

The previous analysis shows the correlation of this thesis and the previous studies in terms of loading and unloading curves, impact duration, and maximum head acceleration; therefore, it is concluded that **the helmet impact simulation has been validated and will be used to asses head Injuries during bicycle impacts.**

4.6.3 EN 1078 Curbstone Anvil Assessment

The same three key aspects as the EN 1078 flat anvil test can be used to assess the correctness of the set-up for the curbstone anvil, the conditions now are the following:

1. Impact Duration: It is observed from the previous studies that the Average impact duration is 15.3 ms, the maximum impact duration is 16.5 ms and the minimum impact duration is 13.9 ms.
2. Maximum Head Acceleration (measured in g): It is observed from the previous studies that the average of the maximum head acceleration is 81.3 g, the maximum head acceleration is 88.9 g, and the minimum head acceleration is 74.6g`s.
3. Loading and Unloading Curves: The derivative of the function shall be in close terms to the previous functions, it shall not tend to zero or infinite in the loading or unloading curve, and it shall reach the maximum value approximately half-way through the impact period in order to agree with the previous results.

The results for the head Acceleration were obtained from the average of the accelerations of the Cerebrum, Corpus Callosum, Brainstem, and Cerebellum in the curbstone Anvil test are shown in Figure *67* below.

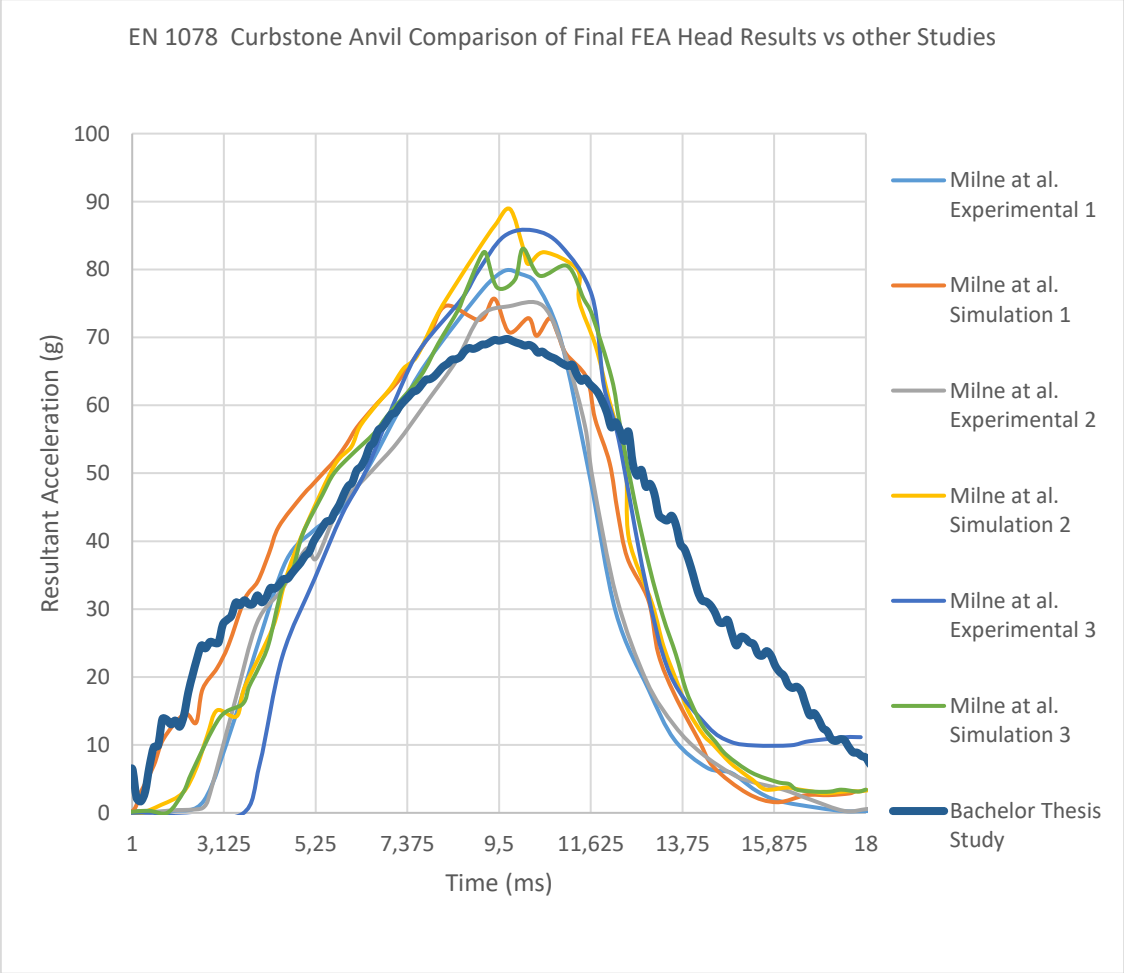

Figure 67: EN 1078 Test Acceleration Results on Curbstone Anvil Comparison with Previous Studies.

The effective impact starts at 1ms and finishes at 18ms. The maximum acceleration of the head is 69.8 g, as shown below in Figure *67*.

Comparing the loading and unloading curve of this study with the previous studies it can be observed that they follow similar patterns on both studies, with a slightly more pronounced slope on the loading and unloading curve of the previous studies, which can be due to the helmet model, validated FEA head used, but the most important reason is the anvil position since the previous studies do not specify the location and orientation of the anvil and that can have drastic changes in the acceleration curves. The maximum value is also reached halfway through the impact period, as seen in previous studies.

The average value of maximum head acceleration in the previous studies is 81.3. The result obtained in this simulation is 69.8 g and has a 16.5 % difference with the mean value of the previous studies, which is reasonable due to the many differences of these studies, mainly seen in helmet model, and FEA head used, but most importantly, in the anvil positioning as previously explained.

The average impact duration of previous studies is 15.3 ms, the simulation has an impact duration of 17 ms which has a 10% difference with the average value of the previous studies.

The comparison shows the correlation in terms of loading and unloading curves, impact duration, and maximum head acceleration on both studies; therefore, the curbstone impact set-up used in this thesis is deemed correct and will be used to assess and identify Head Injury Criteria in Future analyses.

4.6.4 Main Differences between the Acceleration Results between this Thesis and Previous Studies

As shown before, the flat and curbstone anvil impacts agree with the previous studies in terms of loading and unloading curves, maximum head acceleration and impact duration with less than 17% difference in all the previous parameters, validating the previous set-up.

Nevertheless, there is a minor value difference and it may be due to the following reasons:

- The main reason for the difference in the acceleration and impact time values is the helmet model and its properties since all the previous studies use helmets which are different from the one used for this thesis. Some of the previous studies also use helmet designs which are not available on the market and are the author's design, which may affect the results; this is noticeable in the Michael Sandberg et al. [7] study shown in *Figure 66* as this study is not based on a real helmet and the results obtained from this study greatly differ from all the others, with a much shorter impact time duration and a much larger head acceleration.
- The helmet elements that have been modelled greatly differ on each study. Nevertheless, to the author's knowledge, no previous study has been done with all the following elements modelled: EPS Foam, padding, rear and chin straps, shell, validated FEA head, and a helmet design which is available on the market. These elements can have a large influence in the results; for example, as it will

be later demonstrated in the document, the straps keep the head attached to the helmet during the impact. Therefore, the difference in the values can be due to this thesis' modelling of all the helmet elements previously stated.

- Another key difference is found in the head model that has been used. 94.7% of the previous studies used for validation purposes use some kind of head dummy (J head form, ISO head form…) with rigid body properties. As it was seen before in this thesis (*Figure 59*), using a rigid body head produces larger resultant head accelerations. The latest results are obtained using a FEA head model from Dr. Antona-Makhosi which has been extensively validated by the Japan Automotive Research Institute. Therefore, the difference of values in resultant acceleration and impact duration can be due to the head form used, since this thesis uses a head that can yield closer results to a real-life-impact scenario. Therefore, it is concluded that **using a validated FEA head yields more accurate results than a dummy head and the real head acceleration results are lower than those proposed in previous studies.**

5. HEAD INJURY CRITERIA AND OTHER ANALYSES

5.1 Head Injury Criteria

This section analyzes multiple parameters in the following order: first, the graphical sequence of the flat and curbstone impacts are show; afterwards, multiple head injury criterion and head injury modes will be assessed; lastly, the analyses made to the helmet are explained and shown.

There are several ways of assessing head injury criteria and head injury modes that might occur to a head during an impact. Some of them have been extensively validated, while others lack validation. Some of these criteria stands out from the others, for example the Head Injury Criterion (HIC) is widely used in crash testing, specifically in motor vehicles.

For this thesis it is intended to conduct an extensive analysis of the methods that can assess Head Injury Criteria. This analysis will be done for the EN 1078 test, with Flat and Curbstone Anvils, shown in Figure *61* and Figure *65*.

Each of these methods is based upon different characteristics (acceleration, stresses…) that can be obtained from the simulation results in LS-DYNA with the Post Processing tools (LS Pre-Post).

The criteria that will be analyzed is the following: Peak Linear Acceleration (PLA), Gadd Severity Index (GSI), Head Injury Criterion (HIC_{15} and HIC_{36}), Head Protection Criterion (HPC), 3 Ms Criterion (A3MS), 5 Ms Criterion (A5MS), Diffuse Axonal Injuries (DAI), and Skull Fracture Probability.

5.2 EN 1078 Flat Anvil Result Sequence

Previous to the analyses, the sequence of the impact in the Flat Anvil is shown in Figure *68* below to aid in the understanding of how the head behaves during the impact.

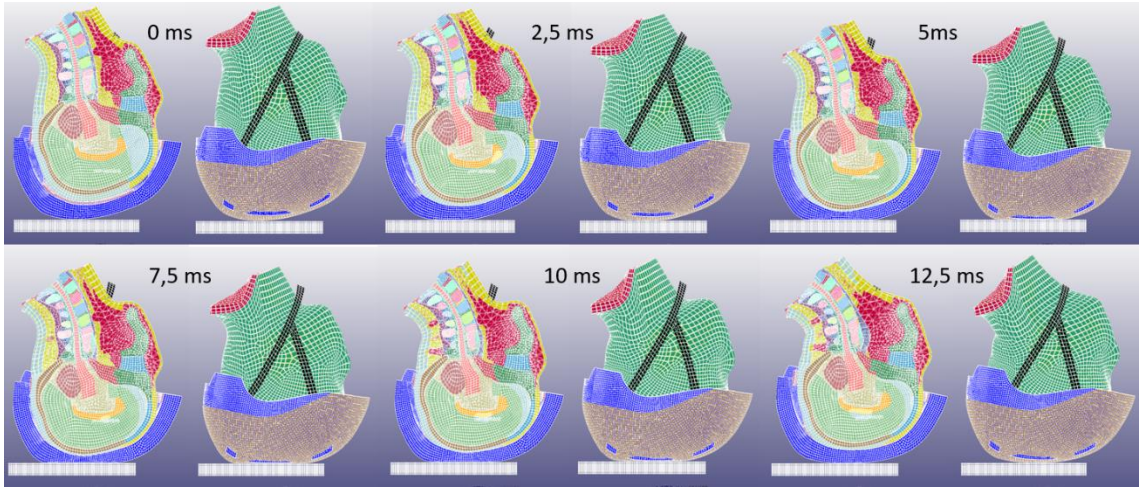

Figure 68: Impact Sequence for EN 1078 Test on Flat Anvil.

It can be seen that initially the helmet and head are not in contact with the anvil. At 2.5ms the PU foam in the helmet has completely deformed and the helmet (shell and EPS Foam) has reached a state of contact with the Anvil.

At 5 ms the EPS Foam has already been deformed and will keep being deformed until it reaches 5.9 ms; afterwards, the EPS will begin to recover its initial shape, as can be seen in the sequence from 7.5 ms onwards where the head starts to gain velocity in the opposite direction.

It must be noted that at 12.5ms the chin straps keep the head attached to helmet, and during all the simulation the rear strap keeps the head in the correct position, which prevents the head from bouncing backwards and forwards.

The previously described graphical sequence agrees with the head acceleration results, where the maximum acceleration is reached at 5.9 ms.

5.3 EN 1078 Curbstone Anvil Result Sequence

Previous to the analyses, the sequence of the impact in the Curbstone Anvil is also shown in Figure *69* below to aid in the understanding of how the head behaves during the impact.

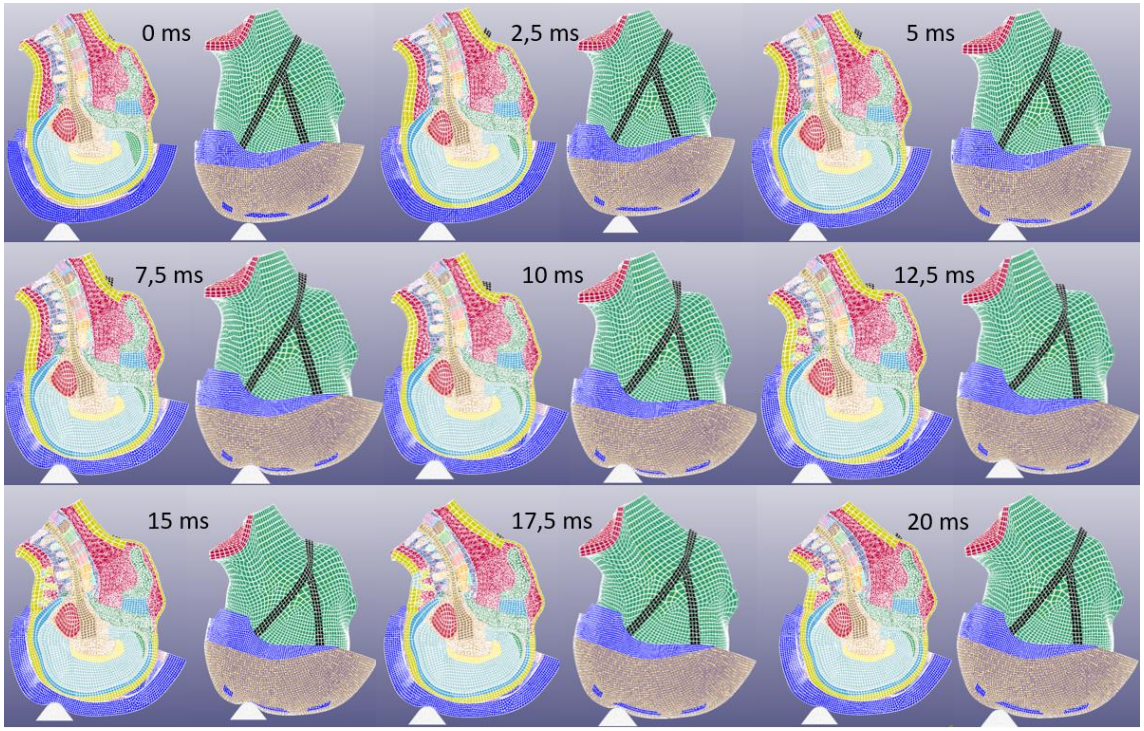

Figure 69: Impact Sequence for EN 1078 Test on Curbstone Anvil.

It can be seen that initially the helmet and head are not in contact with the anvil. At 2.5ms the PU Foam in the helmet has completely deformed and the helmet (shell and EPS Foam) has reached a state of contact with the Anvil.

At 5 ms the EPS Foam has already been deformed and will keep being deformed until it reaches 9.7 ms; Afterwards the EPS will begin to recover its initial shape, as can be seen in the sequence from 10 ms onwards where the head starts to gain velocity in the opposite direction with a different angle than that of the initial contact.

It must be noted that at 17.5ms the chin straps keep the head attached to helmet, and during all the simulation the rear strap keeps the head in the correct position, as happens in the flat anvil simulation.

The previously described graphical sequence agrees with the head acceleration results, where the maximum acceleration is reached at 9.7ms.

5.4 Peak Linear Acceleration Measurement (PLA)

Based on this head injury criterion, there is a 50% probability of skull fracture if the acceleration is larger than 135 g [30], a 50% probability of Concussion if the acceleration is larger than 65.1 g and a 75% probability of concussion if the acceleration is larger than 88.5 g [31].

Flat Anvil Impact: Based on the Peak Linear Acceleration method, this impact would incur in a 50% probability of Skull Fracture and a 75% of probability of Concussion because this impact generates a maximum acceleration of 150.61 g, as shown in Figure *66*.

Curbstone Anvil Impact: Based on the Peak Linear Acceleration method, this impact would incur in a 50% of probability of Concussion because this impact generates a maximum acceleration of 69.8 g, as shown in Figure *67*, but it would not generate skull fracture.

5.5 Severity Index (GSI)

This head Injury Criterion is based upon the Wayne State University Cerebral Concussion Tolerance Curve (WSTC). The WSTC is a curve with acceleration on the Ordinate Axis and Time in the Abscissa Axis. The values that are over the curve cause permanent brain Injury [32] [33].

It was found that when the WSTC is converted into a logarithmic scale it changes into a straight function with a slope of -2.5; therefore, Gadd proposed the Severity Index Criteria shown in equation 5.1. Following this criterion, the GSI values that are over 1000 produce serious internal head injury [34] [33].

$$GSI = \int_0^t a(t)^{2.5} dt \quad eqn.\,5.1$$

Where

a is the linear acceleration (g)

t is the duration of the impact (s)

This head injury criterion can be determined since the output that is obtained from the LS Pre-Post tool are the accelerations every 0.1ms as shown in Figure *66* and Figure *67*.

A way of converting the given acceleration-time curve onto the GSI was needed, it was decided to use MATLAB (R2017B) as an implementation tool for this criteria. A summary of the programming Code for the Flat Anvil case is shown in TABLE *15* below.

TABLE 15: MATLAB CODE IMPLEMENTED TO CALCULATE GSI.

```
% Time Input Inside A Matrix Flat Anvil
A[t1,t2,…,t151];
% Acceleration Input Inside B Matrix Flat Anvil
B[a1,a2,…,a151];
% Integral calculation
GSIValue=0;
for i=1:150
   GSIValue=GSIValue+(A(i+1)-A(i))*(((B(i+1)+B(i))/2)^2.5;
End
disp(GSIValue)
```

Flat Anvil Impact: Based on Gadd Severity Index Criteria and implementing the flat anvil results into the MATLAB code previously shown, this impact has a GSI Value of 1089.6, which means that this impact would incur in serious internal head injuries.

Curbstone Anvil Impact: Based on Gadd Severity Index Criteria and implementing the Curbstone anvil results into the MATLAB code previously shown, this impact has a GSI Value of 259.15, which means that this impact would not incur in serious internal head injuries.

5.6 Head Injury Criterion (HIC) and Head Protection Criterion (HPC)

The head injury criterion (HIC) is one of the most-widely used criteria to assess head injuries. It is currently, and has been used in the safety regulations code in the American motor vehicle regulations. The Head Injury Criterion is defined in equation 5.2 [32]:

$$HIC = \left\{(t_2 - t_1)\left[\frac{1}{t_2 - t_1}\int_{t1}^{t2} a(t)dt\right]^{2.5}\right\}_{max} \qquad eqn.\,5.2$$

Where t_2 is the time at the end of the impact period (s)

t_1 is the time at the beginning of the impact period (s)

a is the acceleration (g)

This function is to be calculated within the timeframe that yields the highest HIC value. Therefore, theoretically, it means that there is an infinite number of possible timeframes, which means that there is a need to use computer processing power to implement this function.

Commonly there are two maximum timeframes used in the automotive safety standards, 36ms and 15ms [35] . Therefore, for this thesis the HIC_{15} and HIC_{36} will be assessed. The calculation will be done with MATLAB and the function used to calculate the Flat Anvil Case is shown in TABLE *16* below.

TABLE 16: MATLAB CODE IMPLEMENTED TO CALCULATE HIC_{15} FOR FLAT ANVIL CASE.

```
% Time Input Inside A Matrix Flat Anvil
A[t1,t2,…,t151]
% Acceleration Input Inside B Matrix Flat Anvil
B[a1,a2,…,a151]
%Function Calculation Flat Anvil
Max=0;
for x=1:150
  for z=(x+1):151;
HICValue=0;
    for i=x:z-1;
   W1=0;
   W2=0;
   W3=0;
   W4=0;
   W5=0;
   W1=A(z)-A(x);
   W2=1/(W1);
   W3=(B(i+1)+B(i))/2;
   W4=W3*0.0001;
   HICValue=HICValue+W4;
      end
HICValue=(HICValue*W2)^2.5;
HICValue=HICValue*W1;
%Timeframe Recorder to evaluate interval
        if HICValue >= Max
    t1=x;
    t2=z;
        end
Max=max(HICValue, Max);
  end
end
disp(Max)
disp (t1)
disp (t2)
```

Regarding the Head Protection Criterion (HPC), it is used in the ECE R94 (norm for the protection of occupants against frontal collision) and R95 (norm for the protection of occupants against lateral collision) regulations. The way of calculating the HPC is the same as the HIC_{36} [36], therefore it will be analyzed in the same criteria.

After calculating the $HIC_{15,}$ HIC_{36} and HPC using MATLAB it was found that they yielded the same results for both timeframes (15 and 36 max); thus, the HIC_{15} and HIC_{36} and HPC will be assessed in the same section.

HIC_{15} and HIC_{36} and HPC on Flat Anvil Impact: The result is a value of 970.2 which happens in the timeframe between 3.4 and 9.1 ms. Based on the table developed in the Forensic Injures Biomechanics study by Wilson C. Hayes et al. [37] which shows the probability of injury based on the HIC values, the injury probability was obtained:

- For the Flat Anvil impact case there is a 0% probability of a Maximum Injury (not treatable) [37].
- For the Flat Anvil impact case there is a 2% probability of a Critical Injury (53.1-58.4% of Fatality Range) [37].
- For the Flat Anvil impact case there is a 15% probability of Severe Injury (7.9-10.6% of Fatality Range) [37].
- For the Flat Anvil impact case there is a 49% probability of Serious Injury (0.8-2.1% of Fatality Range) [37].
- For the Flat Anvil impact case there is a 88% probability of Moderate Injury (0.1-0.4 % of Fatality Range) [37].
- For the Flat Anvil impact case there is a 100% probability of Minor Injury (0% of Fatality Range) [37].

HIC_{15}, HIC_{36} and HPC on Curbstone Anvil Impact: The result is a value of 224.2, which happens in the timeframe between 4.6 and 14.1 ms, the conclusions of this head injury criteria are the following:

- For the Curbstone Anvil impact case there is a 0% probability of a Maximum Injury (not treatable) [37].
- For the Curbstone Anvil impact case there is a 0% probability of a Critical Injury (53.1-58.4% of Fatality Range) [37].
- For the Curbstone Anvil impact case there is a 0% probability of Severe Injury (7.9-10.6% of Fatality Range) [37].
- For the Curbstone Anvil impact case there is a 3% probability of Serious Injury (0.8-2.1% of Fatality Range) [37].
- For the Curbstone Anvil impact case there is a 7% probability of Moderate Injury (0.1-0.4 % of Fatality Range) [37].
- For the Curbstone Anvil impact case there is a 20% probability of Minor Injury (0% of Fatality Range) [37].

5.7 Diffuse Axonal Injuries (DAI)

Diffuse Axonal Injuries are thought to be related to cases where comma has happened to the patient. It is also related to cases where a person has lost consciousness and is one of the main mechanisms of brain injury. Multiple cognitive malfunctions are attributed to DAI, some of which include memory disorder to store new information and a decrease in the capacity of the individual to process information [38].

A 50% probability of Diffuse Axonal Injuries are caused by a Intracranial Von-Misses Stress of 28KPa; therefore, this parameter was measured in the EN 1078 flat anvil and curbstone anvil tests with the following results [22]:

Flat Anvil Impact: For this case, the Intracranial Von-Misses stress-time curve is shown in Figure *70* below:

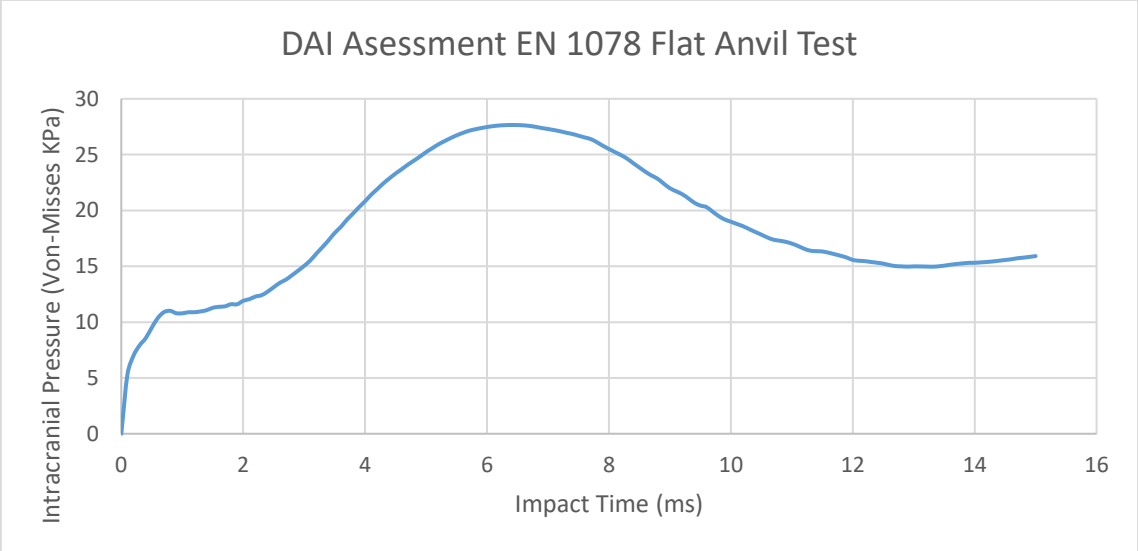

Figure 70: Intracranial Von-Misses Stress for DAI Assessment.

A maximum value of 27.6 KPa is reached in Figure *70*, which means that it does not reach the threshold to sustain a 50% probability of DAI, but it is within 1% of intracranial stress to reach the 50% probability.

Curbstone Anvil Impact: For this case, the Intracranial Von-Misses Stress-time curve is shown in Figure *71* below:

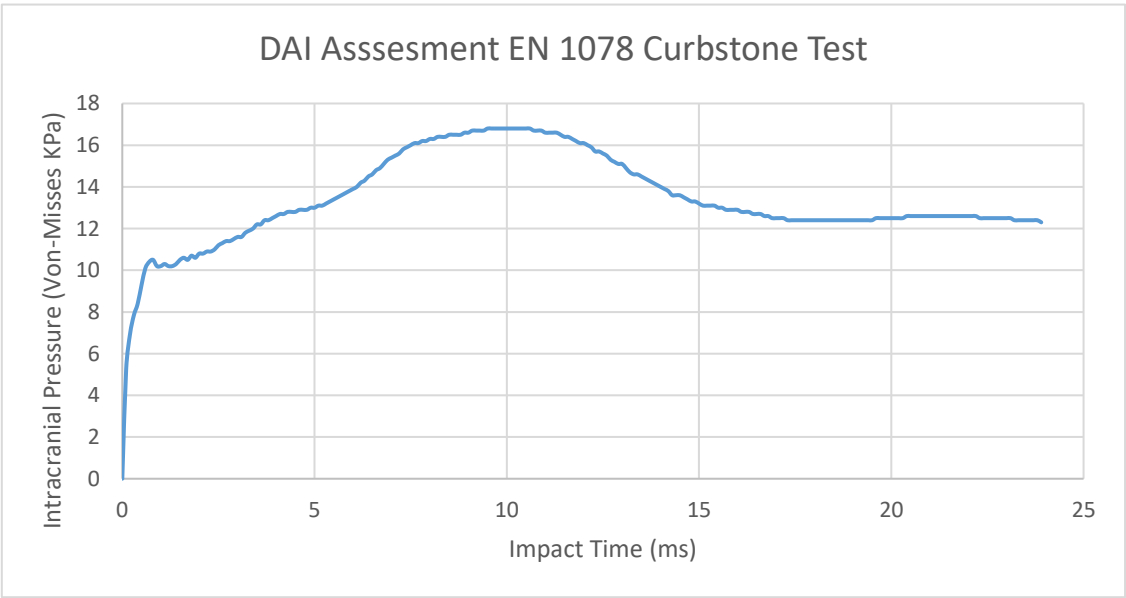

Figure 71: Intracranial Von-Misses Stress for DAI Assessment.

A maximum value of 16.8 KPa is reached in Figure *71*, which means that it does not reach the threshold to sustain a 50% probability of DAI, it is within 39.9% difference of intracranial stress to reach the 50% probability.

5.8 Skull Fracture Probability

The skull is a key element that protects the intracranial elements from harms-way. Therefore, there is a need to evaluate whether it fractures under a normalized EN 1078 test. In order to do so, the probability curve implemented by Philemon Chan in the "development of a generalized linear skull fracture criterion" [1] paper will be used.

This method uses the following equations 5.3, 5.4 and 5.5.

$$SFC = \frac{\Delta V^{HIC}}{\Delta T^{HIC}} \quad eqn\ 5.3\ [1]$$

Where ΔV^{HIC} is the averaged velocity during the HIC Interval

ΔT^{HIC} is the HIC time interval

$$\Delta V^{HIC} = \int_0^t a(t)dt \quad eqn.\ 5.4\ [39]$$

Where a is the resultant acceleration (g)

The relationship between the probability of skull fracture and SFC is given in eqn. 5.5.

$$\ln\left(\frac{P}{1-P}\right) = 6.39\ln(SFC) - 32.53\ eqn\ 5.5\ [1]$$

Where P is the probability of skull fracture.

TABLE 17: MATLAB IMPLEMENTATION OF EQUATION 5.4 FOR FLAT ANVIL CASE.

```
% Time Input Inside A Matrix Flat Anvil
A[t1,t2,…,t151];
% Acceleration Input Inside B Matrix Flat Anvil
B[a1,a2,…,a151];
t1=34; % Start of HIC Interval
t2=91; % End of HIC Interval
%Integral
AV=0
for i=t1:t2
   AV=AV+(A(i+1)-A(i))*(((B(i+1)+B(i))/2))
end
SFC=AV/((t2-t1)/10000)
```

Using the previous equations, the following information was obtained for the flat and curbstone anvil cases:

Flat Anvil Impact: The SFC calculated with equation 5.3 was 122.4 (g). This was then applied to equation 5.5, which gave a probability of 14.04 % of skull fracture. A lower skull fracture probability value than the Peak linear acceleration method.

Curbstone Anvil Impact: The SFC calculated with equation 5.3 was 57.55 (g). This was then applied to equation 5.5, which gave a probability of 0.13 % of skull fracture.

5.9 3 MS Criterion (A3MS)

This criterion does not asses head injuries itself, but it is required that the head acceleration does not go over the threshold value in order to meet multiple regulations and standards.

This head injury criterion imposes a maximum of 80 continuous g for a 3ms impact.

Flat Anvil Impact: This impact does not meet the A3MS regular criterion since it has more than 80 g for a period of 5.3ms. Therefore, this impact and helmet set-up would not meet the criteria required for multiple regulations [40].

Curbstone Anvil Impact: This impact meets the A3MS criterion because at no point this simulation reaches 80 g.

5.10 5 MS Criterion (A5MS)

This criterion is an adaptation to the previously criterion (A3MS) but in this case it is specifically designed to test helmets. It imposes a maximum of 150 continuous g for a 5 ms impact [40].

Flat Anvil Impact: This impact meets the A5MS criterion since it only reaches a value higher than 150 g during 0.3ms.

Curbstone Anvil Impact: This impact meets the A5MS criterion because at no point this simulation reaches 150 g.

5.11 Influence of PU Foam in absorbing Impact Energy on the Helmet Structure

The PU Foam, as previously explained, is mainly used for rider comfort, and some authors claim that it also absorbs some impact energy. Thus, the percentage of energy absorbed by the PU Foam will be calculated to assess the importance of this element in the helmet absorbing capabilities.

In order to assess how much energy is absorbed and the dependence of the speed in the energy absorbed by the PU Foam, the EN 1078 flat anvil test with speed variation was used because the flat anvil is the one that produces the worst-case injury scenario for the impacts. Eight simulations were made in total for this analysis.

The energy absorbed by the PU Foam is compared against the energy in the entire simulation (left ordinate axis), and against the energy absorbed by the EPS Foam (right ordinate axis), as shown in Figure *72* below.

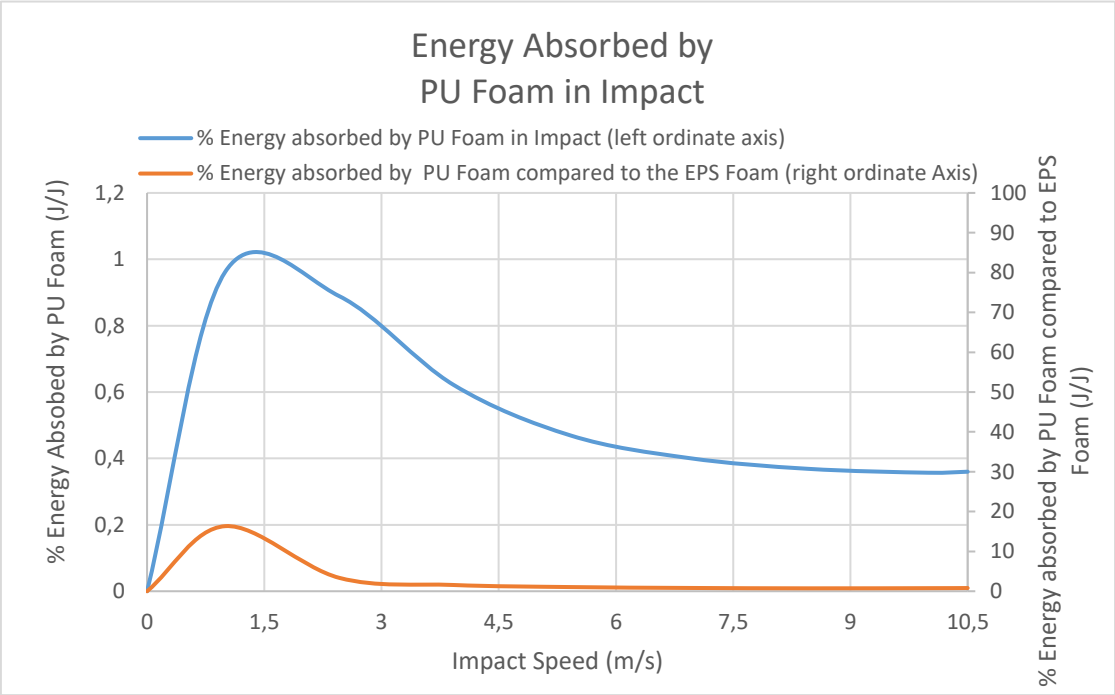

Figure 72: Percentage of Energy absorbed by the PU Foam.

Figure *72* shows that the PU Foam absorbs 1% of the entire impact energy in low speed impacts (less than 3 m/s), at this point it accounts for less than 20% of the energy absorbed by the entire helmet.

When the speed increases the percentage of energy absorbed in the entire impact tends to converge to a value of approximately 0.38%; it also converges to a value 0.8% in the percentage of energy absorbed by the entire helmet.

This study concludes that the PU Foam absorbs less than 1% of the entire energy of the impact, and accounts for less than 1% of the energy absorbed by the helmet at high impact speeds. **Thus, it is concluded that the PU Foam has little effect on the absorption properties of the helmet and its main use is rider comfort.**

5.12 Capacity of the Helmet of absorbing the Impact Energy

The helmet as previously explained, absorbs part of the impact energy; thus, it reduces the energy that goes into the head, which reduces the probability of suffering head injuries.

In order to assess how much energy is absorbed by the helmet and the dependence of the speed in the Energy absorption capabilities, the EN 1078 flat anvil test with speed variation was used because the flat anvil is the one that produces the worst-case injury scenario for the impacts. Eight simulations were made in total for this analysis.

The energy absorbed by the Helmet is compared against the energy in the entire simulation in Figure *73* below.

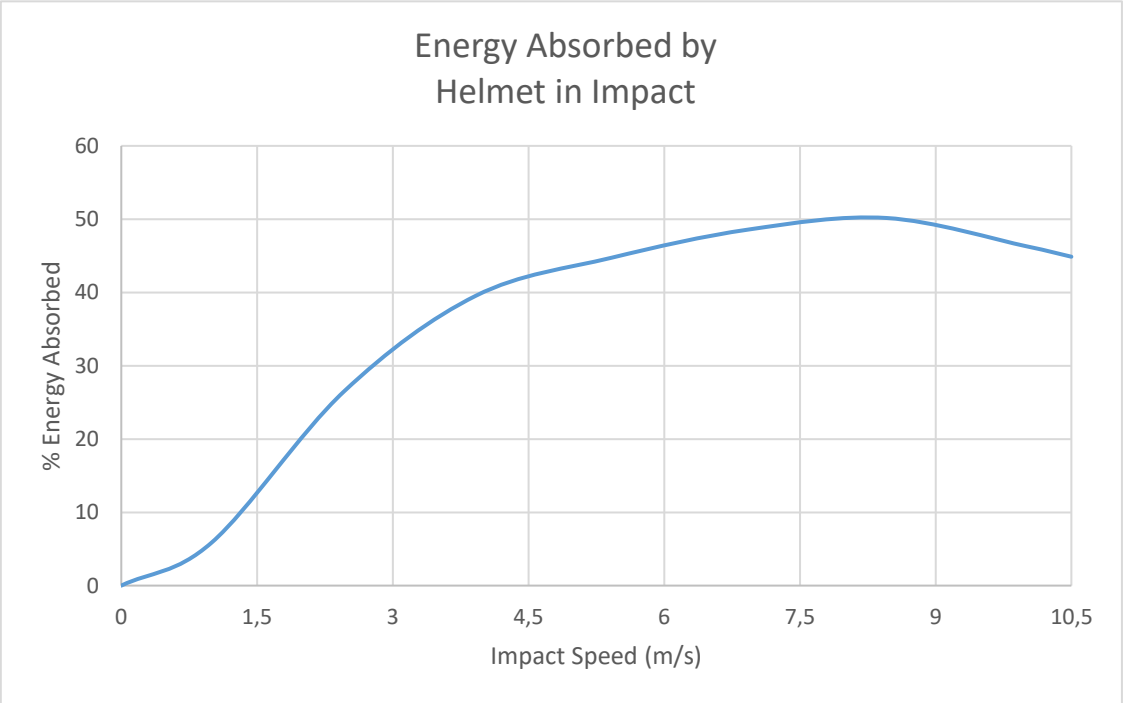

Figure 73: Energy absorbed by Helmet During the Impact.

Figure *73* shows that with increasing speed, the helmet tends to absorb more percentage of the impact Energy. The highest value is achieved at 8.46 m/s where it absorbs 50.15 % of all the impact Energy, then the percentage absorbed starts to decrease.

As it will be shown in later studies performed in this thesis, the critical speed for untreatable damage in the impact is 8.1 m/s (29.4 km/h), which means that the helmet is very effective until the critical damage point is reached.

For a regular 5.42 m/s (19.5 km/h, an EN 1078 standard test) impact, the helmet absorbs 44.7 % of the impact Energy (46.0 J out of 102.9 J).

This study concludes that the helmet is a key element in safety during bicycle accidents; the helmet under normal impact conditions can absorb up to 50.15 % of the impact energy, which otherwise would be absorbed by the head. It also shows that even at low impact speeds (less than 10 km/h or 2.77 m/s) the helmet is very useful and absorbs up to 30% of the impact energy.

Currently, regulations state that the helmet only has to be worn at all times by people under the age of 16. People older than 16 only have to wear it if they leave a city center [41].

Therefore, **it is proposed that bicycle helmets must be made mandatory for all people, regardless of age groups or road type**, since the effectiveness of the helmet has been demonstrated even at low impact speeds.

5.13 Influence of the EPS Foam Density on Head Injuries

As previously stated, there are multiple EPS Foams available on the market. In order to assess the safety and determine the ideal one for this helmet, a comparison was made with foams with a density of 14.8 kg/m^3, 31.2 kg/m^3, 50.6 kg/m^3 and 86.8 kg/m^3.

The EN 1078 flat anvil impact is used for this analysis because it is the one that produces the worst-case injury scenario for the impacts. Four simulations were made in total for this analysis.

The properties of the foams and their stress-strain curves were obtained from the thesis: "crash helmet testing" and design specifications by Van Den Bosch [26]. The stress-strain curves were digitalized using the program Plot Digitizer, and are shown below.

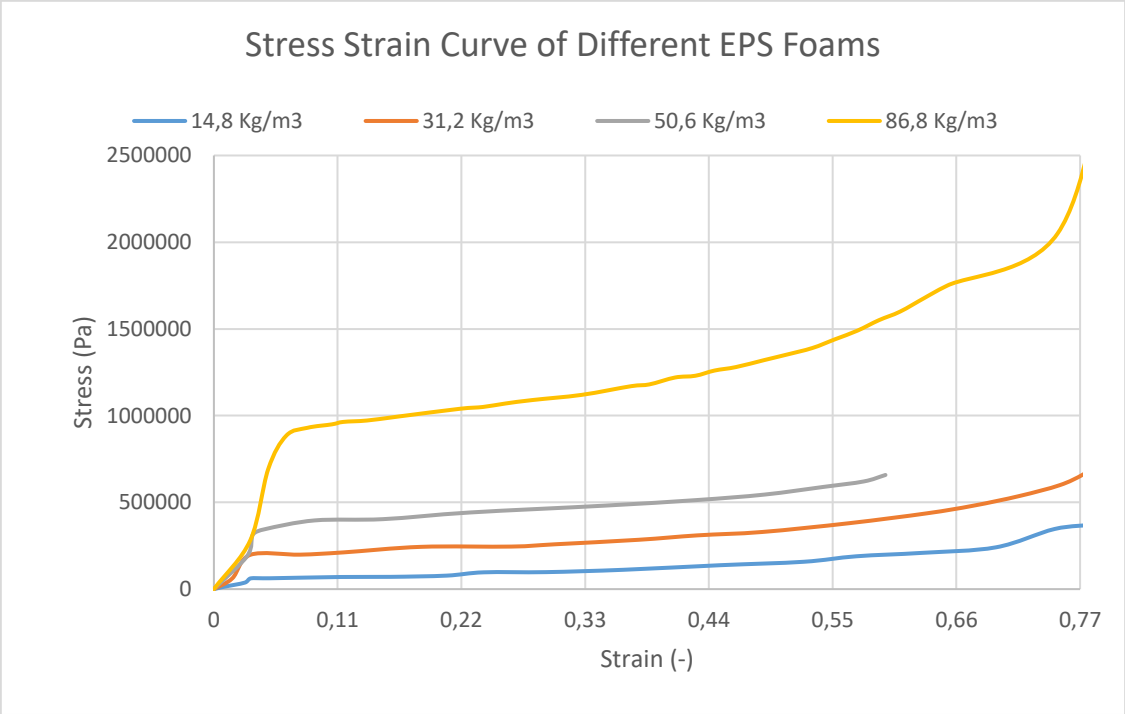

Figure 74: Stress-Strain Curves of Different EPS Foams *[26]*.

The material used to model these foams in LS-DYNA is MAT_LOW_DENSITY_ FOAM_57. The Young's Modulus also differs on each EPS Foam, and must therefore be changed, the values are shown on TABLE *18* below.

TABLE 18: YOUNG'S MODULUS OF DIFFERENT EPS FOAMS *[26]*.

Density (kg/m^3)	E (MPa)
14.8	2.1 [26]
31.2	7.8 [26]
50.6	12.0 [26]
86.8	22.4 [26]

In order to assess the changes, the acceleration-time curve of all the foams was calculated, as shown in Figure 75 below.

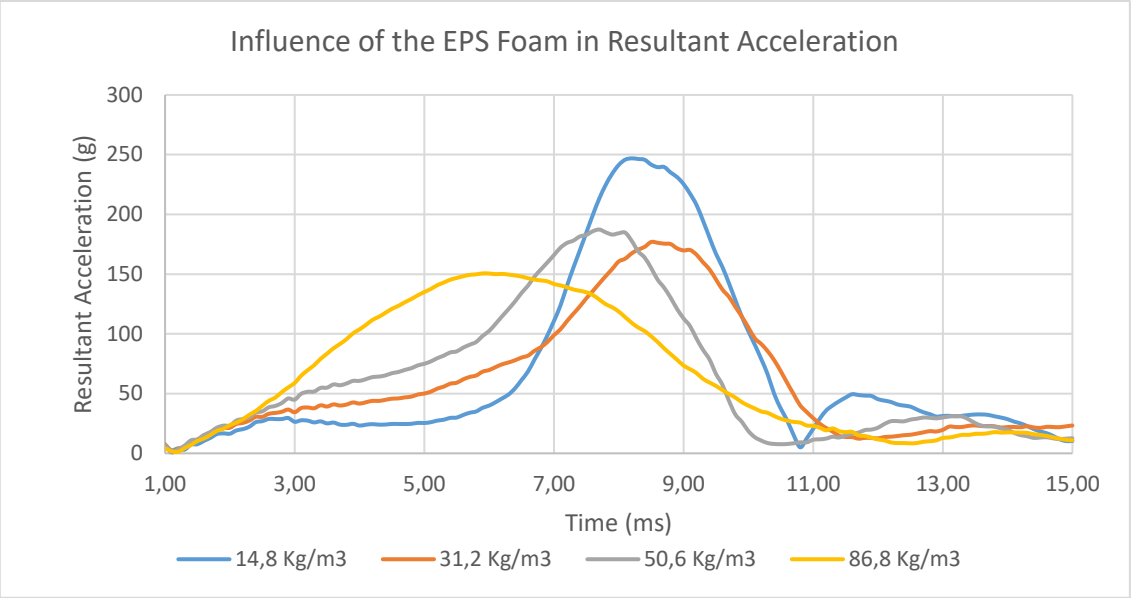

Figure 75: Resultant Head Acceleration depending on EPS Foam Density.

Figure 75 shows that the highest density foam (86.8 kg/m^3) is the one that has the largest effective impact time and lowest maximum acceleration. On the other hand, the lowest density foam (14.8 kg/m^3) has the shortest impact time, but the largest maximum resultant acceleration.

It can be noted that the lower the density, the more that the EPS deforms before it starts to pose resistance to the head, which means that the lower density foams begin to pose resistance very late in the process, and once they start doing it, they cannot deform any longer, which brings the head to a very sudden deceleration, as can be seen in the 14.8 kg/m^3 foam at the 6-7.5 ms timeframe.

The HIC criterion was chosen for Head Injury assessment since it is the most widely used and it is calculated with the results of Figure 75. The HIC time interval is also calculated, as well as the maximum acceleration of the head, which are shown in Figure 76.

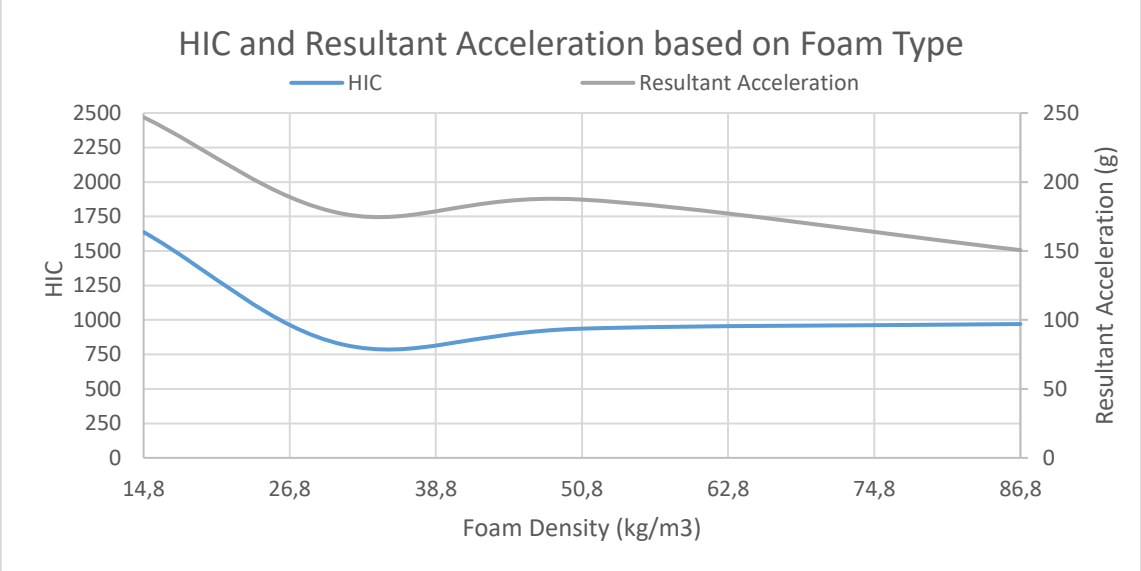

Figure 76: HIC, HIC Time Interval, and Maximum Head Acceleration depending on Foam Properties.

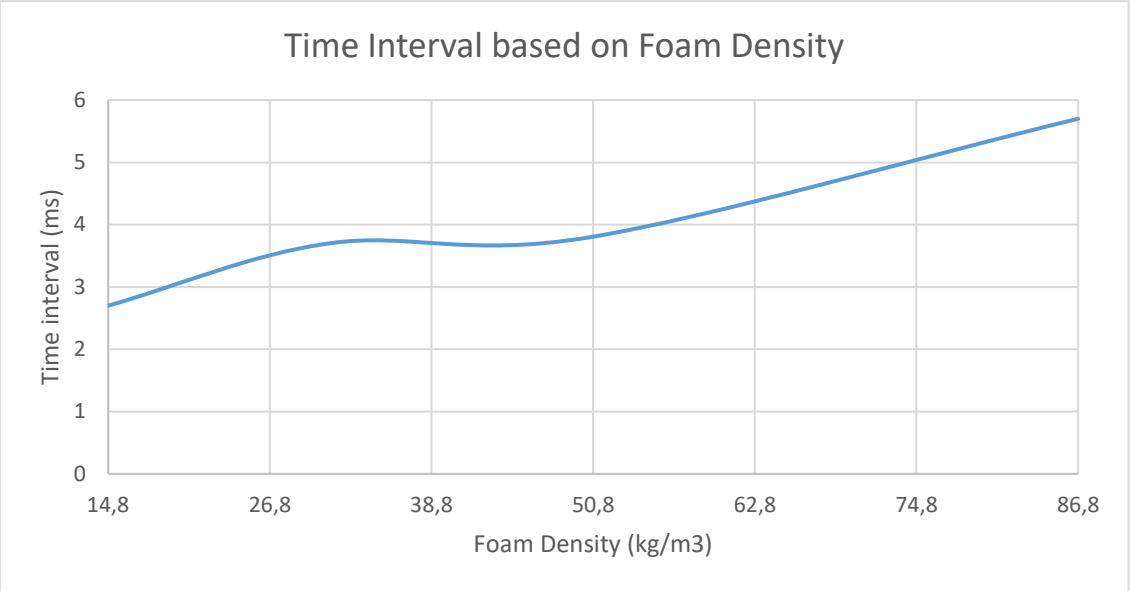

Figure 77: Time Interval depending on Foam Properties.

It is observed that the lower the density, the more abrupt the impact is, which means that the head has to absorb all the energy in a very short period of time. Moreover, the higher the density, the impact energy is distributed more evenly throughout the impact.

The loading and unloading curves differ depending on the density; the higher the density, the lower steepness of the loading and unloading curves are, which means that the head suffers less instant acceleration.

As it can be observed in Figure 76 and *Figure 77*, the highest HIC value is obtained with the lowest Foam density of 14.8 kg/m^3, and then, as the density increases, the HIC value tends to converge to a value of 950.

The time interval on which the HIC happens tends to increase as the density increases, shown in *Figure 77*, due to the energy and acceleration being more evenly distributed throughout the impact, which agrees with the acceleration-time curves shown in Figure *75*. The maximum head acceleration tends to decrease as the density increases, as shown in Figure *76*.

Therefore, **to achieve a more distributed impact, with a low HIC value and low maximum acceleration it is recommended to use an EPS Foam with a large density.**

5.14 Development of Curves for Head Injury Modes based on impact Speed

In order to assess the effect that the impact speed has on head injuries, multiple simulations were made varying impact speeds for the EN 1078 test on a flat anvil because the flat anvil test is the one that produces the worst-case injury scenario.

A total of 8 simulations with the following impact speeds were made: 1m/s, 2.4m/s, 3.92m/s, 5.4m/s, 6.93m/s, 8.46m/s, 10m/s and 10.5m/s; the curves of the resultant acceleration against time are shown in Figure *78*. Eight simulations were made in total for this analysis.

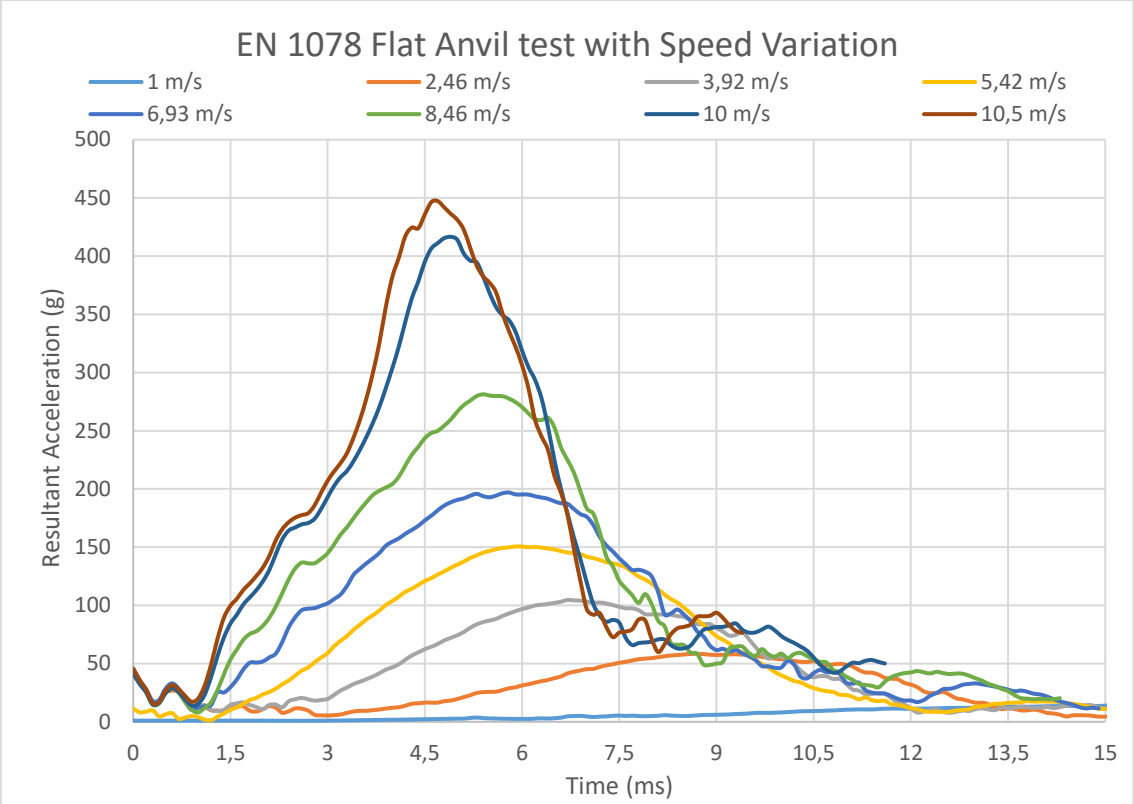

Figure 78: Resultant Head Acceleration based on Impact Speed (Flat Anvil EN 1078 Test).

Figure *78* shows that the higher the impact speed is, the higher that the maximum resultant acceleration is. The impact duration is reduced when the speed increases.

In order to assess the probability of head injuries, the HIC criterion was used since it is one of the methods most widely used. The results obtained in Figure *78* were implemented into the MATLAB code (TABLE *16*) that was designed to implement the equation number 5.2, which gave the following results:

TABLE 19: HIC VALUE AND DURATION DEPENDING ON IMPACT SPEED.

Impact Speed (m/s)	HIC	t1 (s)	t2 (s)
1	5.2	4.9	16.2
2.46	100.64	5.9	12.2
3.92	390.7	4.2	10.3
5.42	970.2	3.4	9.1
6.93	1786.2	2.7	8.3
8.46	3436.1	2.6	7.5
10	6589.6	3.1	6.7
10.5	7645.9	3.1	6.6

In order to obtain the probability of the different injury types (severe, moderate…) it was necessary to know the HIC values every 0.01m/s. There were two options to obtain these results: the first one was conducting a total of 1050 simulations to obtain each result individually, and the second one was to approximate the HIC values previously obtained as a function which is dependent of the impact speed.

The second option was chosen due to the time and storage limitations of the computer.

It was found that a polynomial function of grade 6 was the one that fitted the previously obtained results best (better than, logarithmic, exponential, potential and lineal functions), the function is shown in equation 5.5 below:

$$y = -0.2351x^6 + 7.7705x^5 - 97.951x^4 + 600.7x^3 - 1809.9x^2 + 2567.3x - 1262.8 \quad \text{for } (1 < x < 10.5) \quad \text{eqn. } 5.5$$

Where: *y* is the HIC value

x is the impact speed (m/s)

Thus, the function in equation 5.5 was implemented for speed values that range from 1 to 10.5 m/s every 0.01m/s, the results are shown in the annex A.

After the previous implementation, the HIC-probability of Injury curve was obtained from the Forensic Injury Biomechanics paper by Wilson C. Hayes et al. [37]. The curve was digitalized using Plot Digitizer. This curve determines the probability of injury based on the different injury modes (minor, moderate, serious, severe, critical and maximum injuries) and HIC value. The meaning of each injury mode is shown in TABLE *20* below:

TABLE 20: SEVERITY CODE EXPLAINED *[37]*.

AIS CODE	Severity Code	Fatality rate (range %)
1	Minor	0.0
2	Moderate	0.1–0.4
3	Serious	0.8–2.1
4	Severe	7.9–10.6
5	Critical	53.1–58.4
6	Maximum	Untreatable

Knowing the injury probability based on the HIC value and knowing the HIC value based on the impact Speed (eqn. 5.5), the curves shown in Figure *79* were developed.

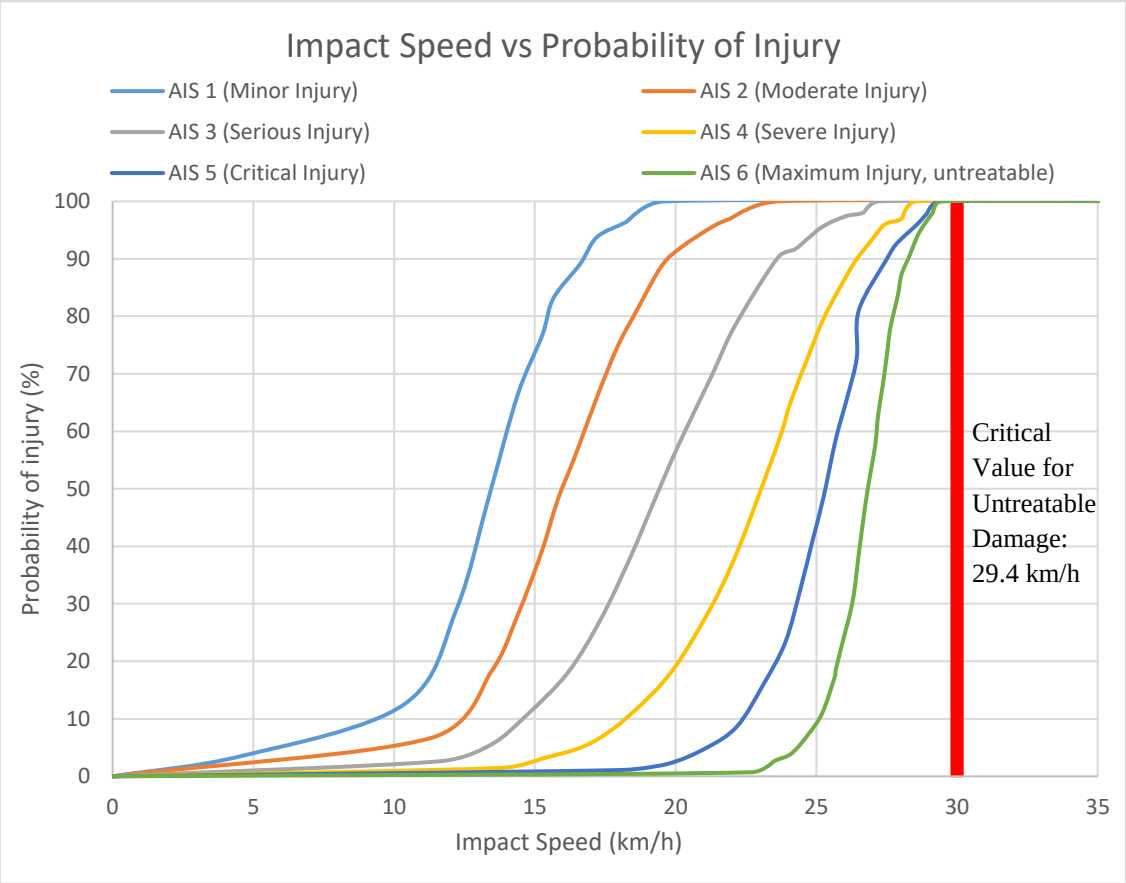

Figure 79: Curves for Development of Head Injury Modes based on Impact Speed.

The curves developed in Figure *79* determine the head injury modes based on impact speed against a flat anvil wearing a Bicycle helmet, and show the following results:

- From the curves, it is observed that minor injuries (minor and moderate) start to have a high probability of occurrence when the impact speed is over 20 km/h (5.55 m/s) and they start to happen at 10 km/h (2.77 m/s).
- Severe injuries (serious and severe) start to occur with a speed of 15 km/h and have a high probability of occurrence at 27 km//h (7.5 m/s).
- The most extreme injuries (critical and maximum) start to happen at 20 km/h (5.55 m/s). The critical value for untreatable damage in the impact is 29.4 km/h.

Even though the effectiveness of the helmet has been proven in this study, it has also been found that at high speeds (more than 29.4 km/h) the cyclist can suffer untreatable damage; therefore, new research on helmets and cyclist safety is required to increase the likelihood of survival.

Based on the previous probability findings, it is possible to recommend a speed limit for the bicycle users to limit the probability of serious injuries. It must be noted that the speed limitation should be within reasonable parameters so that the bicycle still is a fast and convenient method of commuting and exercising, and it must also be noted that the curves previously developed are for the worst-case-impact scenario.

As of now, the main limitation on bicycle speed in Spain are set by the DGT (Dirección General de Tráfico) with a speed limit of 45 km/h [42]. According to the Boletín Oficial

del Estado (885-2014 Interior) of Spain, [43], in order to promote the use of bicycles, many streets within the cities will be limited to 30 km/h.

A full implementation of the speed limitation to 30 km/h started to take place in the year 2018 in large cities such as Madrid [44] with the introduction of new shared pathways for bicycles and cars. This means that in these pathways, bicycles also have a speed limit of 30 km/h.

Regarding electric bikes, the European Normative, as well as the normative in Spain, states that assisted electric bikes are the ones that reach 25 km/h without pedaling input from the rider [45].

A maximum speed of 20 km/h means that the minor injuries have more than 90% of probability, the severe injuries have between 20% and 60% of happening and the most severe injuries have less than 3% probability of happening.

Using the electric input, electric bikes can reach 25 km/h, at this speed untreatable damage has 9% probability of occurrence and critical injury has 44% probability. Therefore, it **is proposed to limit the maximum speeds of electric bikes so that they can reach a maximum of 20 km/h without pedaling input** to keep the most severe and extreme injury modes within reasonable values during the worst-case-scenario impact.

Cyclist have to follow the traffic rules [46]; therefore, they have the same speed limits as other vehicles (with a maximum of 45 km/h) on all roads, even though they are less protected, when compared, for example, to cars and trucks. Using the new implementation of slower pathways (30 km/h) for shared use between cars an bicycles in the cities; and knowing that setting a 20 km/h speed limit on bicycles greatly diminishes the injury modes, **it is proposed to lower bicycle speed limits to 20 km/h in shared pathways in the cities** to keep the most severe and extreme injury modes within reasonable values during the worst-case-scenario impact**.**

6. CONCLUSIONS

6.1 Objectives Accomplished

The main hypothesis of this thesis was that the results obtained would be able to assess the importance of bicycle helmets on rider's safety, and it would also help to identify the main injuries that might happen during the impact.

- The main hypothesis was deemed correct since the results obtained from this thesis state that up to 50.15% of the total impact energy is absorbed by the helmet, which means that helmets are a key element to improve safety.
- The main injuries that happen under the EN 1078 standard have also been identified and will be explained in the following section of the document.

These previous hypotheses were achievable since the helmet that was simulated has been validated against previous real-life experiments and simulations. It only differs in 15.3% in the maximum head acceleration and 4.5% in impact duration with the previous studies.

The difference in head acceleration and impact duration is due to multiple reasons, the most important ones being the helmet model, which differs with those of the previous studies, and the validated FEA head that has been used. The validation that has been made gives legitimacy to the derived results.

The main impact scenario that was to be replicated was the EN 1078 energy absorption test on a flat anvil. Moreover, additional tests such as using a curbstone anvil, changing the impact speeds and EPS Foam properties have been done, the results will be assessed later in the following sections of the document.

6.1.1 Conclusions of Initial Steps and Procedures

Helmet Design:

- The real helmet available on the market has been replicated using a three-dimensional coordinate system. It has achieved high fidelity by using the CAD Software CATIA, which has allowed to replicate all the elements of the helmet: rear and chin straps, shell, EPS Foam, PU Foam, upper, side and rear padding.

Helmet Adaptability for further designs and analyses:

- Moreover, the helmet has been designed and implemented in such a way that it allows for future "nimble modifications". Meaning that parameters such as the thickness of the EPS Foam, geometry and location of the ventilation holes can easily be changed in order to assess the increase or decrease in safety.

Meshing technique used to obtain an accurate geometrical mesh:

- The meshing implemented has also been able to adapt to the exact geometry of the three-dimensional design due to the development of multiple meshing techniques that allow for a meshing of the most critical parts.

- The most crucial development was meshing the EPS Foam using the “solid map” and “solid edit” command by dividing the solid part into 38 mappable solids.

Mesh element type implemented:

- Further development in the mesh was seen in the element type used, since all the previous studies used tri and tetrahedral elements, and the techniques used for this thesis allowed for meshing with quadrilateral and hexahedral elements. This has a significant outcome in the convergence time of the simulations and can help increase the accuracy of the results.

Mesh adaptability and convenience for entire impact set-up:

- The number of elements used for the helmet in the simulation is also considered adequate since it accounts for 19.8% and 17% of all the elements used in the simulation including the FEA head and the anvils.

6.1.2 Head Injury Conclusions based on the Final Simulation Results

Regarding the final simulations performed with the validated FEA head provided by the Japan Automotive Research Institute, the following results were obtained.

The resultant acceleration-time curve results were validated for the EN 1078 Flat anvil case previously explained, and for the EN 1078 curbstone test the set-up was deemed correct (no absolute validation could be done due to the lack of abundant data from previous studies).

Therefore, the two tests were used for assessing the head injuries that might have occurred under the EN 1078 shock absorption capacity test, as shown below:

The Peak Linear Acceleration (PLA) deemed that:

- For the EN 1078 flat anvil test: a 50% probability of skull fracture and a 75% of probability of concussion would occur.
- For the EN 1078 curbstone anvil test: a 50% of probability of concussion would occur but it would not generate skull fracture.

The Gadd Severity Index (GSI) deemed that:

- For the EN 1078 flat anvil test: a GSI value of 1086.6 meant that the impact would incur in serious internal head injuries.
- For the EN 1078 curbstone anvil test: a GSI value of 259.15 meant that the impact would not incur in serious internal head injuries.

The Head Injury Criterion (HIC_{15} and HIC_{36}) deemed that:

- For the EN 1078 flat anvil test there is a 100% probability of minor injury, 88% of moderate injury, 49% of serious injury, 15% probability of severe injury, 2% of critical injury and 0% of maximum injury.

- For the curbstone anvil test it was found that there is a 20% probability of minor injury, 7% of moderate injury, 3% of serious injury, 0% probability of severe injury, 0% of critical injury and 0% of maximum injury.

The Head Protection Criterion (HPC) is similar to the Head Injury criterion; therefore, it yielded the same results as the HIC test previously explained.

Diffuse Axonal Injuries (DAI) were assessed for both tests and the results were the following:

- For the EN 1078 flat anvil test the results of this analysis did not reach the 50% probability of DAI, but it is within 1% of stress difference to reach the 50% probability threshold.
- For the EN 1078 curbstone anvil test the result of this analysis does not reach the threshold to sustain a 50% probability of DAI, it has a 39.9% difference of stress to reach the 50% probability threshold.

Skull fracture probability under impacts was determined using a probability function developed by Philemon Chan [1]:

- For the EN 1078 flat anvil test the result of this analysis predicts a probability of 14.04% of skull fracture, a lower value than that proposed by the PLA criterion.
- For the EN 1078 curbstone anvil test the result of this analysis predicts a probability of 0.13% of skull fracture.

The 3 MS Criterion (A3MS) criterion deemed that:

- For the EN 1078 flat anvil test the impact does not meet the A3MS criterion since it has more than 80 g for a period of 5.3ms. Therefore, this impact would not meet the criteria which is required by multiple regulations.
- For the EN 1078 curbstone anvil test the impact meets the A3MS criterion because at no point this simulation reaches 80 g.

The 5 MS Criterion (A3MS) criterion deemed that:

- For the EN 1078 flat anvil test the impact meets the A5MS criterion since it only reaches a value higher than 150 g during 0.3ms.
- For the EN 1078 curbstone anvil test the impact meets the A5MS criterion because at no point this simulation reaches 150 g.

6.1.3 Conclusions of other Analyses to Test the Safety of the Bicycle Helmet and its Individual Components

Influence of the Straps in the Simulation:

The results of the simulation show the importance of the modeling the straps in the simulation, as can be seen in the graphical sequences shown in Figure *68* and Figure *69*. The straps keep the head attached to the helmet at the end of the impact, which may lead to obtaining more accurate results.

The straps are not used in many of the previously mentioned studies, which may be a big influence factor in their results. Therefore, **it is proposed for all future simulations the use of straps in the simulation to achieve closer results to real impacts.**

Influence of the Padding (PU Foam) in absorbing the Impact Energy:

The PU Foam absorbs 1% of the entire impact energy at low speeds (less than 3 m/s), at that speed it absorbs 20% of the total energy absorbed by the helmet.

As speed increases (larger than 3 m/s) the energy absorbed in the entire impact converges to a value of approximately 0.38% and to 0.8% in the percentage of energy absorbed in the helmet.

Therefore, it is concluded that **the PU Foam has almost no effect on the absorption properties of the helmet and its main use is rider comfort.**

Capacity of the Helmet to absorb Energy depending on Impact Speed:

The EN 1078 flat anvil test was used with speed variations to test the energy absorption capabilities of the helmet depending on the impact speed.

It was found that with increasing speed, the helmet absorbs a higher percentage of energy. At 8.46 m/s is where it absorbs the maximum amount of impact energy 50.15 %. Then, the percentage absorbed starts to decrease. The critical speed for untreatable damage in the impact is 8.1 m/s (29.4 km/h), which means that the helmet is very effective until the critical damage point is reached.

For a regular 5.42 m/s (19.5 km/h, an EN 1078 standard test) impact, the helmet absorbs 44.7 % of the impact Energy (46.0 J out of 102.9 J).

The previous findings conclude that the helmet can absorb up to 50.15 % of the impact energy, which otherwise would be absorbed by the head. Even at low impact speeds the helmet absorbs up to 30% of the impact Energy.

Currently, under the regulations, the helmet only has to be worn at all times by people under the age of 16 and people older than 16 only if they leave a city center [41]. Therefore, **it is proposed that bicycle helmets must be made mandatory for all people, regardless of age groups or road type**, since the effectiveness of the helmet has been demonstrated even at low impact speeds.

Influence of the EPS Foam Density on Head Injuries

Four different densities of EPS Foam (14.8 kg/m^3, 31.2 kg/m^3, 50.6 kg/m^3 and 86.8 kg/m^3) were used to assess multiple aspects of helmet absorption capabilities. The main results obtained were the HIC values, HIC time interval acceleration-impact time curves, and maximum acceleration in the head.

It was found that the highest density foam (86.8 kg/m^3) is the one that has the largest effective impact time and lowest maximum acceleration. On the other hand, the lowest density foam (14.8 kg/m^3) has the shortest impact time, but the largest maximum resultant acceleration.

The lower the EPS density, the more abrupt the impact is, which means that the head has to absorb all the energy in a very short period of time. Moreover, the higher the density, the impact energy is distributed more evenly throughout the impact.

The highest HIC value happens with the lowest Foam density 14.8 kg/m^3, and then, as the density increases, the HIC value tends to converge to a value of 950.

The time interval on which the HIC happens tends to increase as the density increases, due to the energy and acceleration being more evenly distributed, which agrees with the acceleration-time curves developed. The maximum head acceleration tends to decrease as the density increases.

Therefore, to **achieve a more distributed impact, with a low HIC value and low maximum acceleration it is recommended to use an EPS Foam with a large density.**

Development of Curves for Head Injury Modes Based on Impact Speed.

In order to assess the effect that the impact speed has on head injuries, multiple simulations were made changing the speeds (1 m/s, 2.4 m/s, 3.92 m/s, 5.4 m/s, 6.93 m/s, 8.46 m/s, 10 m/s and 10.5 m/s) for the EN 1078 test on a flat anvil.

The HIC criterion was used, and a function was developed to obtain the HIC value based on the impact Speed. Afterwards, the HIC-probability of Injury curve was obtained from the Forensic Injury Biomechanics by Wilson C. Hayes et al. [37].

Knowing the injury probability based on the HIC value and knowing the HIC value based on the impact speed, curves that show injury probability based on impact speed were developed. The most meaningful results of the curves are the following:

- From the curves, the minor injuries (minor and moderate) start to occur with speeds of 20 km/h (5.55 m/s) and start to happen at 10 km/h (2.77 m/s).
- The severe injuries (serious and severe) start to occur with a speed of 15 km/h and have a high probability of occurrence at 27 km//h (7.5 m/s).
- The most extreme injuries (critical and maximum) start to happen at 20 km/h (5.55 m/s). The critical value for untreatable damage in the impact is 29.4 km/h.

Even though the effectiveness helmets has been proven in this study, it has also been found that at high speeds (more than 29.4 km/h) the cyclist can suffer untreatable damage in the worst-case-scenario impact. Thus, new research to optimize helmet designs for high speed impacts, the introduction of new materials and new laws to increase safety are required to increase the likelihood of cyclist survival.

Based on the curves for head injury modes developed in this thesis, it was found that a speed of 20 km/h means that the minor injuries have over 90% of occurrence probability, severe injuries have between 20% and 60% probability, and the most extreme injuries have less than 3% probability of occurrence. Therefore, at 20 km/h the probability of occurrence of the most extreme injury modes is kept at reasonable values in the worst-case-scenario impact.

Due to the increasing implementation of slower pathways with a 30 km/h speed limit for shared use between cars an bicycles in the cities and knowing that at 30 km/h untreatable damage can happen in the worst-case-scenario impact, a lower speed limit is needed for cyclist to lower the probability of critical injuries. Knowing that a 20 km/h speed limit on bicycles greatly diminishes the probability of the most extreme injury modes**; it is proposed to lower the bicycle speed limits from 30 km/h to 20 km/h in the shared pathways of the cities** to keep the most severe and extreme injury modes within reasonable values during the worst-case-scenario impact.

The European and Spanish normative states that assisted electric bikes can reach 25 km/h without input from the rider [45]. At 25 km/h untreatable damage has 9% probability of occurrence and critical injury has 44% probability . Thus, it **is proposed to limit the maximum speed of electric bikes so that they can reach a maximum of 20 km/h without pedaling input** to keep the most severe and extreme injury modes within reasonable values during the worst-case-scenario impact.

6.2 Future Lines of Work

1. A further improvement of the FEA analyses could include artificial ageing of the material properties, which could be done by changing the material properties to include the effects that age and weather can have.

2. Additional improvement of the FEA analyses could include a test of the helmet at extremely high and low temperatures (-20ºC, +45ºC) which would simulate the most adverse scenarios on which a helmet could be used. This would be done by changing the material properties to the ones that the helmet has at those temperatures.

3. Testing all the standards with the same FEA helmet, which would give significant data on how much energy is absorbed by the helmet on each standard. Therefore, the most thorough helmet standard could be determined.

4. Performing the “determination of retention system strength and ease of release” test, which would give further information on how much stress is required for the straps to become detached from the head.

5. Testing the influence of changing the dynamic and static coefficient friction in the acceleration results; which can show the importance of the roughness of the materials used for the helmet and the effect that each ground type (grass, steel, rock) can have in the outcome of the analyses.

6. Testing the helmet impact that has been simulated in this thesis using a real head dummy and the real helmet. This test is expected to take place in the summer of 2019 at the laboratories of Universidad Carlos III de Madrid.

7. REFERENCES

[1] P. Chan, Z. Lu, P. Rigby, E. Takhounts, J. Zhang, N. Yoganandan and F. Pintar, "Development of a generalized linear skull fracture criterion,," *Journal of Chemical Information and Modelling,* vol. 53, pp. 1-11, 2007.

[2] European Road Safety Observatory, "European Commission, Traffic Safety Basic Facts on Cyclists," June 2018. [Online]. Available: https://ec.europa.eu/transport/road_safety/sites/roadsafety/files/pdf/statistics/dacota/bfs20xx_cyclists.pdf. [Accessed 31 Marzo 2019].

[3] National Highway Traffic Safety Administration, U.S Department Of Transportation, "Bicyclists and Other cyclists," 2018 May. [Online]. Available: https://crashstats.nhtsa.dot.gov/Api/Public/ViewPublication/812507. [Accessed 31 Marzo 2019].

[4] Save Life Foundation, "Road Statistics Involving Bicycle Users in India," 28 November 2017. [Online]. Available: http://savelifefoundation.org/wp-content/uploads/2017/11/Road-Statistics-Involving-Bicycle-Users_111017.pdf. [Accessed 31 March 2019].

[5] I. Popa, O. E. Ferraro, C. Orsi, A. Morandi and C. Montomoli, "Bicycle helmet use patterns in Italy. A description and analysis of survey data from an Italian friends of cycling association," *Elsevier: Accident Analysis and Prevention,* vol. 108, pp. 268-274, 2017.

[6] P. L. Ramage-Morin, "Cycling in Canada," Statistics Canada, Canada, 2017.

[7] M. Sandberg, K. M. Tse, L. B. Tan and H. P. Lee, "A computational study of the EN 1078 impact test for bicycle helmets using a realistic subject-specific finite element head model," *Computer Methods in Biomechanics and Biomedical Engineering,* pp. 1-9, 2018.

[8] CEN, European Comitte for Standardization, "Helmets for pedal cyclists and for users of skateboards and roller skates," EUROPEAN STANDARD, Brussels, 1997.

[9] BELL HELMETS, "HISTORY & FACTS," 2019 Bell Helmets Europe s.a - All rights reserved., 2019. [Online]. Available: https://www.bellracing.eu/about-us/history-and-facts.html. [Accessed 2 April 2019].

[10] Dirección General De Tráfico, "Las bicis y las motos protagonistas de la nueva campaña de concienciación de la DGT.," DGT, Gobierno de España, Ministerio del Interior, 2016. [Online]. Available: http://www.dgt.es/es/prensa/notas-de-

prensa/2016/20160520-bicis-y-motos-protagonistas-nueva-campania-concienciacion-dgt.shtml. [Accessed 02 April 2019].

[11] London Department for transport, "Bicycle Helmets - A review of their effectiveness: A critical Review of the Literature, Road Safety Research Report No. 30," 2002. [Online]. Available: http://dacota-project.eu/Links/erso/knowledge/Fixed/40_Pedestrians/ref.%2054%20helmets.pdf. [Accessed April 02 2019].

[12] T. A. Conno, S. Meng, D. Zouzias, R. Burek, A. Cernicchi, G. D. Bruyne, M. Gilchrist, P. Halldin and J. Ivans, "Current Standards for Sports and Automotive Helmets: A review," Head Protection: A European Training Network for Advanced Designs in Safety, 2016.

[13] Consumer Product Safety Commission, "Bicycle Helmets Business Guidance," CPSC, [Online]. Available: https://www.cpsc.gov/Business--Manufacturing/Business-Education/Business-Guidance/Bicycle-Helmets. [Accessed 04 April 2019].

[14] United States Census Bureau, "U.S. Census Bureau Current Population," United States Census Bureau, 04 April 2019. [Online]. Available: https://www.census.gov/popclock/print.php?component=counter. [Accessed 04 April 2019].

[15] Standards Australia/Standards New Zealand, "Australian/New Zealand Standard, Bicycle Helmets," December, Sydney & Wellington, 2009.

[16] General Administration of Quality Supervision, Inspection and Quarantine of the People's Republic of China, "Sports helmets - Safety requirements for sports helmets for cyclists and users of skateboards and roller skates," National Standard, 2009.

[17] European Committee for Standarization, "What is a European Standard (EN)?," [Online]. Available: https://www.cencenelec.eu/standards/DefEN/Pages/default.aspx. [Accessed 08 April 2019].

[18] M. Bíla, M. Dobiášb, R. Andrášika, M. Bílováa and P. Hejnac, "Cycling fatalities: When a helmet is useless and when it might save your life," *Elsevier, Safety Science*, no. 105, pp. 71-76, 2018.

[19] N. Mills and A. Gilchrist, "Finite-element analysis of bicycle helmet oblique impacts," *Elsevier, International Journal of Impact Engineering*, no. 35, pp. 1087-1101, 2008.

[20] A. AG, V. d. P. G, V. I and G. J, "A TRANSIENT FINITE ELEMENT STUDY REVEALS THE IMPORTANCE OF THE BYCICLE HELMET MATERIAL PROPERTIES ON HEAD PROTECTION DURING AN IMPACT," *Proceedings*

of the International Research Council on the Biomechanics of Injury conference, no. 37, pp. 357-360, 2009.

[21] T.-L. Teng, C.-L. Liang and V.-H. Nguyen, "Development and validation of finite element model of helmet impact test," *Journal of Materials Design and Applications,* vol. I, no. 227, pp. 82-88, 2012.

[22] G. Milne, C. Deck, R. Carreira, Q. Allinne and R. Willinger, "Development and validation of a bicycle helmet: assessment of head injury risk under standard impact conditions," *Computer Methods in Biomechanics and Biomedical Engineering,* vol. 15, no. S1, pp. 309-310, 2012.

[23] G. Milne, C. Deck, N. Bourdet, R. Carreira, Q. Allinne, A. Gallegob and R. Willinger, "Bicycle helmet modelling and validation under linear and tangential impacts," *International Journal of Crashworthiness,* vol. 19, no. 4, pp. 323-333, 2014.

[24] H. Mustafa, T. Y. Pang, T. Perret-Ellena and A. Subic, "Finite element bicycle helmet models development," *Elsevier,* no. 20, pp. 91-97, 2015.

[25] M. Fahlstedt, P. Halldin and S. Kleiven, "The protective effect of a helmet in three bicycle accidents—A finite element study," *Elsevier, Accident Analysis and Prevention,* no. 91, pp. 135-143, 2016.

[26] H. L. A. v. d. Bosch, Crash Helmet Testing and Design Specifications, Eindhoven: Technische Universiteit Eindhoven DOI: 10.6100/IR613094, 2006.

[27] D. Brands, J. Thunnissen and J. Wismans, "Modelling Head Injury Countermeasures: a 3D helmet model," *Proceedings of the AGARD Specialists' Meeting on Impact Head Injury*, pp. 26-1 to 26-8, 1997.

[28] J. ANTONA-MAKOSHI, THESIS FOR THE DEGREE OF DOCTOR OF PHILOSOPHY In MACHINE AND VEHICLE SYSTEMS: "Traumatic Brain Injuries: Animal Experiments and Numerical Simulations to Support the Development of a Brain Injury Criterion", Gothenburg, Sweden: Vehicle Safety Division, Department of Applied Mechanics, CHALMERS UNIVERSITY OF TECHNOLOGY, 2016.

[29] LS-Dyna, "LS-Dyna Support Contact Types," [Online]. Available: https://www.dynasupport.com/tutorial/contact-modeling-in-ls-dyna/contact-types. [Accessed 15 May 2019].

[30] Y. PENG, C. DECK, J. YANG, D. OTTE and R. WILLINGER, "A Study of Adult Pedestrian Head Impact Conditions and Injury Risks in Passenger Car Collisions Based on Real-World Accident Data," *Taylor & Francis Group, Traffic Injury Prevention,* no. 14, pp. 639-646, 2013.

[31] A. S. Mcintosh, D. A. Patton, B. Frechede, P.-A. Pierre and E. Ferry, "The Biomechanics of Concussion in Unhelmeted Australian Football Players," *British medical journal, British Medical Association,* vol. 4, no. (5), pp. 1-41, 2014.

[32] J. Hutchinson, M. J. Kaiser and H. M. Lankarani, "The Head Injury Criterion (HIC) functional," *Applied Mathematics and Computation,* no. 96, pp. 1-16, 1998.

[33] L. Nokes, A. Roberts and B. Knight, "Use of the Gadd severity index in forensic medicine: a case study," *Forensic Science International,* no. 76, pp. 85-90, 1995.

[34] C. W. Gadd, "CRITERIA FOR INJURY POTENTIAL," *Impact Acceleration Stress, A symposium,* pp. 141-144, 1961.

[35] H. Kimpara, Y. Nakahira, M. Iwamoto, S. Rowson and S. Duma, "Head injury prediction methods Based on 6 Degree of Freedom Head Acceleration Measurements during Impact," *International Journal of Automotive Engineering,* vol. 2, pp. 13-19, 2011.

[36] K.-U. Schmitt, P. F. Niederer, D. S. Cronin, M. H. Muser and F. Walz, Trauma Biomechanics, An introduction to Injury Biomechanics, Berlin Heidelberg: Springer, ISBN: 978-3-642-53920-6, 2014.

[37] W. C. Hayes, M. S. Erickson and E. D. Power, "Forensic Injury," *Annual Review of Biomedical Engineering,* vol. 9, pp. 55-86, 2007.

[38] J. M. Meythaler, J. D. Peduzzi, E. Eleftheriou and T. A. Novack, "Current Concepts: Diffuse Axonal Injury–Associated Traumatic Brain Injury," *Archives of Physical Medicine and Rehabilitation,* vol. 82, pp. 1461-1471, 2001.

[39] M. V. Vorst, P. Chan, J. Zhang, N. Yoganandan and F. Pintar, "US National Library of Medicine, National Institutes of Health," THE ASSOCIATION FOR THE ADVANCEMENT OF AUTOMOTIVE MEDICINE, 2004. [Online]. Available: https://www.ncbi.nlm.nih.gov/pmc/articles/PMC3217435/. [Accessed 30 May 2019].

[40] K.-U. Schmitt, P. F. Niederer, M. H. Muser and F. Walz, Trauma Biomechanics, Accidental Injury in Traffic and Sports DOI: 10.1007/978-3-642-03713-9, Berlin: Springer, 2010.

[41] ABC Motor, "¿Es obligatorio el casco en bicicleta?," *ABC,* 04 July 2018.

[42] Dirección General de Tráfico, "Limites de Velocidad en Vías Interurbanas," DGT, 2018. [Online]. Available: http://revista.dgt.es/es/sabia-que/normas/2018/0103velocidad-a-la-que-debe-circular.shtml#.XPmfs4gzZPY. [Accessed 06 June 2019].

[43] Agencia Estatal, "Boletín Oficial del Estado," MINISTERIO DE LA PRESIDENCIA RELACCIONES CON LAS CORTES E IGUALDAD, 20

November 2014. [Online]. Available: https://www.boe.es/buscar/doc.php?id=CE-D-2014-885. [Accessed 12 June 2019].

[44] M. Á. MEDINA, "La ordenanza de movilidad limita desde hoy la velocidad a 30 kilómetros por hora en las calles de un carril de Madrid," *El País*, 24 October 2018.

[45] DGT, "Dirección General de Tráfico (Tráfico y Seguridad vial)," 31 May 2019. [Online]. Available: http://revista.dgt.es/es/noticias/nacional/2019/05MAYO/0531-Bicis-electricas-NP.shtml#.XQDbMIgzaUk. [Accessed 2019 June 2019].

[46] Movilidad y transportes, oficina de la bici, "Preguntas frecuentes sobre la bicicleta en la ciudad," Portal web del Ayuntamiento de Madrid, [Online]. Available: https://www.madrid.es/portales/munimadrid/es/Inicio/Movilidad-y-transportes/Oficina-de-la-bici/Preguntas-frecuentes-sobre-la-bicicleta-en-la-ciudad?vgnextfmt=default&vgnextoid=d7a45b1f61fc8210VgnVCM2000000c205a0aRCRD&vgnextchannel=125331dc4f768210VgnVCM20. [Accessed 12 June 2019].

[47] J. Antona-Makoshi, S. Holcombe, Koshiro Ono and J. Davidsson, "Development of a Brain Injury Criterion and Associated Thresholds".

ANNEX A

Results for function in equation 5.5 implemented for speed values that range from 1m/s to 10.5m/s every 0.01m/s:

Impact Speed (m/s)	HIC Value	Impact Speed (m/s)	HIC Value	Impact Speed (m/s)	HIC Value	Impact Speed (m/s)	HIC Value
1	4.88	4	411.37	7	1822.46	10	6560.2
1.01	8.78	4.01	414.85	7.01	1829.68	10.01	6582.59
1.02	12.58	4.02	418.35	7.02	1836.93	10.02	6604.96
1.03	16.28	4.03	421.87	7.03	1844.23	10.03	6627.29
1.04	19.88	4.04	425.39	7.04	1851.56	10.04	6649.6
1.05	23.38	4.05	428.93	7.05	1858.94	10.05	6671.88
1.06	26.78	4.06	432.48	7.06	1866.35	10.06	6694.13
1.07	30.09	4.07	436.04	7.07	1873.81	10.07	6716.35
1.08	33.31	4.08	439.62	7.08	1881.3	10.08	6738.53
1.09	36.43	4.09	443.2	7.09	1888.84	10.09	6760.67
1.1	39.47	4.1	446.8	7.1	1896.42	10.1	6782.78
1.11	42.42	4.11	450.41	7.11	1904.04	10.11	6804.85
1.12	45.28	4.12	454.03	7.12	1911.7	10.12	6826.87
1.13	48.06	4.13	457.67	7.13	1919.4	10.13	6848.85
1.14	50.75	4.14	461.31	7.14	1927.15	10.14	6870.79
1.15	53.36	4.15	464.96	7.15	1934.94	10.15	6892.68
1.16	55.89	4.16	468.63	7.16	1942.77	10.16	6914.53
1.17	58.34	4.17	472.31	7.17	1950.65	10.17	6936.32
1.18	60.72	4.18	476	7.18	1958.57	10.18	6958.06
1.19	63.01	4.19	479.69	7.19	1966.54	10.19	6979.75
1.2	65.24	4.2	483.4	7.2	1974.55	10.2	7001.39
1.21	67.39	4.21	487.12	7.21	1982.6	10.21	7022.97
1.22	69.46	4.22	490.85	7.22	1990.7	10.22	7044.48
1.23	71.47	4.23	494.59	7.23	1998.85	10.23	7065.94
1.24	73.41	4.24	498.34	7.24	2007.04	10.24	7087.34
1.25	75.28	4.25	502.1	7.25	2015.28	10.25	7108.67
1.26	77.08	4.26	505.87	7.26	2023.56	10.26	7129.93
1.27	78.82	4.27	509.65	7.27	2031.89	10.27	7151.13
1.28	80.49	4.28	513.43	7.28	2040.27	10.28	7172.26
1.29	82.1	4.29	517.23	7.29	2048.7	10.29	7193.32
1.3	83.66	4.3	521.03	7.3	2057.17	10.3	7214.3
1.31	85.15	4.31	524.85	7.31	2065.69	10.31	7235.2
1.32	86.58	4.32	528.67	7.32	2074.26	10.32	7256.03
1.33	87.95	4.33	532.51	7.33	2082.88	10.33	7276.78
1.34	89.27	4.34	536.35	7.34	2091.55	10.34	7297.45
1.35	90.53	4.35	540.2	7.35	2100.27	10.35	7318.03
1.36	91.74	4.36	544.05	7.36	2109.04	10.36	7338.53
1.37	92.9	4.37	547.92	7.37	2117.85	10.37	7358.94
1.38	94.01	4.38	551.79	7.38	2126.72	10.38	7379.26

Impact Speed (m/s)	HIC Value	Impact Speed (m/s)	HIC Value	Impact Speed (m/s)	HIC Value	Impact Speed (m/s)	HIC Value
1.39	95.06	4.39	555.68	7.39	2135.64	10.39	7399.49
1.4	96.07	4.4	559.57	7.4	2144.61	10.4	7419.62
1.41	97.03	4.41	563.46	7.41	2153.63	10.41	7439.66
1.42	97.94	4.42	567.37	7.42	2162.7	10.42	7459.59
1.43	98.81	4.43	571.28	7.43	2171.82	10.43	7479.43
1.44	99.63	4.44	575.2	7.44	2181	10.44	7499.17
1.45	100.41	4.45	579.13	7.45	2190.22	10.45	7518.8
1.46	101.14	4.46	583.06	7.46	2199.5	10.46	7538.32
1.47	101.84	4.47	587.01	7.47	2208.84	10.47	7557.73
1.48	102.5	4.48	590.95	7.48	2218.22	10.48	7577.03
1.49	103.11	4.49	594.91	7.49	2227.67	10.49	7596.22
1.5	103.69	4.5	598.87	7.5	2237.16	10.5	7615.29
1.51	104.23	4.51	602.84	7.51	2246.71		
1.52	104.74	4.52	606.82	7.52	2256.31		
1.53	105.21	4.53	610.8	7.53	2265.97		
1.54	105.64	4.54	614.79	7.54	2275.68		
1.55	106.05	4.55	618.78	7.55	2285.45		
1.56	106.42	4.56	622.78	7.56	2295.28		
1.57	106.76	4.57	626.79	7.57	2305.16		
1.58	107.07	4.58	630.8	7.58	2315.09		
1.59	107.35	4.59	634.82	7.59	2325.09		
1.6	107.61	4.6	638.85	7.6	2335.14		
1.61	107.83	4.61	642.88	7.61	2345.24		
1.62	108.03	4.62	646.91	7.62	2355.41		
1.63	108.21	4.63	650.96	7.63	2365.63		
1.64	108.36	4.64	655	7.64	2375.91		
1.65	108.49	4.65	659.05	7.65	2386.25		
1.66	108.59	4.66	663.11	7.66	2396.64		
1.67	108.67	4.67	667.17	7.67	2407.1		
1.68	108.73	4.68	671.24	7.68	2417.61		
1.69	108.77	4.69	675.31	7.69	2428.19		
1.7	108.8	4.7	679.39	7.7	2438.82		
1.71	108.8	4.71	683.47	7.71	2449.52		
1.72	108.79	4.72	687.56	7.72	2460.27		
1.73	108.75	4.73	691.65	7.73	2471.08		
1.74	108.71	4.74	695.75	7.74	2481.96		
1.75	108.64	4.75	699.85	7.75	2492.89		
1.76	108.57	4.76	703.96	7.76	2503.89		
1.77	108.48	4.77	708.07	7.77	2514.95		
1.78	108.37	4.78	712.18	7.78	2526.07		
1.79	108.26	4.79	716.3	7.79	2537.25		
1.8	108.13	4.8	720.42	7.8	2548.49		
1.81	107.99	4.81	724.55	7.81	2559.8		
1.82	107.84	4.82	728.68	7.82	2571.17		

Impact Speed (m/s)	HIC Value	Impact Speed (m/s)	HIC Value	Impact Speed (m/s)	HIC Value
1.83	107.68	4.83	732.82	7.83	2582.6
1.84	107.52	4.84	736.96	7.84	2594.1
1.85	107.34	4.85	741.1	7.85	2605.65
1.86	107.16	4.86	745.25	7.86	2617.28
1.87	106.97	4.87	749.4	7.87	2628.96
1.88	106.78	4.88	753.55	7.88	2640.71
1.89	106.57	4.89	757.71	7.89	2652.53
1.9	106.37	4.9	761.88	7.9	2664.41
1.91	106.16	4.91	766.04	7.91	2676.35
1.92	105.95	4.92	770.21	7.92	2688.36
1.93	105.73	4.93	774.39	7.93	2700.43
1.94	105.51	4.94	778.56	7.94	2712.57
1.95	105.3	4.95	782.74	7.95	2724.78
1.96	105.07	4.96	786.93	7.96	2737.05
1.97	104.85	4.97	791.12	7.97	2749.38
1.98	104.63	4.98	795.31	7.98	2761.79
1.99	104.41	4.99	799.5	7.99	2774.26
2	104.19	5	803.7	8	2786.79
2.01	103.98	5.01	807.9	8.01	2799.4
2.02	103.76	5.02	812.11	8.02	2812.07
2.03	103.55	5.03	816.31	8.03	2824.8
2.04	103.34	5.04	820.53	8.04	2837.61
2.05	103.13	5.05	824.74	8.05	2850.48
2.06	102.93	5.06	828.96	8.06	2863.42
2.07	102.74	5.07	833.18	8.07	2876.43
2.08	102.55	5.08	837.41	8.08	2889.5
2.09	102.36	5.09	841.63	8.09	2902.65
2.1	102.18	5.1	845.87	8.1	2915.86
2.11	102.01	5.11	850.1	8.11	2929.14
2.12	101.85	5.12	854.34	8.12	2942.49
2.13	101.69	5.13	858.58	8.13	2955.91
2.14	101.54	5.14	862.83	8.14	2969.4
2.15	101.4	5.15	867.07	8.15	2982.96
2.16	101.27	5.16	871.32	8.16	2996.58
2.17	101.15	5.17	875.58	8.17	3010.28
2.18	101.04	5.18	879.84	8.18	3024.04
2.19	100.94	5.19	884.1	8.19	3037.88
2.2	100.84	5.2	888.36	8.2	3051.78
2.21	100.76	5.21	892.63	8.21	3065.76
2.22	100.69	5.22	896.9	8.22	3079.8
2.23	100.64	5.23	901.18	8.23	3093.92
2.24	100.59	5.24	905.46	8.24	3108.1
2.25	100.56	5.25	909.74	8.25	3122.36
2.26	100.54	5.26	914.02	8.26	3136.69

Impact Speed (m/s)	HIC Value	Impact Speed (m/s)	HIC Value	Impact Speed (m/s)	HIC Value
2.27	100.53	5.27	918.31	8.27	3151.08
2.28	100.54	5.28	922.61	8.28	3165.55
2.29	100.56	5.29	926.9	8.29	3180.09
2.3	100.6	5.3	931.2	8.3	3194.7
2.31	100.65	5.31	935.51	8.31	3209.38
2.32	100.71	5.32	939.81	8.32	3224.13
2.33	100.79	5.33	944.12	8.33	3238.96
2.34	100.89	5.34	948.44	8.34	3253.85
2.35	101	5.35	952.76	8.35	3268.82
2.36	101.13	5.36	957.08	8.36	3283.85
2.37	101.27	5.37	961.41	8.37	3298.96
2.38	101.43	5.38	965.74	8.38	3314.14
2.39	101.61	5.39	970.07	8.39	3329.39
2.4	101.8	5.4	974.41	8.4	3344.72
2.41	102.01	5.41	978.75	8.41	3360.11
2.42	102.24	5.42	983.1	8.42	3375.58
2.43	102.49	5.43	987.45	8.43	3391.11
2.44	102.75	5.44	991.81	8.44	3406.72
2.45	103.04	5.45	996.17	8.45	3422.4
2.46	103.34	5.46	1000.54	8.46	3438.16
2.47	103.66	5.47	1004.91	8.47	3453.98
2.48	104	5.48	1009.28	8.48	3469.88
2.49	104.36	5.49	1013.66	8.49	3485.84
2.5	104.74	5.5	1018.04	8.5	3501.88
2.51	105.14	5.51	1022.43	8.51	3517.99
2.52	105.56	5.52	1026.83	8.52	3534.18
2.53	106	5.53	1031.23	8.53	3550.43
2.54	106.46	5.54	1035.63	8.54	3566.76
2.55	106.94	5.55	1040.04	8.55	3583.15
2.56	107.44	5.56	1044.46	8.56	3599.62
2.57	107.96	5.57	1048.88	8.57	3616.16
2.58	108.5	5.58	1053.3	8.58	3632.77
2.59	109.07	5.59	1057.74	8.59	3649.46
2.6	109.65	5.6	1062.17	8.6	3666.21
2.61	110.26	5.61	1066.62	8.61	3683.03
2.62	110.88	5.62	1071.07	8.62	3699.93
2.63	111.53	5.63	1075.52	8.63	3716.9
2.64	112.2	5.64	1079.99	8.64	3733.94
2.65	112.9	5.65	1084.45	8.65	3751.05
2.66	113.61	5.66	1088.93	8.66	3768.23
2.67	114.35	5.67	1093.41	8.67	3785.48
2.68	115.11	5.68	1097.9	8.68	3802.8
2.69	115.89	5.69	1102.39	8.69	3820.19
2.7	116.7	5.7	1106.9	8.7	3837.65

Impact Speed (m/s)	HIC Value	Impact Speed (m/s)	HIC Value	Impact Speed (m/s)	HIC Value
2.71	117.53	5.71	1111.4	8.71	3855.18
2.72	118.38	5.72	1115.92	8.72	3872.78
2.73	119.25	5.73	1120.44	8.73	3890.45
2.74	120.15	5.74	1124.98	8.74	3908.2
2.75	121.07	5.75	1129.51	8.75	3926.01
2.76	122.01	5.76	1134.06	8.76	3943.89
2.77	122.98	5.77	1138.61	8.77	3961.84
2.78	123.96	5.78	1143.18	8.78	3979.85
2.79	124.98	5.79	1147.75	8.79	3997.94
2.8	126.01	5.8	1152.33	8.8	4016.1
2.81	127.07	5.81	1156.91	8.81	4034.32
2.82	128.15	5.82	1161.51	8.82	4052.61
2.83	129.26	5.83	1166.11	8.83	4070.97
2.84	130.39	5.84	1170.73	8.84	4089.4
2.85	131.55	5.85	1175.35	8.85	4107.9
2.86	132.72	5.86	1179.98	8.86	4126.46
2.87	133.92	5.87	1184.62	8.87	4145.09
2.88	135.15	5.88	1189.27	8.88	4163.79
2.89	136.4	5.89	1193.93	8.89	4182.55
2.9	137.67	5.9	1198.6	8.9	4201.38
2.91	138.97	5.91	1203.28	8.91	4220.28
2.92	140.29	5.92	1207.97	8.92	4239.24
2.93	141.63	5.93	1212.67	8.93	4258.27
2.94	143	5.94	1217.39	8.94	4277.36
2.95	144.39	5.95	1222.11	8.95	4296.52
2.96	145.81	5.96	1226.84	8.96	4315.74
2.97	147.25	5.97	1231.59	8.97	4335.02
2.98	148.71	5.98	1236.34	8.98	4354.37
2.99	150.2	5.99	1241.11	8.99	4373.79
3	151.71	6	1245.89	9	4393.26
3.01	153.25	6.01	1250.68	9.01	4412.8
3.02	154.81	6.02	1255.48	9.02	4432.41
3.03	156.39	6.03	1260.29	9.03	4452.07
3.04	158	6.04	1265.12	9.04	4471.8
3.05	159.63	6.05	1269.96	9.05	4491.58
3.06	161.28	6.06	1274.81	9.06	4511.43
3.07	162.96	6.07	1279.68	9.07	4531.34
3.08	164.66	6.08	1284.56	9.08	4551.31
3.09	166.39	6.09	1289.45	9.09	4571.34
3.1	168.14	6.1	1294.36	9.1	4591.43
3.11	169.91	6.11	1299.28	9.11	4611.57
3.12	171.71	6.12	1304.21	9.12	4631.78
3.13	173.53	6.13	1309.16	9.13	4652.04
3.14	175.37	6.14	1314.12	9.14	4672.37

Impact Speed (m/s)	HIC Value	Impact Speed (m/s)	HIC Value	Impact Speed (m/s)	HIC Value
3.15	177.24	6.15	1319.1	9.15	4692.74
3.16	179.13	6.16	1324.09	9.16	4713.18
3.17	181.05	6.17	1329.1	9.17	4733.67
3.18	182.98	6.18	1334.12	9.18	4754.22
3.19	184.94	6.19	1339.16	9.19	4774.82
3.2	186.93	6.2	1344.21	9.2	4795.47
3.21	188.93	6.21	1349.28	9.21	4816.18
3.22	190.96	6.22	1354.37	9.22	4836.95
3.23	193.01	6.23	1359.47	9.23	4857.77
3.24	195.09	6.24	1364.59	9.24	4878.63
3.25	197.19	6.25	1369.73	9.25	4899.56
3.26	199.31	6.26	1374.88	9.26	4920.53
3.27	201.45	6.27	1380.05	9.27	4941.55
3.28	203.61	6.28	1385.24	9.28	4962.63
3.29	205.8	6.29	1390.45	9.29	4983.75
3.3	208.01	6.3	1395.67	9.3	5004.92
3.31	210.24	6.31	1400.91	9.31	5026.14
3.32	212.5	6.32	1406.17	9.32	5047.41
3.33	214.78	6.33	1411.45	9.33	5068.72
3.34	217.07	6.34	1416.75	9.34	5090.08
3.35	219.39	6.35	1422.07	9.35	5111.49
3.36	221.74	6.36	1427.41	9.36	5132.94
3.37	224.1	6.37	1432.77	9.37	5154.44
3.38	226.49	6.38	1438.15	9.38	5175.98
3.39	228.89	6.39	1443.55	9.39	5197.56
3.4	231.32	6.4	1448.97	9.4	5219.19
3.41	233.77	6.41	1454.41	9.41	5240.85
3.42	236.24	6.42	1459.87	9.42	5262.56
3.43	238.73	6.43	1465.35	9.43	5284.31
3.44	241.24	6.44	1470.86	9.44	5306.09
3.45	243.78	6.45	1476.38	9.45	5327.92
3.46	246.33	6.46	1481.93	9.46	5349.78
3.47	248.91	6.47	1487.51	9.47	5371.68
3.48	251.5	6.48	1493.1	9.48	5393.62
3.49	254.12	6.49	1498.72	9.49	5415.59
3.5	256.75	6.5	1504.36	9.5	5437.59
3.51	259.41	6.51	1510.02	9.51	5459.63
3.52	262.08	6.52	1515.71	9.52	5481.71
3.53	264.78	6.53	1521.42	9.53	5503.81
3.54	267.49	6.54	1527.16	9.54	5525.95
3.55	270.23	6.55	1532.92	9.55	5548.11
3.56	272.98	6.56	1538.71	9.56	5570.31
3.57	275.76	6.57	1544.52	9.57	5592.53
3.58	278.55	6.58	1550.35	9.58	5614.78

Impact Speed (m/s)	HIC Value	Impact Speed (m/s)	HIC Value	Impact Speed (m/s)	HIC Value
3.59	281.36	6.59	1556.22	9.59	5637.06
3.6	284.19	6.6	1562.11	9.6	5659.36
3.61	287.04	6.61	1568.02	9.61	5681.69
3.62	289.91	6.62	1573.96	9.62	5704.04
3.63	292.8	6.63	1579.93	9.63	5726.41
3.64	295.7	6.64	1585.93	9.64	5748.81
3.65	298.62	6.65	1591.95	9.65	5771.23
3.66	301.57	6.66	1598	9.66	5793.66
3.67	304.53	6.67	1604.08	9.67	5816.12
3.68	307.5	6.68	1610.19	9.68	5838.59
3.69	310.5	6.69	1616.33	9.69	5861.08
3.7	313.51	6.7	1622.49	9.7	5883.59
3.71	316.54	6.71	1628.69	9.71	5906.11
3.72	319.59	6.72	1634.91	9.72	5928.64
3.73	322.65	6.73	1641.17	9.73	5951.18
3.74	325.74	6.74	1647.45	9.74	5973.74
3.75	328.83	6.75	1653.77	9.75	5996.31
3.76	331.95	6.76	1660.11	9.76	6018.88
3.77	335.08	6.77	1666.49	9.77	6041.47
3.78	338.23	6.78	1672.9	9.78	6064.06
3.79	341.4	6.79	1679.34	9.79	6086.65
3.8	344.58	6.8	1685.81	9.8	6109.25
3.81	347.77	6.81	1692.32	9.81	6131.86
3.82	350.99	6.82	1698.86	9.82	6154.46
3.83	354.21	6.83	1705.43	9.83	6177.07
3.84	357.46	6.84	1712.03	9.84	6199.67
3.85	360.72	6.85	1718.67	9.85	6222.28
3.86	363.99	6.86	1725.34	9.86	6244.88
3.87	367.28	6.87	1732.04	9.87	6267.47
3.88	370.59	6.88	1738.78	9.88	6290.06
3.89	373.91	6.89	1745.56	9.89	6312.64
3.9	377.24	6.9	1752.37	9.9	6335.22
3.91	380.59	6.91	1759.21	9.91	6357.78
3.92	383.96	6.92	1766.09	9.92	6380.34
3.93	387.33	6.93	1773.01	9.93	6402.88
3.94	390.73	6.94	1779.96	9.94	6425.4
3.95	394.13	6.95	1786.95	9.95	6447.92
3.96	397.55	6.96	1793.98	9.96	6470.41
3.97	400.99	6.97	1801.04	9.97	6492.89
3.98	404.43	6.98	1808.14	9.98	6515.35
3.99	407.89	6.99	1815.28	9.99	6537.79